CHAPTER 5

Model Estimates of Lifetimes

Lead Authors:
Martyn Chipperfield
Qing Liang

Co-Authors:
Luke Abraham
Slimane Bekki
Peter Braesicke
Sandip Dhomse
Glauco Di Genova
Eric L. Fleming
Steven Hardiman
Daniela Iachetti
Charles H. Jackman
Douglas E. Kinnison
Marion Marchand
Giovanni Pitari
Eugene Rozanov
Andrea Stenke
Fiona Tummon

Contributors:
Jérémie Burgalat
David Cugnet
Stacey M. Frith
Charlotte Pascoe
Matthew Rigby

CHAPTER 5

Model Estimates of Lifetimes

Contents

5.1 Introduction

We discuss how to use three-dimensional (3-D) Chemistry Climate Model (CCM) simulations to estimate atmospheric lifetimes of trace gases, their variability and trends, and to understand the controlling chemical and dynamical processes. We examine the model-estimated lifetimes and uncertainties in the context of the empirically derived values (Chapter 4) and uncertainty estimates in kinetics (Chapter 3). One advantage of CCMs is that they provide a useful tool to extend our current knowledge into the future to quantify how lifetimes will change in a future climate with a recovering ozone layer and a changing circulation and oxidation capacity – processes that are key in determining the lifetimes of Ozone Depleting Substances (ODSs).

The abundance of a species in the atmosphere depends on its rate of emission and its rate of chemical (and/or physical) loss, i.e., its lifetime. CCMs participating in current ozone assessment efforts use mixing ratio boundary conditions (MBC) to simulate the evolution of ODSs and greenhouse gases (GHGs) in the atmosphere, by prescribing surface concentration scenarios at the lowest model layer. Estimated lifetimes are used to predict the rate at which ODSs and GHGs will be removed from the atmosphere, and therefore scenarios used for modelling the future atmosphere. These boundary conditions largely control the time evolution of the atmospheric burden of the source gases, therefore impacting projections for the recovery of the ozone layer. They also affect projections of radiative forcing and climate change. Over the past few years significant doubts have been raised over some of the tabulated lifetimes of major ODSs provide in, for example, World Meteorological Organization/United Nations Environment Programme (WMO/UNEP) Assessments (e.g., Douglass *et al*., 2008; Liang *et al*., 2008). CCMs provide an essential tool, with which we can examine the consistency between annual change in the integrated atmospheric amount, the computed atmospheric loss and the input of ODSs to the atmosphere implied by the MBCs. We can also use CCMs to investigate differences that arise from using flux boundary conditions (FBCs) to specify the input of ODSs and GHGs.

Various definitions of lifetime have been introduced in Chapter 2. The model-calculated lifetime depends on input boundary conditions. In a simulation with time-dependent boundary conditions, dividing the atmospheric abundance of a trace gas by its atmospheric loss yields the instantaneous atmospheric lifetime. This lifetime can differ from the lifetime derived in steady-state conditions when the surface flux (implied by MBC or specified by FBC) is balanced by atmospheric removal. We will use two types of model simulations, transient and steady-state (timeslice) runs, and auxiliary ODS tracers to discuss the difference and connection between instantaneous lifetime and steady-state lifetime, as well as the impact of trends and atmospheric distributions on lifetime.

The atmospheric partial lifetime, τ_{atmos}, of a trace gas is calculated in a model using the globally integrated sum of its loss rate at all locations weighted by the local number density. Note that except for species that have surface losses, i.e., CCl_4, CH_3CCl_3, CH_4, CH_3Cl, CH_3Br, the atmospheric partial lifetime τ_{atmos} is the equivalent of global atmospheric lifetime τ for the majority of the species assessed in this report. Aside from uncertainty associated with kinetic rates (as discussed in Chapter 3), uncertainty in lifetime estimates can also arise from variations in representing transport and chemical processes in a model. For stratospheric removal (SR) species that are removed mainly by ultraviolet (UV) photolysis with maximum loss in the stratosphere, their lifetimes depend not only on the photolysis rate, but are also affected by how fast the atmospheric circulation moves air through the maximum

loss region. The destruction of tropospheric removal (TR) species is dominated by reaction with hydroxyl radical (OH) with the majority of the loss in the troposphere within 30°N/S of the equator. Therefore, species in each group require different validation of the mechanisms for their atmospheric removal.

We present lifetime estimates from six CCMs and one two-dimensional (2-D) model from groups worldwide (Table 5.1) for present day and 2100 conditions. The CCMs participated in the Chemistry-Climate Model Validation Activity (CCMVal) for the WCRP's (World Climate Research Programme) SPARC (Stratospheric Processes and their Role in Climate) Project (Eyring *et al.,* 2005) and so the key processes which impact lifetimes (e.g., photolysis, stratospheric circulation) have already been evaluated extensively (e.g., Waugh and Eyring, 2008; Morgenstern *et al.,* 2010; Butchart *et al.,* 2011; SPARC CCMVal, 2010). CCMVal has provided a framework for model evaluation and a focus of ongoing model improvement by research groups. For the lifetime assessment, we will focus on processes of particular relevance to model estimates of ODS lifetimes and evaluate CCMs in three major areas (i) photolysis, (ii) thermal reactions, (iii) atmospheric transport to address how differences in dynamical and photochemical processes in various models influence their lifetime estimates.

We aim to provide the best model lifetime estimates for the present day as well as to quantify how future climate change may affect these lifetimes. The remainder of this chapter is structured to cover three main areas: (i) experiment design, (ii) model evaluation, and (iii) lifetime estimates. Section 5.2 describes how simulations for the lifetime experiments are formulated. The main results of model evaluation are contained in Section 5.3. Section 5.4 discusses our model-based estimates of the lifetimes based on different model experiments and tracers. Section 5.5 discusses our results and Section 5.6 contains our summary and recommendations.

5.2 Model Descriptions and Experiments

This section summarizes the details of the participating models and describes the experiments performed.

5.2.1 Participating Models

Lifetime calculations in this chapter are conducted using results from six three-dimensional (3-D) CCMs and one two-dimensional CCM, GSFC2D (Chapter 3). The GSFC2D serves as a bridge between Chapter 3 and Chapter 5 to examine (i) how well does the GSFC2D performance compare with the 3-D models, and (ii) how should the uncertainty in kinetics derived in Chapter 3 be translated into 3-D CCM calculated atmospheric lifetimes. Model simulations conducted for this assessment used the same kinetic recommendations from JPL 10-6 (Sander *et al*., 2011) and are driven with the same surface GHG and ODS boundary conditions, and sea surface temperatures (except GSFC2D – see Appendix A). However, models differ in dynamical schemes, e.g., advection, convection, cloud parameterisation, as well as the inclusion of various atmospheric processes, e.g., solar cycle, quasi-biennial oscillation (QBO). In this chapter we attribute the differences in model-calculated lifetimes to variances due to model transport. A short description of each 3-D CCM model and the GSFC2D model is given in Appendix A (Section 5.7). The six 3-D CCMs contributing results to this chapter all participated in SPARC CCMVal-2. The report from this activity, SPARC CCMVal (2010), provides a detailed description of these models and contains a

detailed process-based evaluation. Here we concentrate mostly on evaluation of chemical and dynamical aspects critical to lifetime calculations.

Table 5.1. List of CCMs and 2-D model contributing to this chapter.

Model	Institutes	Researchers	Reference
GEOSCCM	NASA GSFC, USA	Q. Liang A.R. Douglass S. Frith	Pawson *et al.* (2008)
GSFC2D	NASA GSFC, USA	E. Fleming C. Jackman	Fleming *et al.* (2011)
LMDZrepro	CNRS, France	S. Bekki M. Marchand J. Burgalat D. Cugnet	Jourdain *et al*. (2008)
SOCOL	PMOD-WRC, ETH, Switzerland	E. Rozanov A. Stenke F. Tummon	Egorova *et al.* (2005)
UMUKCA	U. Cambridge, UK Met Office, UK U. Leeds, UK	P. Braesicke N.L. Abraham J.A. Pyle S. Hardiman N. Butchart S. Dhomse	Morgenstern *et al.* (2009)
ULAQ	U. L'Aquila, Italy	G. Pitari D. Iachetti G. Di Genova E. Mancini	Pitari *et al.* (2002)
WACCM	NCAR, USA	D. Kinnison	Garcia *et al.* (2007)

5.2.2 Description of Lifetime Experiments

We use a number of model simulations and types of tracers to investigate the relationships between surface fluxes, atmospheric burden, removal rates and lifetime.

5.2.2.1 Model Simulations

The model simulations considered here consist of a transient simulation from 1960-2010 (TRANS) and two timeslice simulations with 2000 conditions (TS2000) and 2100 conditions (TS2100) to calculate present-day and future lifetimes, respectively. Simulations TRANS and TS2000 allow us to compare lifetimes calculated in a full transient experiment with a steady-state experiment. All models participating in the lifetime assessment were required to use the same mixing boundary conditions for greenhouse gases from Coupled Model Intercomparison Project (CMIP) Representative Concentration Pathways (RCP) Scenario 4.5, ODSs according to WMO (2011), and HFCs based primarily on Velders *et al.* (2009). All model simulations used in this chapter, including the GSFC2D simulations, were conducted with the same chemical kinetics and photolysis rates recommended by JPL 10-6 (Sander *et al*., 2011). Note that some differences may arise due to ambiguity in JPL recommendations. Sea surface temperatures and sea ice concentrations in all six 3-D CCMs are prescribed as

monthly mean boundary conditions following the global sea ice concentration and sea surface temperature (HadISST1) data set provided by the UM Met Office Hadley Centre (Rayner *et al.*, 2003). We present here a brief description of simulation setup for this assessment. For more detailed information about model simulations see Appendix B and the individual model descriptions for any deviations from the prescribed setup in Appendix A.

TRANS is a 50-year transient run from 1960 to 2010, based on the definition of the REF-B1 simulation used in CCMVal-2 (SPARC CCMVal, 2010, Chapter 2). It is important to point out that while REF-B1 was a transient simulation with stratosphere-only chemistry schemes, the TRANS simulations from four (SOCOL, ULAQ, WACCM, UMUKCA) of the six 3-D CCMs were run with stratosphere-troposphere coupled chemistry. All forcings in this simulation are taken from observations, and are mostly identical to those described by Eyring *et al.* (2006) and Morgenstern *et al.* (2010) for REF-B1. This transient simulation includes all anthropogenic and natural forcings based on changes in trace gases, solar variability, volcanic eruptions, quasi-biennial oscillation (QBO), and sea surface temperatures/sea ice concentrations (SSTs/SICs). Models that do not include a detailed tropospheric chemistry scheme prescribed their tropospheric OH values to the 3-D monthly OH documented in Spivakovsky *et al.* (2000). For models that have coupled stratosphere-troposphere chemistry schemes, emissions of ozone and aerosol precursors are from the RCP 4.5 Scenario (Lamarque *et al.*, 2011).

TS2000 is a 30-year timeslice simulation for 2000 conditions, designed to diagnose steady-state lifetimes and to facilitate the comparison of model output against constituent observations from various measurement datasets. This simulation is conducted with prescribed GHG, ODS, and HFC surface boundary conditions for 2000, but individual models were run with either repeating or interannually varying solar variability, volcanic eruptions, quasi-biennial oscillation (QBO), and sea surface temperatures/sea ice concentrations (SSTs/SICs) for 2000 conditions. In general the final 20 years are used for analysis.

TS2100 is a 30-year timeslice simulation, driven with 2100 conditions, to diagnose steady-state lifetimes in a future climate with a recovered stratospheric ozone layer and a faster Brewer-Dobson circulation. This simulation was conducted with prescribed GHG, ODS, and HFC surface boundary conditions for 2100, but individual models were ran with either repeating or interannually varying solar variability, quasi-biennial oscillation (QBO), and sea surface temperatures/sea ice concentrations (SSTs/SICs) for 2100 conditions. In general the final 20 years are used for analysis.

One of the key factors dominates the lifetime of TR species is the tropospheric OH abundance. OH is produced in the troposphere mainly through reaction of $O(^1D)$ with H_2O with photodissociation of acetone, peroxides, carbonyls and HONO being important in particular regions (IPCC, 2007). The local abundance of OH involves most of the fast photochemistry in the troposphere and is controlled by a delicate balance between its sources and sinks. The concentration of OH responds to changes in tropospheric carbon monoxide (CO), methane (CH_4), water (H_2O), ozone (O_3), nitrogen oxides (NO_x), as well as overhead O_3 column (e.g., Spivakovsky *et al.,* 2000). The seven models participating in this assessment can be divided into three groups depending upon how tropospheric OH is treated. Models that do not include a detailed tropospheric chemistry scheme, GEOSCCM and GSFC2D, prescribed their tropospheric OH with a recommended 3-D monthly values documented in Spivakovsky *et al.* (2000). SOCOL, ULAQ, UMUKCA, and WACCM have

fully coupled stratosphere-troposphere chemistry schemes and calculate interactive OH in the troposphere. Although tropospheric OH in LMDZrepro is forced with OH taken from a full-chemistry simulation of the TOMCAT 3-D tropospheric CTM (Savage *et al.,* 2004), chemical loss of ODSs is not calculated below 400 hPa. Therefore, we exclude LMDZrepro in the lifetime calculation for all TR species. A detailed evaluation of the performance of CCMs in tropospheric chemistry has yet to be conducted in the ongoing SPARC Chemistry-Climate Modelling Initiative (CCMI). A full evaluation of modelled OH and the related fast photochemistry is beyond the scope of this assessment and difficult due to a shortage of OH observations. In this assessment, we only seek to demonstrate how ranges in simulated OH abundance in models can impact the uncertainty in lifetimes of TR species. In addition, we seek to use CCMs to address how tropospheric OH responds to climate changes under 2100 conditions, including a recovered stratospheric O_3 layer, changes in CH_4 and H_2O, as well as changes in cloudiness. Therefore, models that calculate interactive tropospheric OH were asked to use the same NO_x and non-methane hydrocarbon emissions in TS2100 as TS2000. This chapter also examines how changes in kinetic losses rates due to increasing atmospheric temperature in 2100 impact the lifetime of TR species.

5.2.2.2 Auxiliary ODS tracers

Two additional sets of ODS tracers are embedded in the CCM simulations, but uncoupled from the full chemistry scheme. One set of tracers is calculated with realistic surface emission flux boundary conditions (FBC) and the other with prescribed constant boundary conditions (CONST). Although the FBC and CONST tracers are driven with different boundary conditions, they are destroyed in the atmosphere with the same kinetics as the corresponding full chemistry MBC tracers. Note that potential biases in simulated FBC concentrations do not affect the simulated ozone layer through modified ozone depletion.

FBC tracers. For four high priority species that have ready-to-use bottom up emission estimates, we include their FBC tracers in the CCM simulations: $CFCl_3$(CFC-11)_FBC, CF_2Cl_2(CFC-12)_FBC, CH_3CCl_3_FBC, $CHClF_2$(HCFC-22)_FBC. These FBC tracers are initialised with similar conditions to the MBC tracers at the start of the simulation and evolve with geographically resolved surface emission fluxes released and atmospheric losses via photolysis and thermal reactions with atomic oxygen (first excited state, $O(^1D)$) and OH.

***CONST tracer*s**. Five constant tracers are embedded in the simulations: CFC-11_CONST, CFC-12_CONST, N_2O_CONST, CH_3CCl_3_CONST, and CH_4_CONST. These tracers are lost with the same kinetics as the MBC tracers but have a prescribed constant 100 pptv surface boundary condition.

We use the combination of MBC, FBC, and CONST tracers from the same model runs to examine how surface emission trends, atmospheric abundance and trace gas distribution impact atmospheric lifetime.

5.3 Model Evaluation and Analysis

To illustrate the importance of chemical loss in different regions, Figure 5.1 shows the annually averaged zonal mean loss rates of six ODSs with lifetimes ranging from ~5 years (methyl chloroform (CH_3CCl_3)) to ~120 years (nitrous oxide (N_2O)). CFC-11, CFC-12, and N_2O are SR species with chemical loss occurring solely in the stratosphere. The shorter lived of these (CFC-11) is destroyed lower in the stratosphere compared to the longer-lived species

CFC-12 and N_2O. Although $CBrClF_2$ (Halon-1211) is also primarily destroyed via photolysis, the majority of its loss occurs in the troposphere as it can be removed by photolysis at UV wavelengths up to 320 nm. CH_4 and CH_3CCl_3 are TR species with most of their loss occurring in the troposphere. There are small contributions from stratospheric loss, more so in the case of CH_3CCl_3. For all species, about 75-95% of the atmospheric removal occurs between 60°N-60°S with >50% of the loss occurring in the tropics (within 30° of the equator). Therefore, in this chapter, we focus mainly on model intercomparison and evaluation in the tropical region.

5.3.1 PhotoComp Results

SPARC CCMVal (2010) described the experiments and results from 'PhotoComp 2008', an off-line photolysis rate intercomparison for the CCMVal-2 CCMs. Photolysis is one of the most important processes included in a CCM and is critical for an accurate assessment of the lifetime of most of the species considered in this report. PhotoComp 2008 was a systematic evaluation of the photolysis codes as used in the CCMs by comparison with standalone reference models.

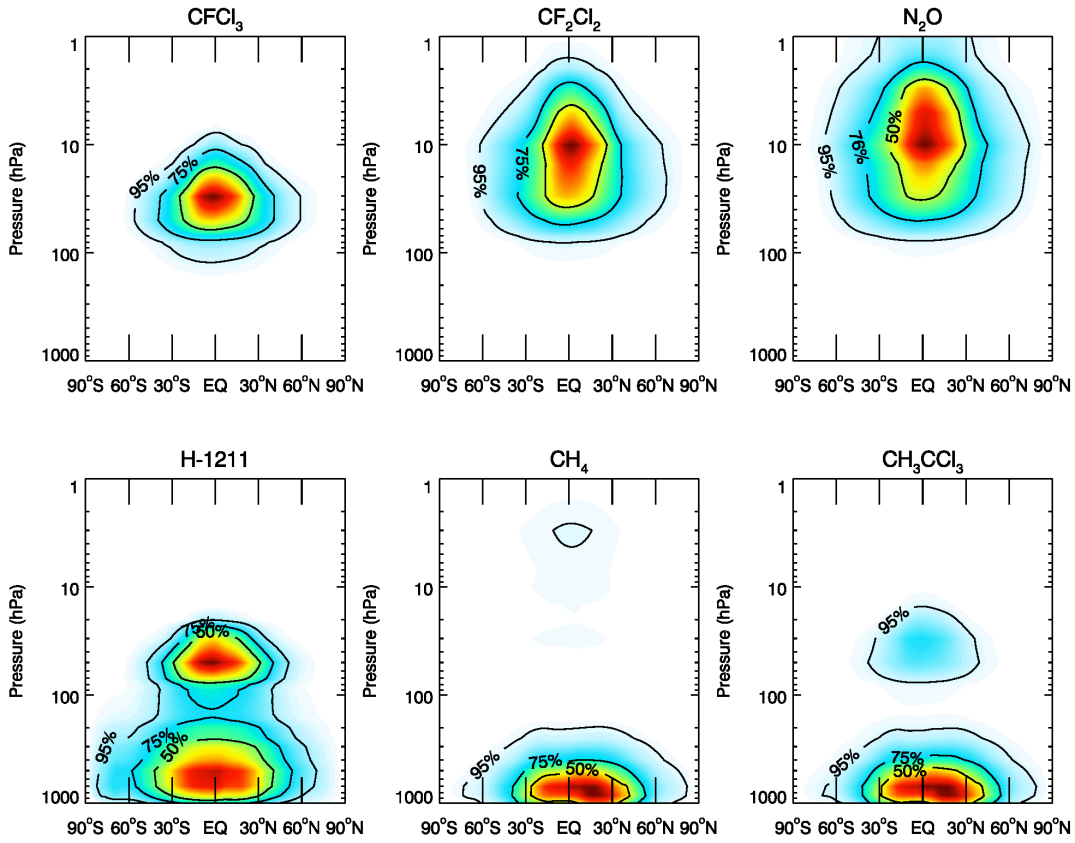

Figure 5.1. Example latitude-pressure cross sections of zonally integrated annual loss rates of $CFCl_3$, CF_2Cl_2, N_2O, Halon-1211, CH_4 and CH_3CCl_3 between 2000-2005 from the WACCM TRANS simulation, with warm colours indicating faster loss rates. The solid contours outline the regions within which 95%, 75% and 50% of the loss occurs.

Not all of the CCMVal-2 CCMs participated in PhotoComp 2008. Only 8 out of the 17 CCMs were able to take part, along with some reference codes. In terms of the models contributing to this assessment the list included GEOSCCM, LMDZrepro, SOCOL, and WACCM. Therefore, a key process for the evaluation of atmospheric lifetimes remained unevaluated for some models participating here. The PhotoComp tests have now been applied to the remaining 3-D models used here (see below).
The CCMs that did participate in PhotoComp 2008 showed a wide range of skill in calculating photolysis rates (SPARC CCMVal (2010) Figure 6-6). GEOSCCM, LMDZrepro and WACCM were consistently in the 0.9 – 1.0 (90-100%) range. NIWA-SOCOL and SOCOL had some occasional problems that could be due either to the radiative transfer solutions or to cross-section implementations.

PhotoComp 2011

The CCMVal project aimed at producing methods for evaluating models that could be archived and returned to in the future as models improve. In this spirit we have used the procedure for PhotoComp 2008 and used it to run new tests for models that did not participate as part of CCMVal-2. This updated intercomparison, PhotoComp 2011, involved the models listed in Table 5.2.

There were three parts to the PhotoComp 2008 photolysis comparison that are described in detail in Chapter 6 of SPARC CCMVal (2010). Parts 1 and 2 have been used for PhotoComp 2011. Briefly, these experiments are:

Part 1 is a basic test of all J-values for high sun (SZA = 15°) over the ocean (albedo = 0.10, Lambertian). Part 1a: Clear sky (only Rayleigh scattering) and no aerosols. Part 1b: Pinatubo aerosol in the stratosphere. Part 1c: Stratus cloud in the troposphere. The primary atmosphere was specified in terms of pressure layers, mean temperature, and column O_3 in each layer. Absorption by NO_2 or other species was not included in calculating optical depths.

Table 5.2. Models contributing to CCMVal PhotoComp 2011. The six CCMs are indicated in bold. Italics indicate new participants compared to PhotoComp 2008.

Group	Model	Label	P1a	P1b	P1c	P2a	P2n	P2m	P3	Participants
GSFC, USA	FastJX	GFJX	√	√	√	√	√	√	√	H. Bian
GSFC, USA	**GEOSCCM**	GEOS	√			√	√	√		R. Kawa R. Stolarski
CNRS, France	**LMDZrepro** (TUV4.1)	LMDZ	√	√	√	√	√	√	√	S. Lefebvre S. Bekki
PMOD-WRC / ETH, CH NIWA, NZ	**SOCOL**	SOCOL	√		√	√	√	√		F. Tummon D. Smale E. Rozanov
UCI, USA	FastJX & UCIref	UCIJ UClr	√	√	√	√	√	√	√	M. Prather
U. L'Aquila	***ULAQ***	*ULAQ*	√	√	√	√	√	√	√	G. Pitari G. Di Genova D. Iachetti
U. Cambridge Met Office	***UMUKCA***	*UKCA*	√			√	√	√		P. Braesicke P. Telford
NCAR, USA	**WACCM**	WACC	√			√	√	√	√	D. Kinnison

Part 2 tests the simulation of a spherical atmosphere and twilight conditions that are critical to the polar regions. It used the same atmosphere as Part 1 without clouds or aerosols and assumed equinox (solar declination = 0°) and latitude of 84°N. The surface SZA (not including refraction) therefore varies from 84º (noon) to 96° (midnight). J-values were reported at noon, midnight, and the 24-hour average (integrating as done in the CCM).

Figures 5.2 and 5.3 show results for species relevant to this lifetimes assessment from PhotoComp 2011 for Part 1a and Part 2 (84^{o}), respectively. The plots show results from the six CCMs listed in Table 5.2, along with three of the reference models used in PhotoComp 2008 between 100 hPa and 1 hPa, a key region of loss for most stratospheric removed species considered here. Overall the level of agreement in the photolysis rates shown is good and the model-model spread is significantly less than seen in SPARC CCMVal (2010). This is due to the iterative improvement in some of the models shown and the removal of some of the outlying models from CCMVal-2. For the high priority species it is interesting to note that the spread in the J rates for CFC-12 is larger than for CFC-11, where the models show an extremely good level of agreement. Other species for which there is a relatively large spread in J rates in the upper stratosphere include HCFC-22, CCl_2FCClF_2 (CFC-113) and CH_3Cl (HCC-40). For the species that are photolysed at short wavelengths, SOCOL produces J rate profiles that tend to differ from other models. Their photolysis rates of CFC-12 and N_2O carry on increasing significantly with height at the top of the region studied (0.01 hPa, not shown). At lower altitudes the agreement is better, but SOCOL does underestimate the photolysis rate of CF_3CClF_2 (CFC-115) and, to some extent, N_2O in the middle stratosphere compared to other models.

Overall, these results show that the models used in this report to evaluate lifetimes calculate accurate and consistent photolysis rates thereby increasing confidence in the model results.

5.3.2 Fast Chemistry Evaluation

No new evaluation of the fast chemistry in the models has been performed for this report. Therefore, we summarize how the participating models performed in the SPARC CCMVal (2010). WACCM was among the group of models that performed very well in the tests using a Photochemical Steady-State (PSS) model to evaluate the models' radical chemistry. GEOSCCM also scored relatively well, giving confidence in the formulation of the model. LMDZrepro and UMUKCA obtained marks in the middle of the range of CCMs. Overall the ULAQ and SOCOL models did not score so highly at that time. However, these two models have been updated since CCMVal-2 (see Appendix A) and so we would expect improvements.

5.3.3 Model Circulation Tests: Mean Age and Comparison with Observations

Figures 5.4 and 5.5 show the stratospheric modelled age-of-air from the CCMs used in this report for 2000 conditions and comparison with values derived from balloon and aircraft observations. For the analysis here the modelled age was set to zero at the tropical tropopause. This procedure had the largest impact on UMUKCA which otherwise produced a tropopause age with a value of around 0.5 years; the shift of reference for the other models was smaller than this. In the lower stratosphere (50 hPa) the CCMs tend to agree well with each other and with the observed variation in age from the tropics to the poles. One exception is SOCOL, which produces mean age-of-air about 1 year younger than the

observations at high latitudes. The models show a large variation in age in the mid and upper stratosphere. At around 50 km SOCOL, WACCM, LMDZrepro, GEOSCCM and UMUKCA produce ages that are 1-2 years younger than ULAQ and GSFC2D. The balloon observations used in Figure 5.5 only provide data up to ~30km but tend to show the models with the older ages are more realistic. Figure 5.5 also shows the gradient in mean age between the northern mid-latitudes and the tropics. This diagnostic tests the recirculation rate of air in the tropical upwelling and mid-latitude downwelling branches of the Brewer-Dobson circulation. The Brewer Dobson circulation itself has transition, shallow and deep branches with vertical ranges of 100-70, 70-30 and above 30 hPa, respectively (Lin and Fu, 2013). ULAQ and UMUKCA have the strongest gradients in mean age and these correspond well with observations. GEOSCCM, GSFC2D, LMDZrepro and WACCM have gradients which are slightly too weak while in SOCOL the gradient is far too week. Overall these results show that ULAQ, GEOSCCM, GSFC2D, LMDZrepro and WACCM have reasonable circulations. UMUKCA appears to have a slow stratospheric circulation, but the slow recirculation into the tropics maintains the young age there. In SOCOL the circulation is too fast.

5.3.4. Online Chemical Diagnostics

The rates of chemical processes which lead to the loss of ODS in the atmosphere have been compared in the lifetime experiments. The fluxes through photolysis, OH and $O(^1D)$ reactions were archived and are intercompared here.

To illustrate the skill of each model in simulating the vertical distribution of species which are factored into the loss rates, we compare ODS vertical profiles with balloon and satellite measurements (Figures 5.6 and 5.7). Figure 5.6 compares the tropical vertical profiles of CFC-11, CFC-12, N_2O, and CH_4 with the annual mean climatology from the Atmospheric Chemistry Experiment (ACE) satellite measurements. Figure 5.7 compares the vertical profiles of CFC-11, CFC-12, N_2O, CH_4, and Halon-1211 with three balloon measurements collected at Ft. Sumner (34.5^{o}N, 104.2^{o}W) in October 2002, September 2003 and 2004. All seven models capture the observed vertical gradients fairly well. The SOCOL model shows consistently higher concentrations in the stratosphere than the other models for all species. This implies more efficient transport of ODSs from the tropical tropopause entrance to the mid and upper stratosphere where maximum loss of the long-lived ODSs occurs, consistent with the younger age-of-air in this model. The UMUKCA model in general performs well, but shows higher CFC-12 and N_2O in the tropical middle stratosphere, related to a weak circulation. Halon-1211 in the UMUKCA model is notably lower than the other models throughout most of the troposphere and stratosphere. For Halon-1211 that has significant removal in the troposphere, such a bias is consistent with the model's (unadjusted) age-of-air being too old at the tropical tropopause.

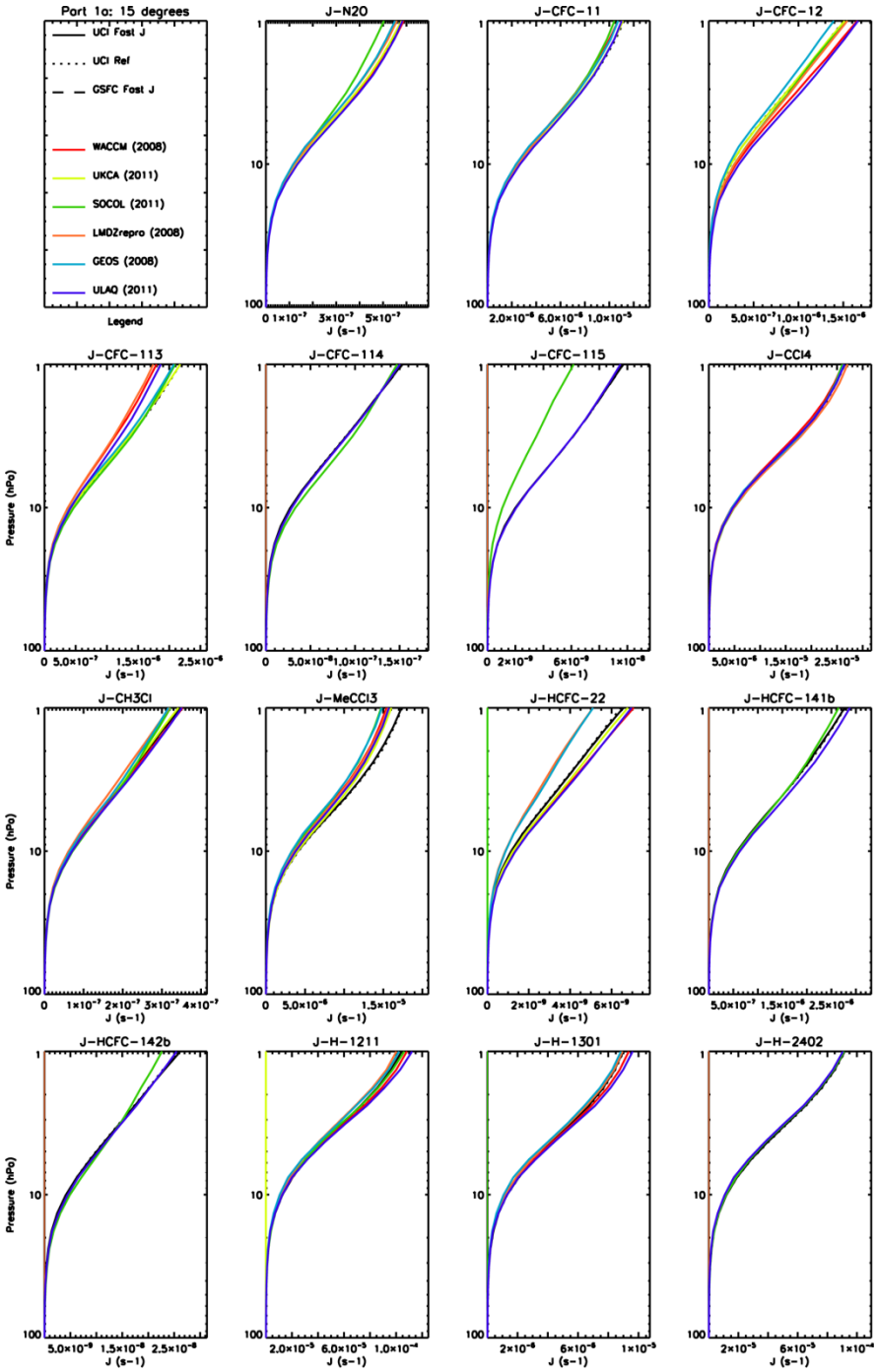

Figure 5.2. Comparison of modelled photolysis rates at 15° (PhotoComp 2011 Part 1a) between 100 hPa and 1 hPa from the WACCM, UMUKCA, GEOSCCM, SOCOL, LMDZrepro and ULAQ CCMs used in this report and 3 reference models from SPARC CCMVal (2010). Note that not all models show results for all species. GSFC2D did not perform PhotoComp tests.

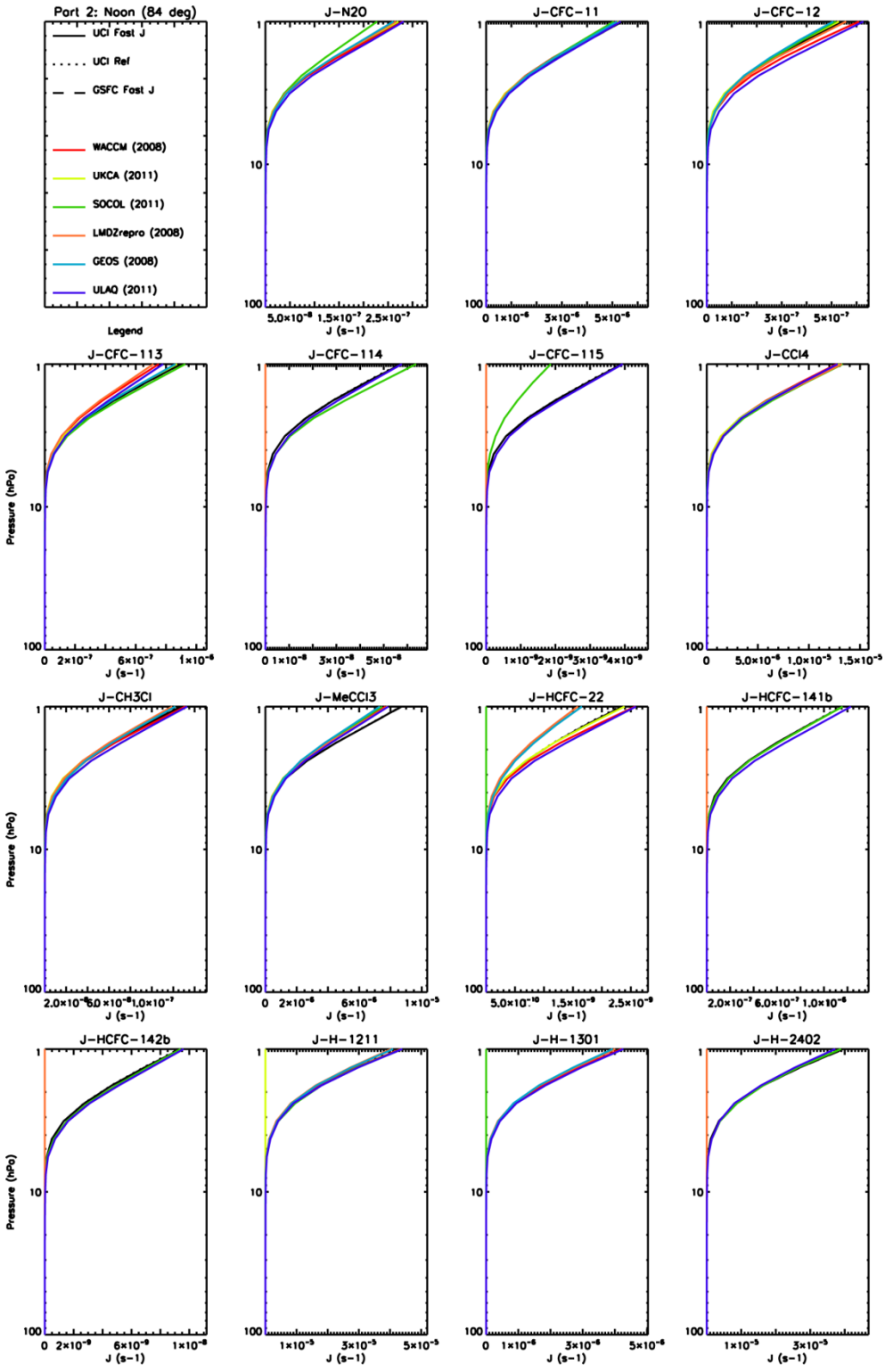

Figure 5.3. As Figure 5.2, but for 84^{o} (PhotoComp 2011 Part 2).

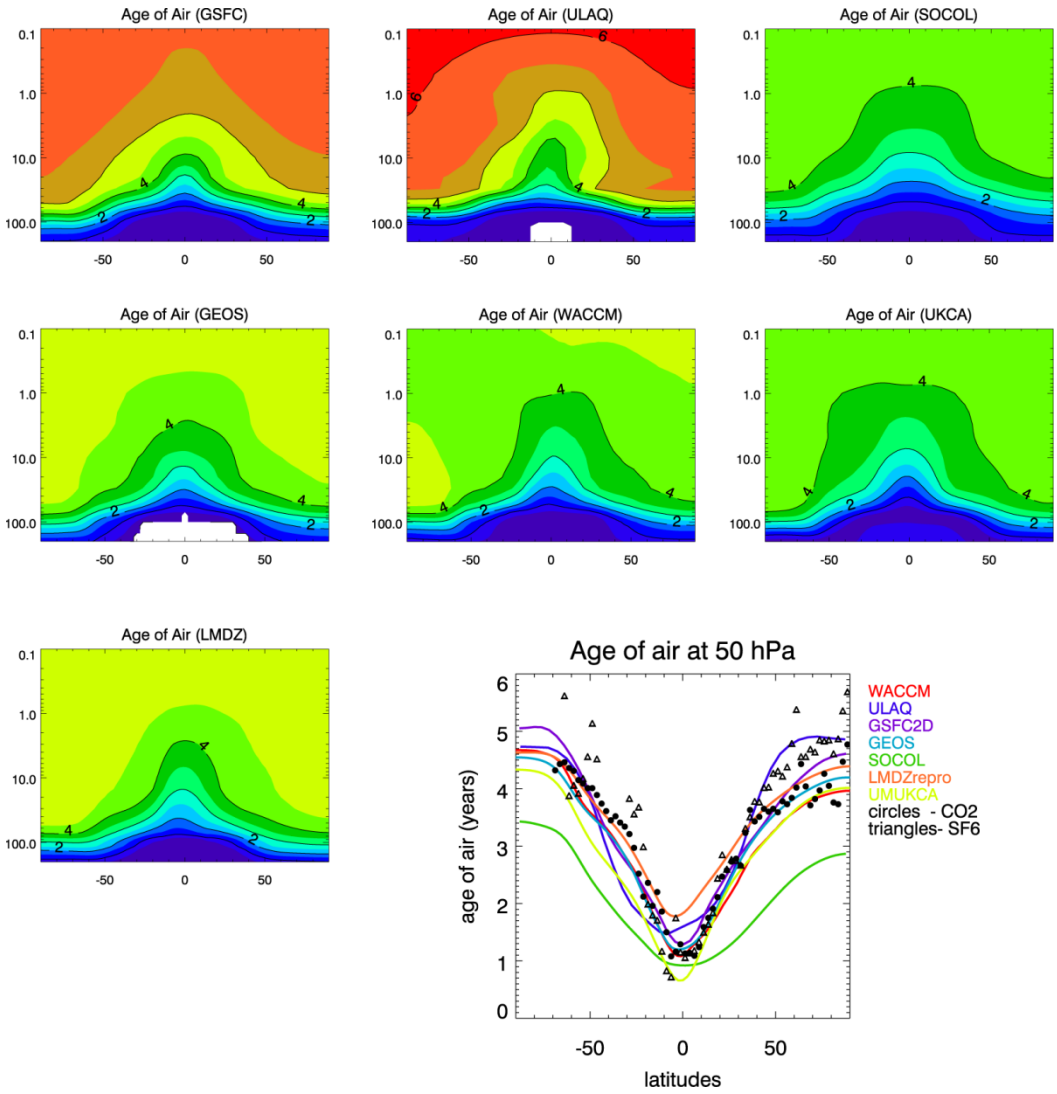

Figure 5.4. Mean age-of-air (years) calculated from present-day CCM simulations. The mean age was calculated using the last 15 years of the TS2000 runs. The lower right panel compares the mean age with observations at 50 hPa and derived age-of-air from CO_2 (filled circles) and SF_6 (triangles) measurements as described in Hall *et al.,* (1999).

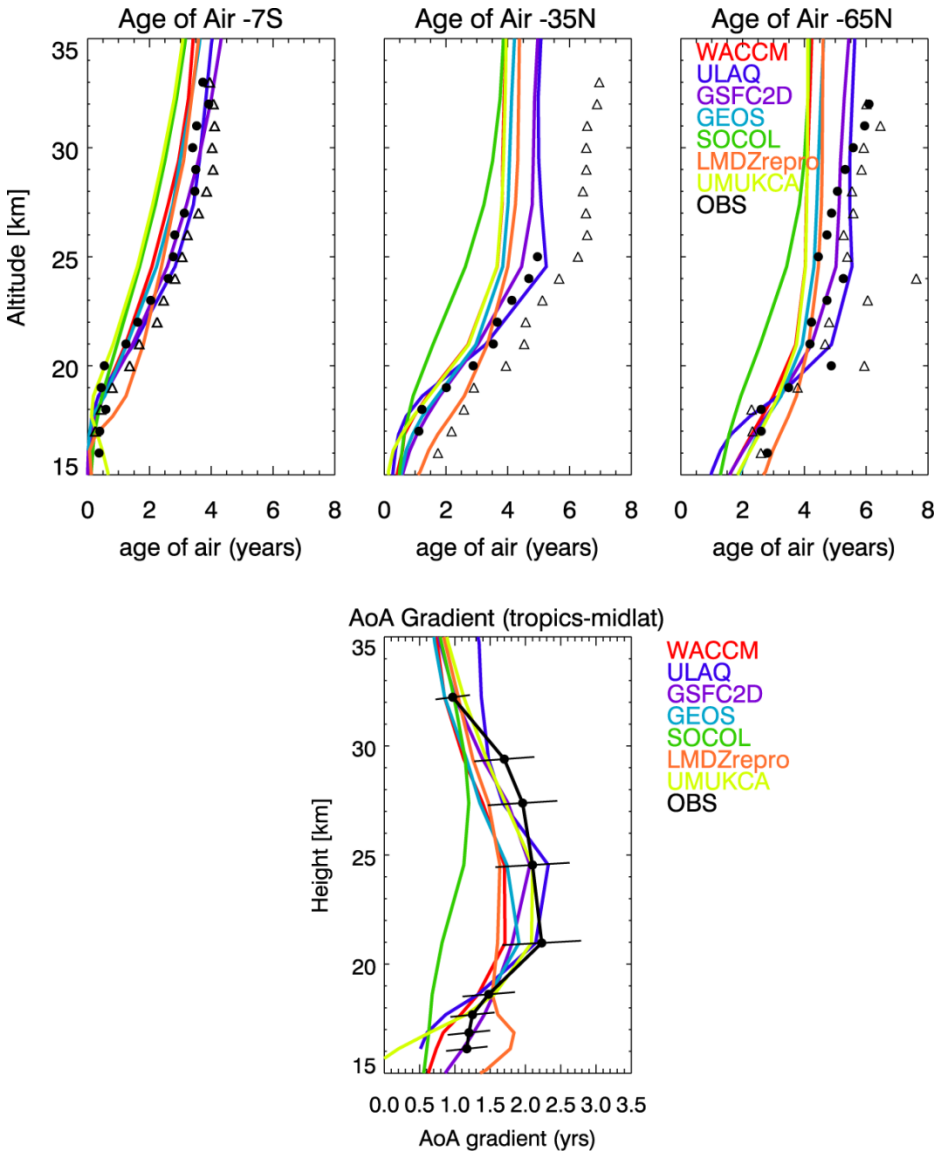

Figure 5.5. (Top) Mean age-of-air from present day CCM simulations for (a, left) 7°S, (b, centre) 35°N and (c, right) 65°N. The ages are 15-year averages of the model zonal mean output from TS2000 runs. The panels also show estimates derived from observations. (Bottom) Mean age gradient between northern midlatitudes (35°N-45°N) and tropics (10°S – 10°N) from model runs and observations with ±25% uncertainties (see Figure 5.5 from SPARC CCMVal (2010)).

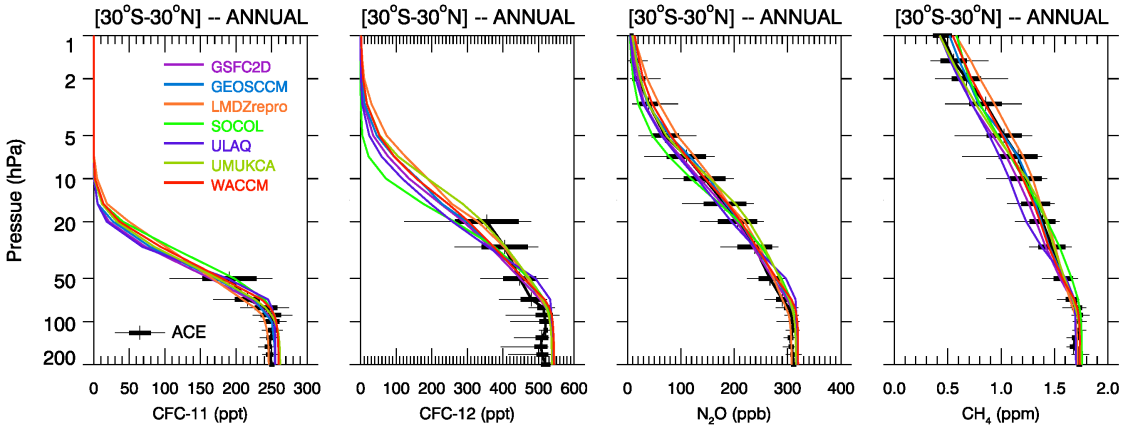

Figure 5.6. Comparison of tropical annual mean CFC-11, CFC-12, N_2O, and CH_4 profiles from the TRANS CCM simulations with ACE Climatology.

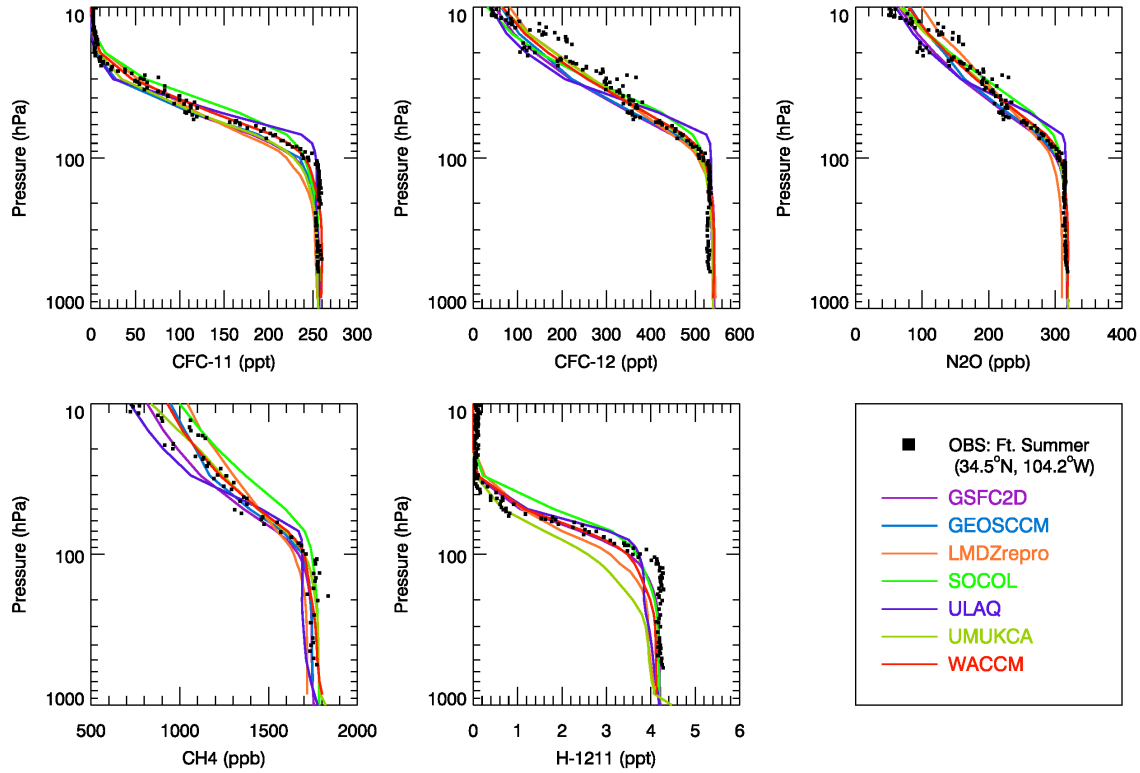

Figure 5.7. Comparison of ODS profiles from the TRANS CCM simulations with balloon measurements obtained at Ft. Sumner (34.5°N, 104.2°W) in Sep/Oct 2002-2004. Models are sampled at the closest location in the corresponding month.

5.3.4.1 Comparison of J[ODS]

Figure 5.8 compares the mean rate of the photolysis reactions from run TS2000 in the tropics. Overall, the seven models show a fair level of agreement in the magnitude of the loss rate and the altitude where maximum loss occurs. The SOCOL model shows rates consistently larger than the other models. A further comparison of the mean J rates in the tropical stratosphere (Figure 5.A1) shows that while the SOCOL model displays higher J values for some of the ODSs between 1-10 hPa, its J values between 10-100 hPa are not notably different from the other models. The higher photolysis loss fluxes in the SOCOL model (Figure 5.8) are mostly due to higher modelled ODS concentrations, a result of its faster circulation. Note that Halon-1202 is removed by photolysis at UV wavelengths up to 340 nm and Halon-1211 and Halon-2402 are removed by photolysis at UV wavelengths up to 320 nm, so a major part of the removal of these halons occurs in the troposphere. The SOCOL model differs significantly from the other four models that carry these halons in its loss rates in the troposphere, possibly due to the absence of long wavelength photolysis.

5.3.4.2 Comparison of k[ODS][OH]

Figure 5.9 compares the mean rate of the OH reactions from run TS2000 in the tropics for species significantly affected by this process. The models exhibit significant differences in the loss rates due to OH, particularly below 500 hPa where more than half of the loss occurs. The simulated OH loss rates near the surface differ by as much as a factor of 2-3 among individual models. Since all models use the same prescribed surface concentrations for the TR species, and are driven by the same sea surface temperature, this implies the difference in the OH loss rates is most likely due to differences in modelled OH.

As a further check, we compare the modelled OH concentration from all participating models (Figures 5.10 and 5.11, and Table 5.3). As explained in Section 5.2.2.1, two of the participating models (GEOSCCM and GSFC2D) use the same prescribed OH in the troposphere (Spivakovsky *et al.,* 2000) while SOCOL, ULAQ, UMUKCA and WACCM calculate interactive tropospheric OH based on surface emissions of NO_x and non-methane hydrocarbons (NMHC). Table 5.3 lists the global mean tropospheric OH concentrations ($[OH]_{GM}$) from all models and compares with previous published values. The global mean tropospheric OH (below 200 hPa) for present-day conditions ranges from 1.01×10^6 molecules/cm^3 to 1.30×10^6 molecules/cm^3 among models, with the four CCMs that calculate their own 'full chemistry' displaying $[OH]_{GM}$ higher than 1.20×10^6 molecules/cm^3. While previous reported OH concentrations show significant differences due to differences in model domain and spatial resolution (Lawrence *et al*., 2001), the majority of the published $[OH]_{GM}$ range from 0.94×10^6 to 1.0×10^6 molecules/cm^3 for $[OH]_{GM}$ below 200hPa. A detailed comparison of zonal mean distribution (Figure 5.10) and tropical mean vertical profiles of OH (Figure 5.11) suggests all models show higher OH concentrations than Spivakovsky *et al*. (2000). The modelled OH mixing ratios in the lower tropical troposphere, where OH loss plays a critical role in determining the atmospheric lifetime of TR species, differ by a factor of two between individual models. Even when models produce similar $[OH]_{GM}$, they still display significant differences in OH abundance at different altitudes. Interestingly, though the GEOSCCM and GSFC2D models both use the same prescribed OH in the troposphere, their modelled OH differ slightly from each other and from the prescribed OH fields. As prescribed OH is input into models in units of molecules/cm^3, this difference likely reflects model variations in online temperature and pressure fields used in the unit conversions between mole mixing ratio and concentration units for the other model species.

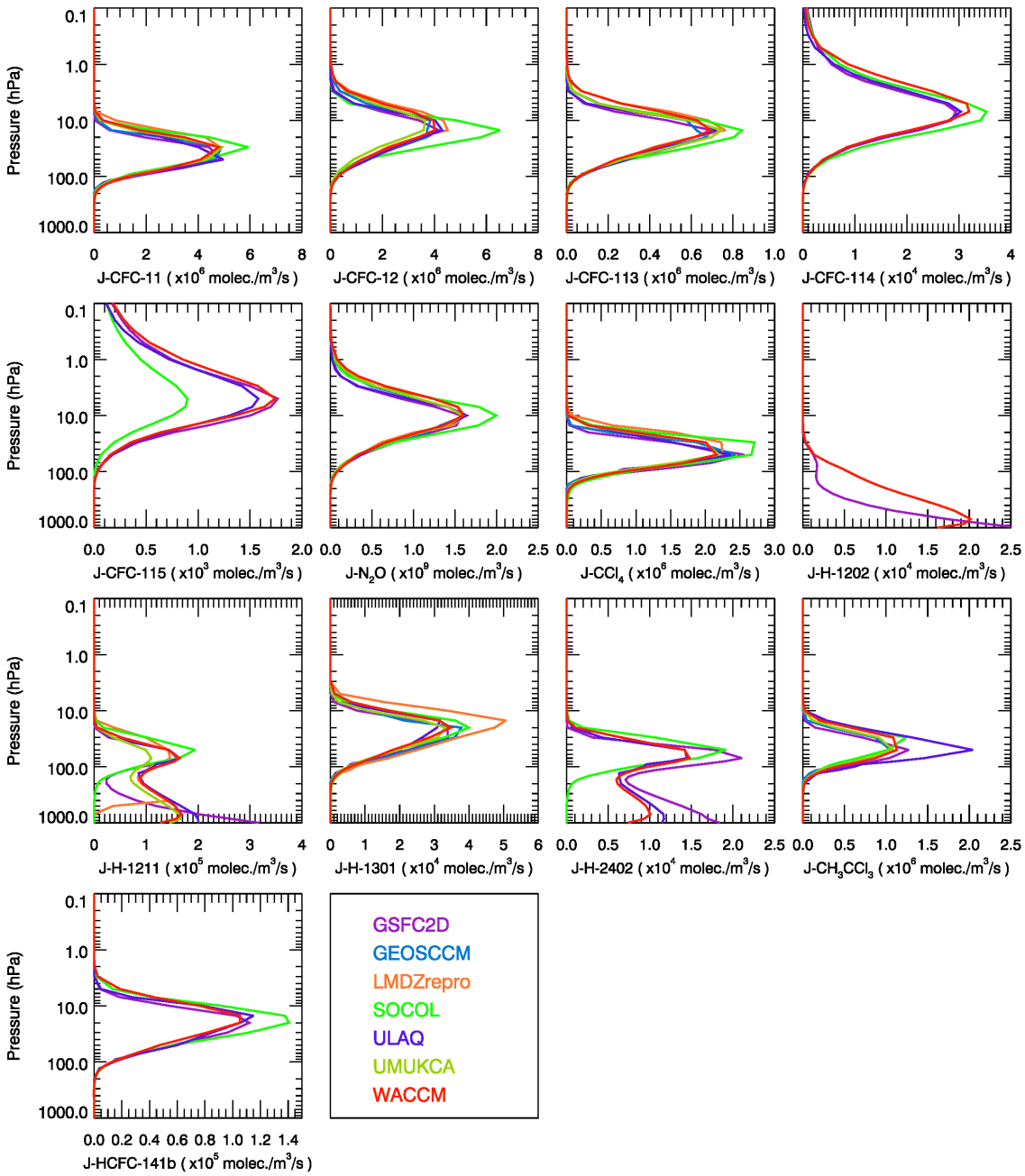

Figure 5.8. Comparison of modelled 30-year mean photolytic loss fluxes J[ODS] from the TS2000 simulation averaged between 30°S-30°N.

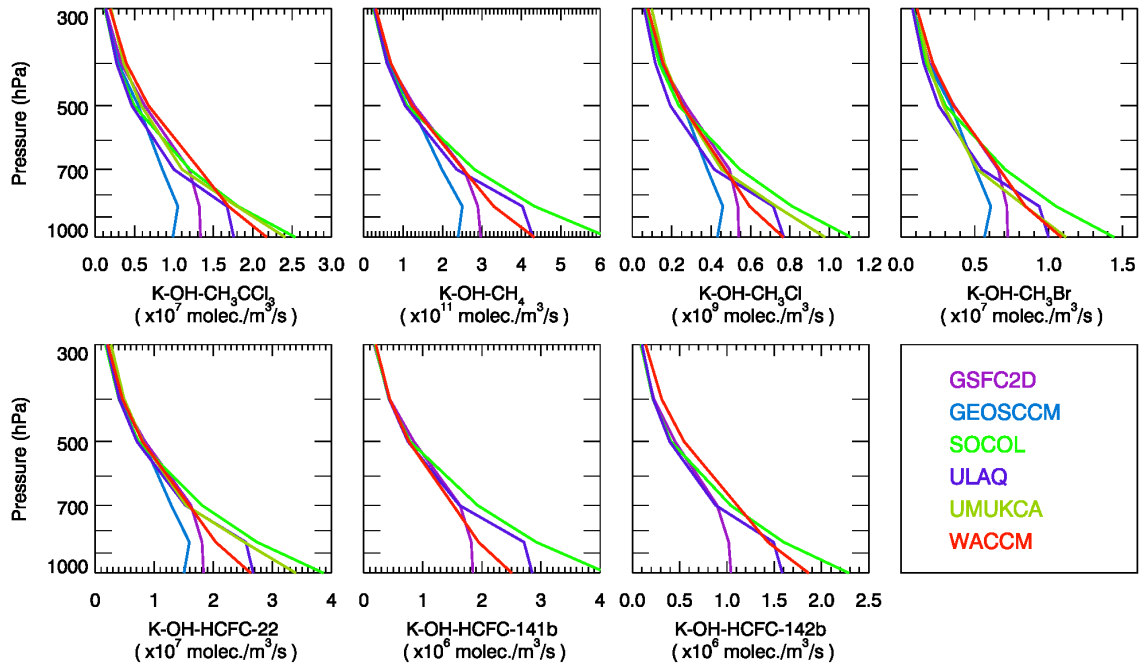

Figure 5.9. Comparison of modelled 30-year mean k[ODS][OH] loss fluxes from the TS2000 simulation averaged between 30°S-30°N.

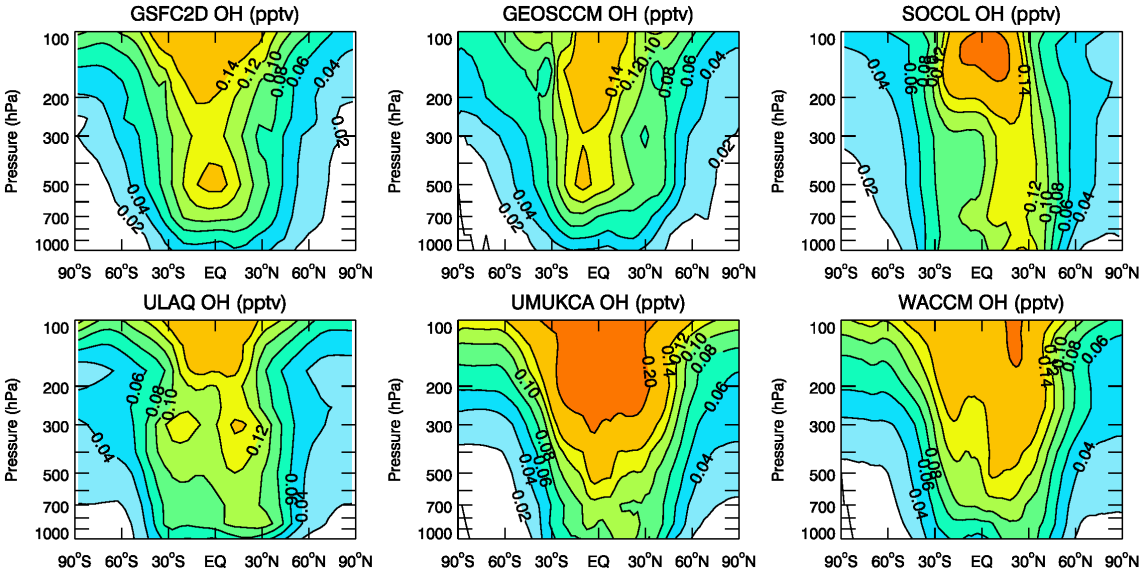

Figure 5.10. Comparison of modelled zonal mean OH (pptv) from the TS2000 simulation for the GSFC2D, GEOSCCM, SOCOL, ULAQ, UMUKCA and WACCM models.

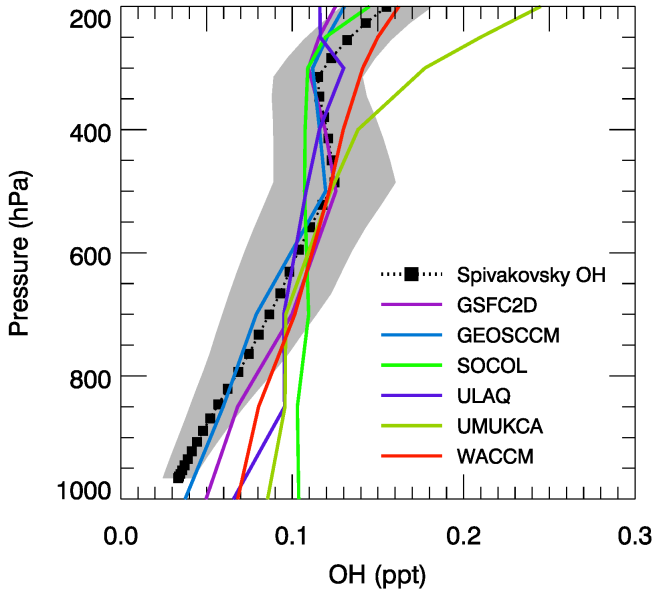

Figure 5.11. Comparison of tropical [30°S-30°N] mean OH profiles from the GSFC2D, GEOSCCM, SOCOL, ULAQ, UMUKCA and WACCM models. Mean tropical OH profile and 1-σ variance (gray shading) from Spivakovsky TS2000 simulations for *et al*. (2000) is also shown.

Table 5.3. Global mean tropospheric OH concentrations (x10^6 molecules/cm^3, mass weighted). Results for the 2000s and 2100s are calculated using the final 10 years of model output from the TS2000 simulations and results for the 1960s are 10-year averages between 1960-1969 from the TRANS simulations.

$[OH]_{GM}$	Published values *	GSFC2D	GEOSCCM	SOCOL	ULAQ	UMUKCA	WACCM
2000s (below 100 hPa)	**0.7 – 1.24**	0.91	0.87	1.07	0.99	1.22	1.07
2000s (below 200 hPa)	**0.94 – 1.0**	1.05	1.01	1.26	1.20	1.30	1.23
1960s (below 200 hPa)	N/A	1.05	1.01	1.25	1.25	1.28	1.14
2100s (below 200 hPa)	N/A	1.05	1.01	1.08	1.25	1.37	1.30

* The published values of mass weighted OH concentration adapted from Lawrence *et al.* (2001):
a) Spivakovsky *et al*. (1990): 0.8 x10^6 molecules/cm^3 below 100 hPa
b) Prather and Spivakovsky (1990): 0.8 x10^6 molecules/cm^3 below 100 hPa
c) Crutzen and Zimmermann (1991): 0.7 x10^6 molecules/cm^3 below 100 hPa
d) Prinn *et al*. (1995): 0.97 x10^6 molecules/cm^3 below 200 hPa
e) Wang *et al*. (1998): 1.0 x10^6 molecules/cm^3 below 200 hPa
f) Prinn *et al*. (2001): 0.94 x10^6 molecules/cm^3 below 200 hPa
g) Poisson *et al*. (2000): 1.24 x10^6 molecules/cm^3 below 100 hPa
h) Spivakovsky *et al*. (2000): 1.16 x10^6 molecules/cm^3 below 100 hPa within ±32° latitude and up to 200 hPa outside that region.

More recent published values since Lawrence *et al.* (2001):
i) Krol *et al.* (2003): 1.03x10^6 molecules/cm^3
j) Prinn *et al*. (2005): 1.10x10^6 molecules/cm^3
k) Bousquet *et al*. (2005): 0.99x10^6 molecules/cm^3
l) Wang *et al*. (2008): 1.06x10^6 molecules/cm^3

5.3.4.3 Comparison of k[ODS][O(^{1}D)]

Reaction with O(^{1}D) provides a minor loss mechanism for many of the ODSs and accounts for as much as ~10-40% of the total atmospheric loss for some species, e.g., CFC-114, CFC-115, and N_2O. Figure 5.12 compares the mean loss flux of the O(^{1}D) reactions from run TS2000 in the tropics. Models show a large spread in loss fluxes for all CFCs in the peak loss regions with differences of ~30-40% with respect to model mean values for four of the five CFCs and a factor of 4 for CFC-115. This large spread is mainly the result of the spread of modelled k[O(^{1}D)] rates (Figure 5.A2). While all models show a consistent and similar logarithmic dependence of k[O(^{1}D)] rates as a function of pressure, the actual rates differ by as much as 30-60% for CFC-11, CFC-12, CFC-113, and CFC-114 between models. The SOCOL and ULAQ models show $k_{O1D\text{-}CFC115}$[O(^{1}D)] rates 3-4 times higher than those from the GSFC2D and WACCM. Instead of a reaction rate constant of $1.5\text{x}10^{-11}$ cm^{-3} molecule s^{-1} ($0.3\times5.0\times10^{-11}$ cm^{-3} molecule s^{-1}, for 30% reaction) recommended by JPL 10-6, the full 5.0×10^{-11} cm^{-3} molecule s^{-1} (reaction + quenching) rate was used in the SOCOL and ULAQ models. The models agree fairly well in calculated $k_{O1D\text{-}N2O}$[O(^{1}D] and $k_{O1D\text{-}CH4}$[O(^{1}D)]. UMUKCA shows reasonable $k_{O1D\text{-}ODS}$[O^{1}D] rates for all species except N_2O; the UMUKCA $k_{O1D\text{-}N2O}$[O(^{1}D] rate is only half of those from the other models due to an implementation error.

5.4 Model Lifetime Calculations

We calculate the atmospheric lifetime, τ_{atmos}, of an ODS by dividing its global burden, B (moles), with its global integrated loss, L (moles/yr). The global burden is calculated as:

$$B = \int q_{i,j,k} \cdot \frac{\rho_{i,j,k} A_{i,j} dz_k}{mw_{air}} = -\frac{1}{g \cdot mw_{air}} \int q_{i,j,k} A_{i,j} dp_k \qquad (5.1)$$

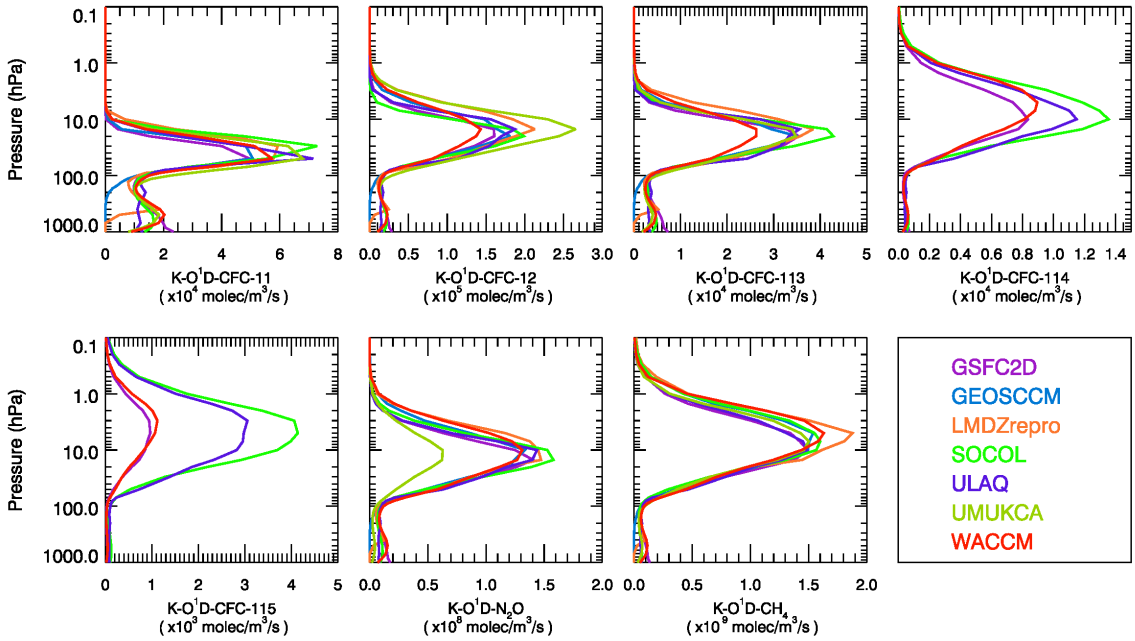

Figure 5.12. Comparison of modelled 30-year mean k[ODS][O(^{1}D)] reaction rates from the TS2000 simulation averaged between 30°S-30°N.

Similarly, L can be calculated as

$$L = -\frac{1}{g \cdot mw_{air}} \int (J_{i,j,k} + k_{i,j,k}) A_{i,j} dp_k \tag{5.2}$$

where $q_{i,j,k}$ is the mole mixing ratio and $\rho_{i,j,k}$ is air mass density at a model grid box (the *i*-th grid in the longitude dimension, *j*-th in the latitude and *k*-th in the vertical) and $A_{i,j}$ is area of grid box. $J_{i,j,k}$ and $k_{i,j,k}$ are photolytic loss rates (mole/mole/s) and thermal loss rates, respectively. dz_k is vertical thickness, and dp_k is the pressure thickness of the grid box. g is gravity and mw_{air} is the molecular weight of air.

5.4.1 Present-Day Lifetime Estimates

5.4.1.1 Evolution of Lifetimes from 1960s to Present

Figure 5.13 shows the time evolution of modelled instantaneous τ_{atmos} of seven high-priority species (CFC-11, CFC-12, CCl_4, N_2O, CH_4, CH_3CCl_3, HCFC-22) from the TRANS run. Time series of modelled instantaneous τ_{atmos} for all species of interest are included in Appendix D Figures 5.A3 to 5.A5. Note that while the TRANS run extends from 1960-2010, only the results between 1960-2006 are shown. This is because the TRANS runs from SOCOL and LMDZrepro stop in 2006 and the missing lifetime values from these two models result in a misleading increase in multi-model mean lifetime between 2006-2010. Overall, the model calculations clearly show a decrease in lifetime for all SR species. A primary reason for the decrease in the calculated lifetimes of CFCs and other man-made ODSs is the diminishing imbalance between surface fluxes and atmospheric losses as the atmosphere approaches steady-state conditions (Martinerie *et al.,* 2009). The contrast in lifetime between CFC MBC and CONST tracers, shown in Figure 5.14, clearly demonstrates that the main cause of the decrease in CFC-11 and CFC -12 lifetimes can be attributed to trends in their atmospheric concentrations. A secondary cause of the decrease in lifetime of the SR species is likely due to the combination of higher-altitude O_3 depletion that increases photolytic destruction and the speed-up of the Brewer-Dobson circulation. The CONST tracers implemented in the GEOSCCM and WACCM models suggest that the changes in photolysis and circulation together explain a decrease of ~5 years (~8% with respect to the ~57-58 years in the 2000s) in CFC-11 lifetime and ~7 years (~7% with respect to the ~93-96 years in the 2000s) in CFC-12 lifetime between the 1960s and the 2000s. Changes in atmospheric concentrations lead to a decrease of ~15 years in CFC-11 lifetime and ~30 years in CFC-12 lifetime. The small difference between the lifetimes of N_2O and its CONST tracer implies that the lifetime of N_2O is not affected by the relatively small change in its atmospheric concentration. The ~7 years (6% with respect to a 115-year lifetime in the 2000s) small decrease in N_2O lifetime from the 1960s to the 2000s is mainly due to changes in photolysis and atmospheric circulation. The instantaneous τ_{atmos} of the SR species also display significant interannual variations with year-to-year 1-σ variance of ±3-5%.

Box 5.1. The Impact of Topography on Lifetime Calculations

While differences in modelled transport and photochemistry lead to variations in calculated atmospheric lifetimes, significant differences may also arise due to differences in model output methods used to calculate atmospheric burden. Table 5.4 compares the steady-state global CFC-11 burden, $\boldsymbol{B}_{CFC\text{-}11}$, from the TS2000 simulation from all seven models. The calculated $\boldsymbol{B}_{CFC\text{-}11}$ varies by ~9% (with respect to a multi-model mean of 4.34×10^{10} moles) between models despite all using the same prescribed MBC condition and outputting data on the same pressure levels. The three CCMs, LMDZrepro, SOCOL and ULAQ, that do not report missing values in atmospheric concentrations when output grid points fall below model terrain all give relatively high $\boldsymbol{B}_{CFC\text{-}11}$. The GSFC2D model, which has a surface pressure extending down to 1013 hPa everywhere, also yields a similarly high $\boldsymbol{B}_{CFC\text{-}11}$. The relatively coarse vertical output resolution in the troposphere (1000, 850, 700, 500, 400, 300hPa, in compliance with the CCMVal-2 output format) requested for this assessment appears to be inadequate for an accurate burden calculation. Therefore, the three 3-D CCMs (GEOSCCM, UMUKCA, and WACCM) that account for topography in model output also yield a 0.17×10^{10} mole difference in their atmospheric burden due to detailed differences in how topography is treated on output layers.

Since SR species are uniformly mixed in the troposphere, it is possible to simply account for the topography effect on the burden calculation by assuming a constant atmospheric mixing ratio at all model grid points below 400 hPa and applying the following mass correction factor, α, to the calculated burden below 400 hPa:

$$\alpha = \frac{985hPa - 400hPa}{1013hPa - 400hPa} = 0.954$$

where 985 hPa is the global mean surface pressure. The topography-corrected $\boldsymbol{B}_{CFC\text{-}11}$ for all seven models is given in Table 5.4.

For TR species, the topography effect applies to both the burden and the loss calculation. Since the above correction is only valid when mixing ratios or losses are uniform in the troposphere, it is not feasible to apply a similar correction for the TR species. However, our calculation (not shown) suggests that for these species, the topography impact on loss and burden approximately cancel with each other with the calculated lifetime accurate within ~1%.

For model lifetimes reported in this chapter, we apply the topography correction to all SR species and halons, for both MBC tracers and CONST tracers. No correction is done for the FBC tracers, as these are not uniformly mixed in the troposphere. This results in a slight difference in calculated lifetimes between MBC tracers and their corresponding FBC tracers.

Table 5.4. The original and topography-corrected global burdens of CFC-11 from the TS2000 runs.

	GSFC2D (76 layers)	GEOSCCM	LMDZ-repro [a]	SOCOL [a]	ULAQ [a]	UMUKCA	WACCM
$\boldsymbol{B}_{CFC\text{-}11}$ ($\times10^{10}$ moles)	4.46	4.15	4.35	4.54	4.48	4.22	4.32
Topography-corrected $\boldsymbol{B}_{CFC\text{-}11}$ ($\times10^{10}$ moles)	4.31	4.25	4.27	4.40	4.36	4.29	4.34

[a] 3-D CCMs with topography not accounted for in model output.

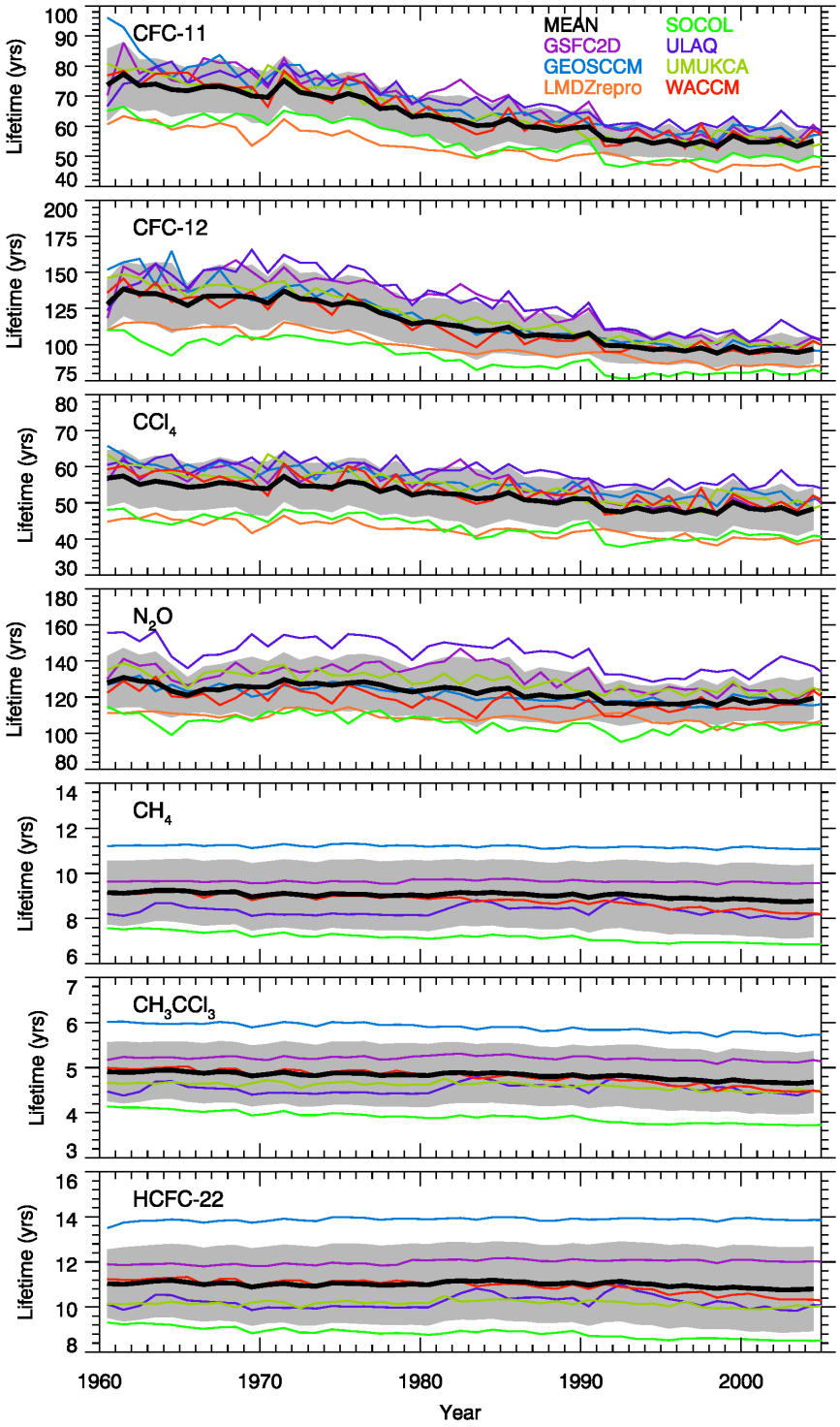

Figure 5.13. Time evolution of modelled atmospheric lifetimes (yrs) of seven high priority species between 1960 and 2006 from the TRANS simulations. Model mean lifetimes (thick black lines) and 1-σ variance (gray shading) are also shown.

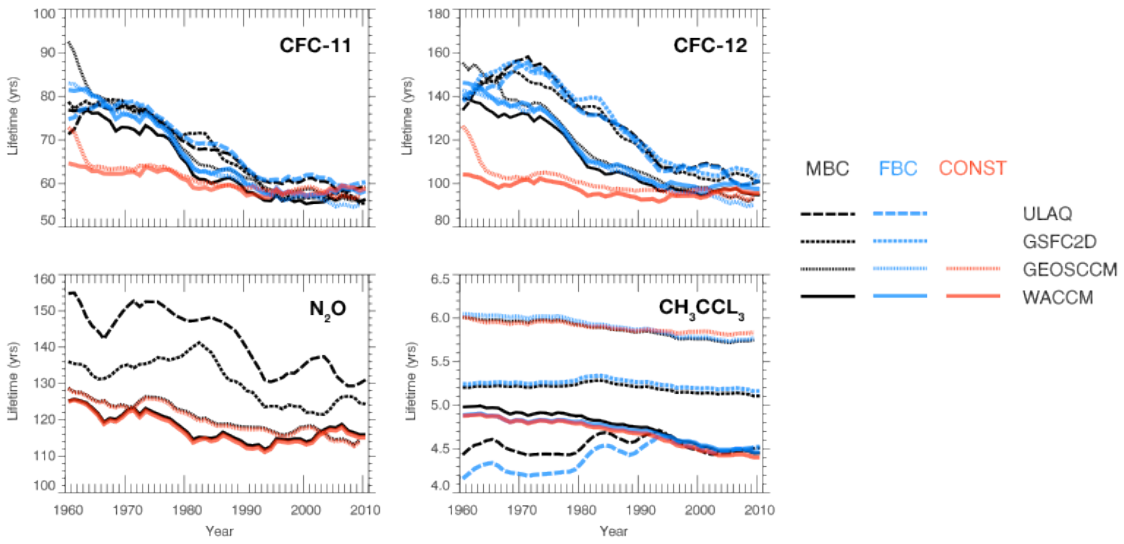

Figure 5.14. Time evolution of modelled atmospheric lifetimes of MBC CFC-11, CFC-12, N_2O, and CH_3CCl_3 (black lines) between 1960 and 2010 from the TRANS simulations and their corresponding FBC (blue lines) and CONST (red lines) tracers when available. For better visualization, the lifetimes are smoothed with a 5-year running mean filter.

While FBC tracers show significant differences in atmospheric distributions and total burden compared to MBC tracers in the same model (Figure 5.15), their modelled lifetimes are not notably different from the lifetime of MBC tracers. A detailed comparison between the 2000 steady-state lifetime and instantaneous lifetime of MBC, FBC, CONST tracers is shown in Table 5A-1 in Appendix C. Note that the instantaneous lifetimes in 2000 for all seven high priority species are not statistically different from their year 2000 steady-state lifetimes, despite their different trends in atmospheric concentrations (decreasing trends for CFC-11, CFC-12, CH_3CCl_3, CCl_4, and increasing trends for N_2O, CH_4 and HCFC-22).

The time dependencies of the lifetimes of TR species vary between models as they differ in how OH is treated or calculated in the troposphere. While GSFC2D (prescribed OH), ULAQ, and UMUKCA (interactive OH) show little trend between 1960 and 2010, SOCOL and WACCM display a ~5-10% decrease in the lifetime of three high priority TR species, CH_4, CH_3CCl_3, and HCFC-22. GEOSCCM shows a ~5% decrease in $\tau_{atmos,CH3CCl3}$, a smaller decrease in the lifetime of $\tau_{atmos,CH4}$, and little change in $\tau_{atmos,HCFC-22}$. The decrease in calculated $\tau_{atmos,CH3CCl3}$ in GEOSCCM (prescribed OH) mostly reflects the lifetime response to a warmer tropical troposphere while the decrease in SOCOL and WACCM (interactive OH) is likely due to the combined impact of a warmer troposphere and increases in OH concentrations (Table 5.3). The slightly different responses in CH_4, CH_3CCl_3, and HCFC-22 lifetimes in GEOSCCM are most likely due to differences in the trends of their atmospheric concentrations between 1960 and 2010, but this difference is less noticeable in WACCM and SOCOL as lifetime changes due to a warmer troposphere and changing OH are more dominant.

Figure 5.14 also shows the differences in calculated lifetime between the MBC, FBC and CONST tracers for CH_3CCl_3. In contrast to SR species where all models show consistent differences between each type of tracer, the differences in lifetime of CH_3CCl_3 between models overwhelm the differences between different types of tracers within a given model.

This implies that the main uncertainty in model-calculated lifetime of the TR species is dominated by the models' skill in simulating atmospheric OH (see Section 5.3.4.2).

5.4.1.2 Present-Day Steady-State Lifetimes

Table 5.5 lists the steady-state τ_{atmos} of ODSs and their substitutes for 2000 conditions from all models. The models agree fairly well in lifetime estimates for many SR species, with calculated lifetimes in general within 10% of the multi-model mean. Lifetimes of several major SR species, e.g., CCl_4, CFC-11, CFC-12, N_2O, from the SOCOL and LMDZrepro models are lower than the other models, most likely due to their fast tropical ascent (see Sections 5.3.3 and 5.4.3). The modelled steady-state τ_{atmos} of TR species differ greatly among models, with the range of estimates varying between 30%-40% for all species, mainly due to differences in modelled OH. One major caveat of the model mean lifetimes of HFCs is that these lifetime estimates are based on only two models (GSFC2D and GEOSCCM), both with prescribed OH fields. It is important to point out in addition to differences in OH, variations in air temperature, particularly in the tropical lower troposphere, can also exert a minor impact on the lifetime against loss by OH via their effects on thermal reaction rates. An increase in air temperature of 3K can lead to loss rate increases, therefore lifetime decreases, by as much as 3-5% for some of the temperature-sensitive species, e.g., HCFC-22, CH_4, CH_3CCl_3. However, for simulations conducted for this lifetimes assessment, since all 3-D CCMs are driven with the same sea surface temperature, variation in TR lifetimes due to differences in air temperature is minimized.

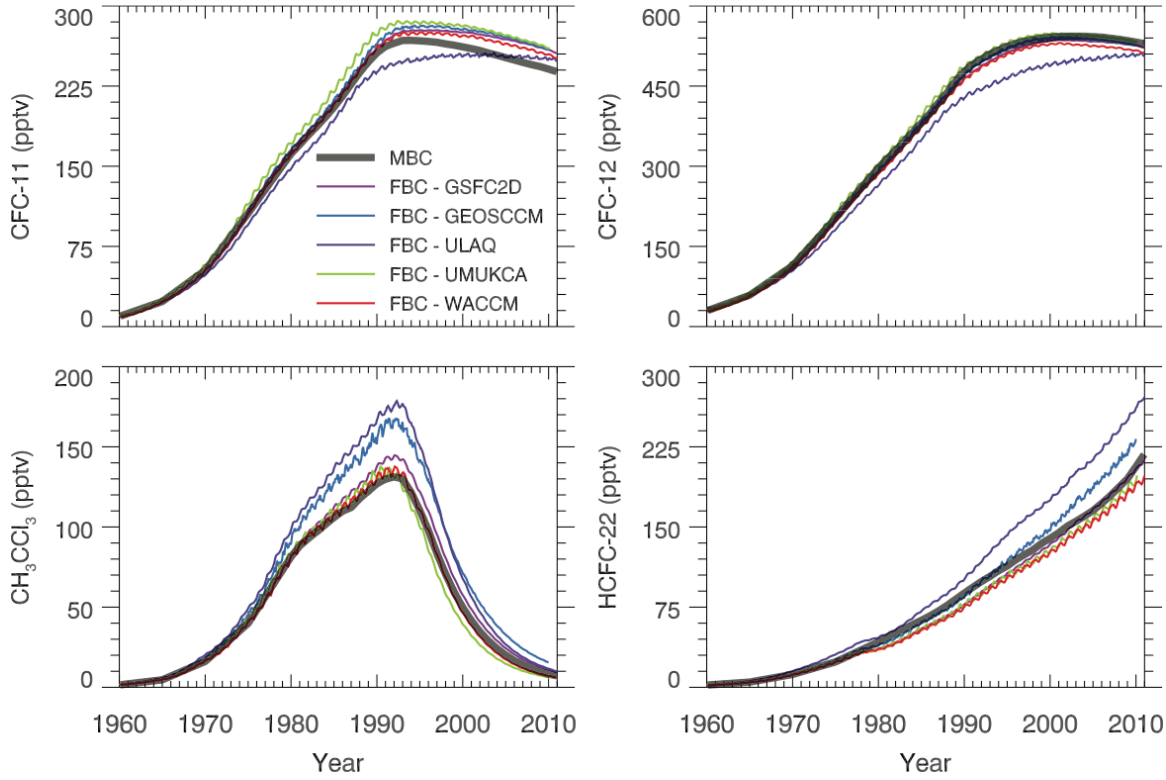

Figure 5.15. Time evolution of global mean surface concentration (pptv) of the modelled FBC tracers (dotted lines) compared with the prescribed MBC tracer scenario between 1960 and 2010 from the TRANS simulations.

Table 5.5. Steady-state τ_{atmos} (yrs) for Year 2000 from the TS2000 model runs**.** For best-estimate lifetimes for all targeted species, refer to Tables 6-1, 6-2 and 6-3 in Chapter 6.

Species	Chemical Formula	Model Mean	GSFC2D	GEOSCCM	LMDZ-repro	SOCOL	ULAQ	UMUKCA	WACCM
CFC-11	CCl_3F	**55.3**	58.6	58.3	49.1	50.8	58.6	56.8	56.9
CFC-12	CCl_2F_2	**94.7**	103.7	96.0	88.2	84.1	99.4	101.5	93.1
CFC-113	CCl_2FCClF_2	**87.3**	95.4	88.9	81.1	80.5	92.8	87.4	87.4
CFC-114	$CClF_2CClF_2$	**189**	204	--	--	169	205	--	184
CFC-115	CF_3CClF_2	**991** [a,b]	961	--	--	*	*	--	1022
CCl_4	CCl_4	**48.6**	50.7 [c]	52.2	42.0	41.4	54.3	52.0	51.3
N_2O	N_2O	**115**	125	117	105	107	127	*	112
Halon-1202	CBr_2F_2	**1.8**	2.1	--	--	--	--	--	1.6
Halon-1211	$CBrClF_2$	**11.5**	13.5	--	--	--	9.8	12.3	11.0
Halon-1301	$CBrF_3$	**72.2**	77.4	72.8	66.0	67.1	78.0	74.7	71.4
Halon-2402	$CBrF_2CBrF_2$	**14.5**	13.9	--	--	--	13.9	--	15.9
CH_4	CH_4	**8.7**	9.6	11.1	--	7.3	8.2	--	8.4
CH_3CCl_3	CH_3CCl_3	**4.6**	5.2	5.8	--	4.0	4.1	4.3	4.6
CH_3Cl	CH_3Cl	**1.3**	1.5	1.7	--	1.1	1.2	1.1	1.3
CH_3Br	CH_3Br	**1.5**	1.7	1.9	--	1.3	1.4	1.4	1.5
HCFC-22	$CHClF_2$	**10.7**	12.0	14.0	--	9.1	10.1	9.5	10.6
HCFC-141b	CH_3CCl_2F	**8.0**	9.2	--	--	7.1	7.8	--	8.1
HCFC-142b	CH_3CClF_2	**14.2**	17.5	--	--	13.6	14.7	--	12.2
HFC-23	CHF_3	**242**	226	260	--	--	--	--	--
HFC-32	CH_2F_2	**5.5**	5.2	5.9	--	--	--	--	--
HFC-125	CHF_2CF_3	**31.3**	29.3	33.7	--	--	--	--	--
HFC-134a	CH_2FCF_3	**14.4**	13.6	15.4	--	--	--	--	--
HFC-143a	CF_3CH_3	**53.2**	50.1	56.8	--	--	--	--	--
HFC-152a	CH_3CHF_2	**1.5**	1.5	1.6	--	--	--	--	--
HFC-227ea	CF_3CHFCF_3	**45.3**	42.4	48.6	--	--	--	--	--
HFC-245fa	$CHF_2CH_2CF_3$	**7.8**	7.8	--	--	--	--	--	--

[a] We calculate the mean lifetime of CFC-115 as the average of the GSFC2D and WACCM lifetimes as SOCOL and ULAQ specified a too large reaction rate constant for $O(^1D)$ and CFC-115 in their calculations.

[b] The CFC-115 lifetime calculated in Chapter 5 is significantly higher than the value in Chapter 6 (540 yr) due to differences in CFC-115 photolysis rates in the JPL 10-6 recommendation and the SPARC Lifetime recommendation (Chapter 3).

[c] The CCl_4 lifetime from GSFC2D is the τ_{phot}, instead of the τ_{atmos} which includes loss against photolysis and OH listed in Chapter 3.

In Table 5.6 we summarize the present-day model mean steady-state τ_{atmos} and 1-σ variance of the targeted species. The model mean lifetimes and their variances are calculated from the inverse of the mean and the variance of all available modelled loss rates. Partial lifetimes in different regions of the atmosphere, stratosphere vs. troposphere, and partial lifetimes associated with different loss processes, i.e., photolysis, reaction with OH, $O(^1D)$ and Cl, are also listed. The model mean lifetime estimates for CFC-11, CCl_4 and all four halons are significantly different from the WMO (2011) values. Considering the large range of modelled lifetime for the TR species, the modelled mean lifetimes of the TR species agree fairly well with the values given in WMO (2011). Photolytic destruction is the dominant loss process for all SR species with reaction with $O(^1D)$ as a minor loss channel for CFCs and N_2O. Reaction with $O(^1D)$ is particularly important for CFC-114 and CFC-115, accounting for 27% and 38% of their global loss, respectively. Although photolysis is the predominant removal process for Halons, for three (H-1202, H-1211, and H-2402) of the four targeted, the majority of the removal occurs in the troposphere. Removal of the TR species occurs primarily through reaction with OH, with photolysis, reaction with $O(^1D)$ and Cl being two minor loss channels for individual species.

5.4.1.3 Global OH Abundance Inferred from CH_3CCl_3

The 2-D model inverse method has been traditionally used with surface observations of CH_3CCl_3 to derive the atmospheric lifetime of CH_3CCl_3 and global mean OH abundance (e.g., Prinn *et al*., 1995, 2001; Montzka *et al*., 2011; Rigby *et al*., 2013). However, it is difficult to conclude whether the inferred OH concentration is representative of the true atmosphere due to a shortage of OH observations. Since CH_3CCl_3_FBC mimics well the long-term as well as short-term variations of CH_3CCl_3 in the atmosphere (Wang *et al*., 2008), one useful application is to substitute surface CH_3CCl_3 observations with 3-D CCM-modelled CH_3CCl_3_FBC in the 2-D model (see Chapter 4 and Rigby *et al*., 2013) to derive the corresponding lifetime and OH abundance. Table 5.7 compares the 2-D model inversely derived τ_{OH} and $[OH]_{GM}$ using surface CH_3CCl_3_FBC from WACCM and GEOSCCM as pseudo-observational constraints with those calculated directly using model output. The close agreement between the 2-D model inferred and 3-D CCM calculated τ_{OH} and $[OH]_{GM}$ confirms the robustness of the 2-D model inverse method and the inferred $[OH]_{GM}$ of 1.09×10^6 molecules/cm^3 is likely representative of the true global OH abundance. This is consistent with the findings in Wang et al. (2008), who inversely derived OH using a 3-D chemistry transport model and CH_3CCl_3 observations. They found that the global OH abundance can be well constrained in a Bayesian inverse approach and reported a similar $[OH]_{GM}$ of 1.06×10^6 molecules/cm^3 between 1988 and 1994.

Table 5.6. Present-day modelled steady-state τ_{atmos} (yrs). SR species whose WMO (2011) lifetimes are less (or more) than model mean – (+) 1-σ variance are highlighted in bold. For best-estimate lifetimes for all targeted species, refer to Tables 6.1, 6.2, and 6.3 in Chapter 6.

Species	WMO (2011)	Model Mean τ_{atmos}	Model Variance % (yrs)	τ_{strat}	τ_{trop}	τ_{phot}	τ_{OH}	τ_{O1D}	τ_{Cl}
CFC-11	45	**55.3**	8% (4.2)	57.0	1870	56.4	--	2930	--
CFC-12	100	94.7	8% (7.3)	95.5	11600	100	--	1750	--
CFC-113	85	87.3	6% (5.5)	88.4	7620	92.9	--	1460	--
CFC-114	190	189	10% (18.0)	191	19600	261	--	684	--
CFC-115	1020	991[a]	4% (43.1)	997	126000	1590	--	2610	--
CCl_4 [b]	35	**48.6**	12% (5.6)	50.6	1230	48.7	--	--	--
N_2O	114[c]	115	8% (9.0)	116	15600	127	--	1180	--
Halon-1202	2.9	**1.8**	21% (0.4)	15.3	2.0	1.8	--	10600	--
Halon-1211	16	**11.5**	14% (1.6)	33.5	17.3	11.5	--	8040	--
Halon-1301	65	**72.2**	7% (4.7)	73.5	4490	73.3	--	5260	--
Halon-2402	20	**14.5**	8% (1.1)	33.8	25.1	14.4	--	6790	--
CH_4	8.7[c]	8.7	16% (1.4)	152	9.3	--	8.9	462	598
CH_3CCl_3	5	4.6	14% (0.6)	37.7	5.2	45.8	5.1	--	--
CH_3Cl	1.5[d]	1.3	14% (0.2)	30.4	1.3	436	1.3	--	259
CH_3Br	1.9[d]	1.5	14% (0.2)	26.3	1.6	51.8	1.6	5180	466
HCFC-22	11.9	10.7	15% (1.6)	161	11.3	4090	10.8	654	--
HCFC-141b	9.2	8.0	11% (0.8)	72.3	8.9	91.5	8.8	1720	--
HCFC-142b	17.2	14.2	15% (2.1)	212	15.3	1510	14.8	398	--
HFC-23	222	242	[*]*15% (36.9)*	4420	256	--	244	31100	--
HFC-32	5.2	5.5	[*]*15% (0.8)*	124	5.8	--	5.5	5210	2110
HFC-125	29	31.3	[*]*15% (4.8)*	351	34.5	--	32.8	705	--
HFC-134a	13.4	14.4	[*]*15% (2.2)*	267	15.3	--	14.5	3100	--
HFC-143a	47.1	53.2	[*]*15% (8.1)*	612	58.3	--	55.6	1230	--
HFC-152a	1.5	1.5	[*]*15% (0.2)*	39.0	1.6	--	1.5	2600	401
HFC-227ea	38.9	45.3	[*]*15% (6.9)*	782	48.0	--	45.3	--	--
HFC-245fa	7.7	7.8	[*]*15% (1.2)*	149	8.2	--	7.8	--	--

[a] The CFC-115 lifetime calculated in Chapter 5 is significantly higher than the value in Chapter 6 (540 yr) due to differences in CFC-115 photolysis rates in the JPL 10-6 recommendation and the SPARC Lifetime recommendation (Chapter 3).

[b] The CCl_4 lifetime from models is τ_{phot}, compared with τ_{atmos} from WMO (2011), which accounts for losses due only to photolysis and reaction with OH.

[c] CH_4 lifetime from IPCC (2007) which includes both atmospheric and soil sinks. The soil sink accounts for <10% of the total loss.

[d] The τ_{atmos} which are listed instead of τ.

[*] For HFCs, since results are only from two models, both driven with the same prescribed OH fields, we adopted the largest variance (15%) calculated for the TR species with reaction with OH being the predominant loss, HCFC-22, as model variance.

Table 5.7. The comparison of the 2-D model inferred lifetimes and $[OH]_{GM}$ with 2-σ uncertainties (in parentheses) using CH_3CCl_3_FBC from WACCM and GEOSCCM as pseudo-observational constraints with those calculated directly using model output. CH_3CCl_3 lifetimes and $[OH]_{GM}$ (2-σ uncertainties shown in parentheses) derived using surface observations from Chapter 4 are also shown.

	Observation-derived (Chapter 4)	GEOSCCM		WACCM	
		3-D CCM	2-D inverse model	3-D CCM	2-D inverse model
$[OH]_{GM}$ ($\times 10^6$ molecules/cm^3)	1.09 (1.02-1.16)	1.01	0.96 (0.90-1.02)	1.21	1.29 (1.21-1.37)
τ_{atmos} (yrs)	5.4 (5.1-5.7)	5.8	6.1 (5.8-6.5)	4.6	4.7 (4.5-5.0)
τ_{OH} (yrs)	6.2 (5.8-6.6)	6.7	7.1 (6.7-7.5)	5.0	5.3 (5.0-5.6)
τ_{strat} (yrs)	43	46.5	46.5	46.7	46.7

5.4.2 Relative Lifetimes from Tracer-Tracer Correlations

For SR species under steady-state conditions tracer-tracer correlations can be used to derive relative lifetimes (see Chapter 2 for the theory and Chapter 4 for applications to observations). The relative lifetime of two tracers is given by:

$$\frac{\tau_2}{\tau_1} = \frac{q_2}{q_1}\frac{dq_1}{dq_2} \tag{5.3}$$

where q_1 and q_2 are volume mixing ratios. We have derived relative lifetimes from simulation TS2000 by correlating model tracers with respect to CFC-11 ($CFCl_3$). For this we analyzed the last 15 years of the run when the steady-state assumption should be valid. The method is illustrated by Figure 5.16. To evaluate the lifetime using Equation (5.3) mean tracer values at/below 100 hPa in the tropics and extra-tropics were used. Table 5.8 shows the derived relative stratospheric lifetimes, along with the corresponding absolute lifetime assuming a lifetime of $CFCl_3$ of 55 years, which is close to the model mean in Table 5.5. Results for CH_4 are also included; at steady state this method gives an estimate of the stratospheric lifetime of TR tracers such as this.

The relative lifetimes shown in Table 5.8 show a generally good level of agreement between the models. For example, ignoring UMUKCA, the relative lifetime of CFC-12 varies from 89.7 years in WACCM to 97.9 years in LMDZrepro. This range is a lot narrower than the range of absolute lifetimes of 84.1 to 103.7 given in Table 5.5. This is also the case for CFC-113 (84.2-89.1 yrs versus 80.5-95.4 yrs), CCl_4 (45.1-48.4 yrs versus 41.4-54.3 yrs), Halon 1301 (68.2-74.3 yrs versus 66.0-78.0 yrs) and N_2O (108.9-118.8 yrs versus 105–127 yrs). Also, while LMDZrepro, for example, generally produces low absolute lifetimes in Table 5.5, this is not the case for the relative lifetimes. Evidently, the models are showing a greater degree of overall self-consistency in the relative SR lifetimes. Relative lifetimes depend more strongly on chemical loss processes, and are less sensitive to differences in stratospheric circulation. Halons 1211 and 2402 have significant tropospheric loss, as does CH_4. The tracer-tracer correlation method will diagnose stratospheric lifetimes (compare to Table 5.6). However, the method appears to produce a wide range in values and more work is needed to test the usefulness of this approach for TR species.

Table 5.8. Relative steady-state τ_{atmos} for year-2000 conditions for high priority SR species from the TS2000 model simulations, derived from tracer-tracer correlations compared to CFC-11 ($CFCl_3$). Values in parentheses are the corresponding lifetime assuming τ_{CFCl3}=55 yrs. Also shown are results for the stratospheric lifetime of CH_4. For best-estimate lifetime for all targeted species, please refer to Tables 6-1, 6-2 and 6-3 in Chapter 6.

Species	GSFC2D	GEOSCCM	LMDZrepro	SOCOL	ULAQ	UMUKCA	WACCM
CFC-12	1.65 (90.1)	1.68 (92.4)	1.78 (97.9)	1.64 (90.2)	1.67 (91.9)	1.99 (109.5)	1.63 (89.7)
CFC-113	1.53 (84.2)	1.56 (85.8)	1.62 (89.1)		1.56 (85.8)	1.67 (91.9)	1.54 (84.7)
CFC-114	3.14 (172.7)				3.30 (181.5)		3.23 (177.7)
CFC-115	14.3 (786.5)						20.4 (1122.0)
CCl_4	0.87 (47.9)	0.88 (48.4)	0.86 (47.3)	0.82 (45.1)	0.88 (48.4)	0.87 (47.9)	0.88 (48.4)
N_2O	1.98 (108.9)	2.04 (112.2)	2.16 (118.8)	2.11 (116.1)	2.10 (115.5)	2.34 (128.7)	1.97 (108.4)
Halon-1211	0.69 (38.0)		0.63 (34.7)		0.37 (20.4)	[a]	0.57 (31.4)
Halon-1301	1.27 (69.9)	1.24 (68.2)	1.35 (74.3)	1.31 (72.1)	1.31 (72.1)	0.89 (49.0)	1.25 (68.8)
Halon-2402	0.63 (34.7)			0.63 (34.7)	0.45 (24.8)		0.64 (35.2)
CH_4	2.28 (125.4)	2.74 (150.7)	3.06 (168.3)	3.18 (174.9)	1.27 (69.9)	2.26 (124.3)	2.48 (136.4)

[a] Derived UMUKCA stratospheric lifetime by this method is very short (<10 years).

The relative lifetimes derived for UMUKCA appear to differ significantly from the other models. For UMUKCA it seems that the tracer-tracer correlations in the lower stratosphere do not produce such a compact correlation compared to other models (see Figure 5.16). This may be due to processing output from native model levels to pressure levels for analysis or may be due to the semi-Lagrangian advection scheme used in UMUKCA and the impact of this scheme on advected tracers as discussed by Morgenstern *et al*., (2009). Therefore, the objectively fitted slope of this UMUKCA line deviates from that which would fit the outer envelope of the tracer-tracer correlation plot and lead to a relative lifetime more consistent with the other models. This behaviour might be related to the larger offset seen in the mean age-of-air in the tropical upper troposphere/lower stratosphere (which is reset to zero at the tropical tropopause for analysis of all models in any case).

Clearly, the lifetime of a SR tracer depends on the rate of circulation of the species through the stratosphere, i.e., in the Brewer-Dobson circulation. The rate of this stratospheric circulation is illustrated by the age-of-air (see Section 5.3.3.1). In this section we explore the quantitative relationship between the derived lifetimes and age-of-air for individual models.

5.4.3 Variation of SR Species Lifetimes with Modelled Age-of-Air

Figure 5.17 shows correlation plots of derived lifetimes with stratospheric mean age-of-air for selected SR species (not including results from LMDZrepro – see below). For this analysis the mean age-of-air for each model has been reset to zero at the tropical tropopause (see Section 5.3.3.1). Overall there is a positive correlation: Models with older mean age-of-air give longer lifetimes. The correlation is relatively compact for the CFCs, CCl_4 and N_2O (r > 0.81). Overall, this confirms the results of relative lifetimes discussed above and shows the

influence of modelled mean age-of-air on the lifetimes of SR species. Given an observational estimate of the mean age-of-air in the stratosphere, the correlations in Figure 5.17 could be used to derive an optimal atmospheric lifetime.

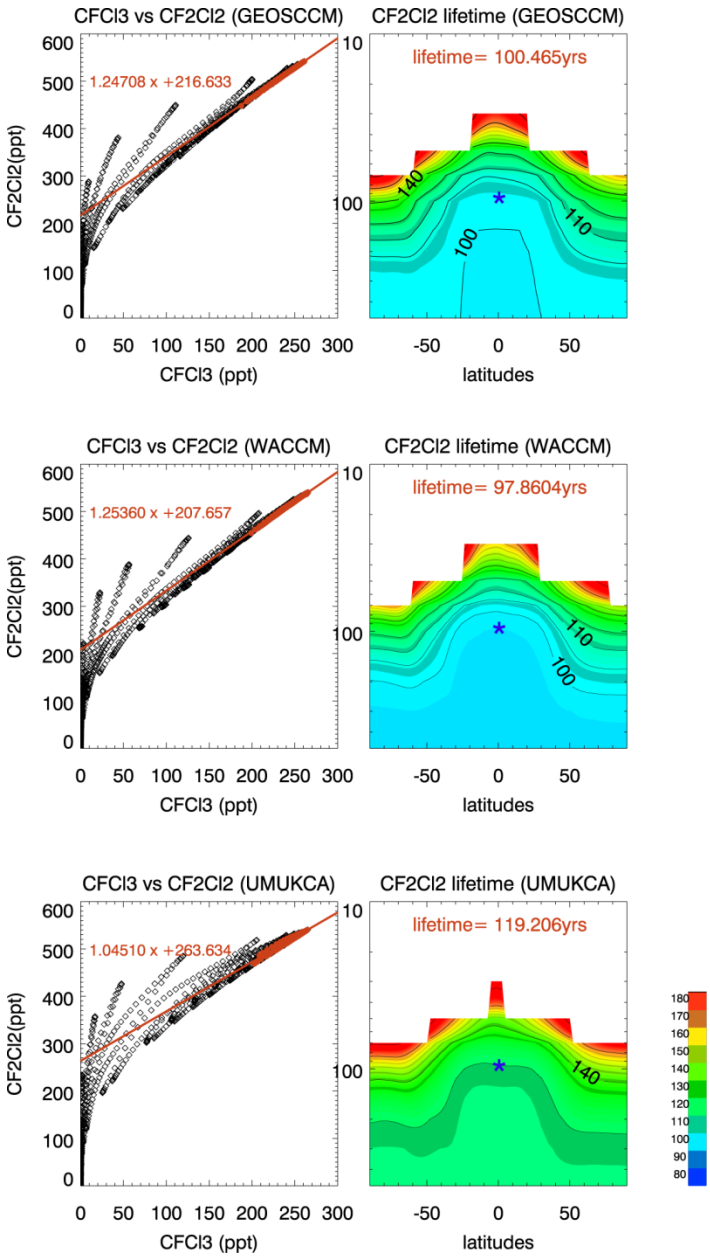

Figure 5.16. Example plots showing the calculation of relative lifetime for CFC-12 (CF_2Cl_2) from tracer-tracer correlation plots for the GEOSCCM, WACCM and UMUKCA models. Results are shown for average of last 15 years of the TS2000 runs. The left panels show the CFC-12 (CF_2Cl_2) vs. CFC-11 ($CFCl_3$) correlation plot. The points in orange (selected as the points between 60°S and 60°N, below 100 hPa and within 30% of the maximum tracer values in this region) are fitted to a straight line (equation in panel). The right panels show the example relative lifetime of CF_2Cl_2 evaluated using Equation (5.3) (see text) and an assumed approximate CFC-11 lifetime of 60 years. See text for more accurate model-based estimates. The lifetime at 100 hPa in the tropics (location of blue star) is shown in the right panels and used in Table 5.8.

As noted above Figure 5.17 does not include results from LMDZrepro. The equivalent figure which also includes these results is given in Appendix D Figure 5.A6. With results from LMDZrepro included, the correlation between lifetime and age is a lot less strong, for example for CFC-11 *r* decreases from 0.87 to 0.22. Evidently, the transport in LMDZrepro in the critical region for SR species loss cannot be represented by the simple metric of global mean age-of-air. Figure 5.18 shows the correlation between modeled lifetimes and the difference in mean age between two levels in the tropical lower stratosphere for CFC-11 and CFC-12. The chosen altitudes span the lower stratosphere up to an altitude above the main loss region for each species. This quantity is therefore a measure of the time taken for air to ascend through this loss region, allowing for vertical advection and mixing between the tropics and mid-latitudes (i.e., recirculation of ascending air). In Figure 5.18 the models display a better correlation than in Figure 5.A6, i.e., modeling the correct mean ascent rate through the tropical lower-mid stratosphere is key. The better models have the larger age difference, i.e., they have values that approach the observed difference. Although LMDZrepro gives a reasonable overall simulation of stratospheric age-of-air (Figure 5.4), the metric in Figure 5.18 shows that the model has a fast ascent rate in the key loss region, which leads to short modelled lifetimes.

5.4.4 Variation of TR Species Lifetimes and OH

While all participating models show a fair level of agreement in their estimated atmospheric lifetime of SR species, modelled lifetimes of TR species display a large range, mainly due to differences in their representation of OH in the troposphere. Figure 5.19 plots the derived partial atmospheric lifetimes of TR species against tropospheric mean OH, $[OH]_{trop}$. There is a clear anti-correlation between modelled lifetime and $[OH]_{trop}$ (r = -0.91 to -0.95). The differences in detail in the modelled OH distributions (interactive or specified) appear to play a secondary role in determining the lifetime, compared to the simple overall tropospheric mean OH.

We conducted two sensitivity TS2000 simulations with the GSFC2D model, differing from TS2000 by increasing and decreasing the prescribed OH field by 20%, to investigate the impact of OH abundance on the lifetimes of the TR species. Results suggest that lifetimes of TR species respond rather linearly to the OH abundance. A 20% increase in OH leads to ~16% decrease in TR species lifetimes against OH on average, while a 20% decrease leads to ~19% increase in lifetime against OH. Although all three simulations were run with the same MBC at the surface, the change in OH leads to a slight decrease (increase) in tropospheric ODS concentrations in the high-OH (low-OH) simulation. The asymmetric response is due to a smaller relative change in ODS concentrations in the high-OH simulation than in the low-OH simulation. The slightly larger relative response in the low-OH case implies higher efficiency in ODS-destruction at lower OH concentrations.

Figure 5.20 plots the OH partial lifetimes, τ_{OH}, of CH_4, HCFC-22, CH_3Cl, and CH_3Br against τ_{OH} of CH_3CCl_3 from all available models as well as the observation-derived τ_{OH} from Chapter 4. While models differ greatly in their calculated lifetime of TR species against OH, τ_{OH} of a TR species is tightly correlated with that of CH_3CCl_3 (r = 0.991-0.996), independent of differences in OH abundances in individual models. The multi-model regression slope of τ_{OH} of a TR species against $\tau_{OH,CH3CCl3}$ agrees well with the reverse ratio of their thermal reaction rates with OH, $k_{OH\text{-}CH3CCl3}/k_{OH\text{-}TR}$, at 272K, as noted in Spivakovsky *et al*. (2000). An important implication of this is that it is possible to derive τ_{OH} of a TR species by scaling up $\tau_{OH,CH3CCl3}$ using the ratio of thermal reaction rates.

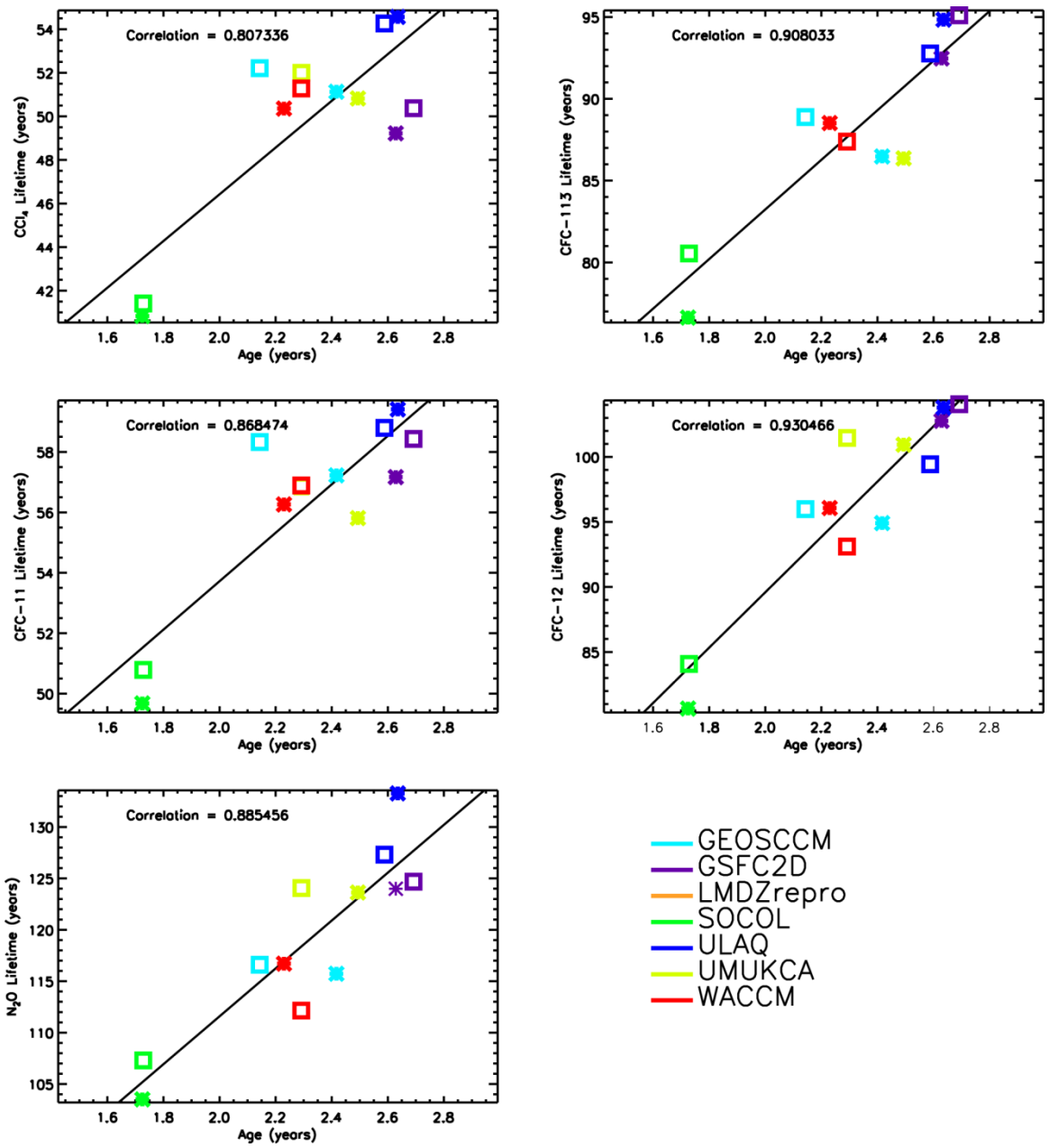

Figure 5.17. Correlation of modelled lifetimes (yrs) with the global mass-weighted average of stratospheric mean age-of-air from 100 hPa to 1 hPa (yrs) for (a) CCl_4, (b) CFC-113, (c) CFC-11, (d) CFC-12 and (e) N_2O. Results are shown from runs TS2000 (square) and TRANS (asterisk). Note that results from LMDZrepro are not included – see Figure 5.A6 in Appendix D.

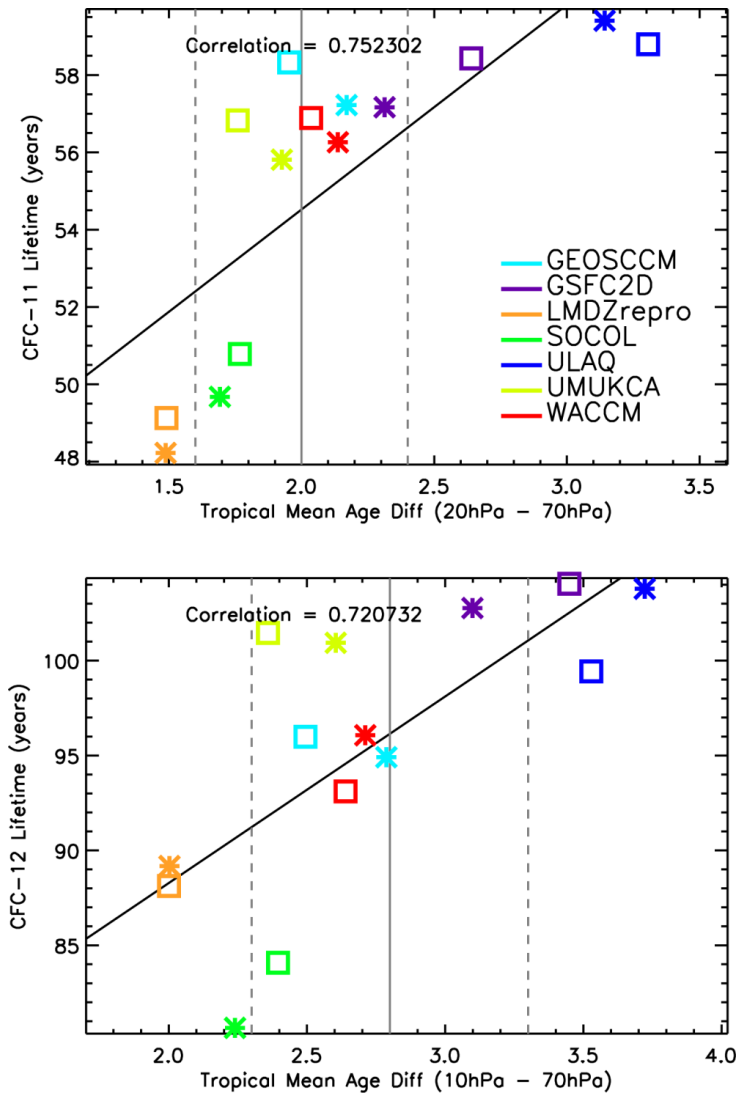

Figure 5.18. Correlation of modelled lifetimes (yrs) with the difference in mean age-of-air between two levels in the tropics for (a, top) CFC-11 (age difference between 70 hPa and 20 hPa), and (b, bottom) CFC-12 (age difference between 70 hPa and 10 hPa). Results are shown from runs TS2000 (square) and TRANS (asterisk). Also shown are estimates of the observed tropical mean age difference (vertical solid line) and its uncertainty (dashed vertical lines).

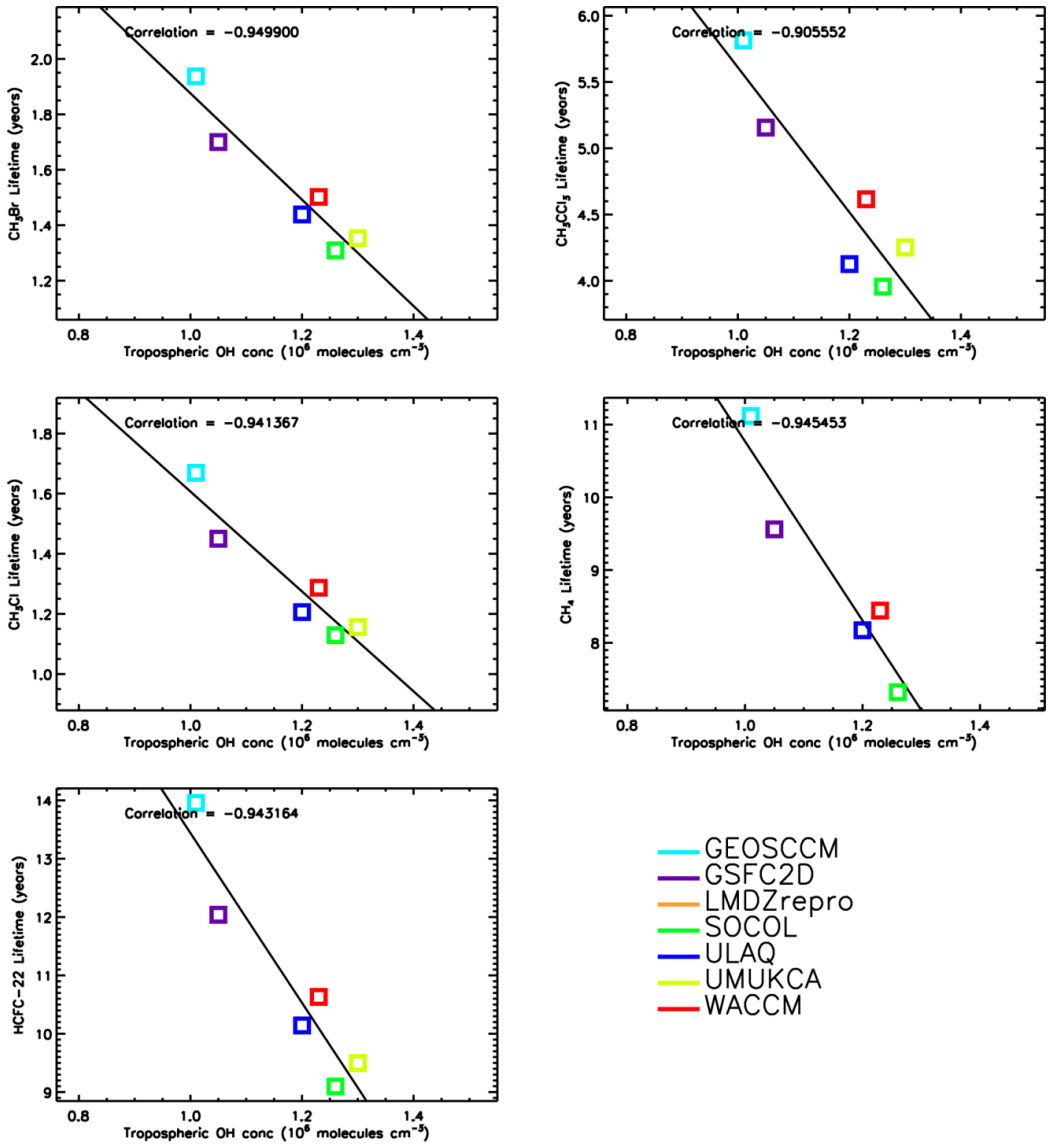

Figure 5.19. Correlation of modelled lifetimes (yrs) with tropospheric mean OH concentration (x 10^6 molecules cm^{-3}) for (a) CH_3Br (b) CH_3CCl_3, (c) CH_3Cl, (d) CH_4 and (e) HCFC-22. Results are shown from TS2000 runs (square). Results from LMDZrepro were not used for TR species and are not plotted here.

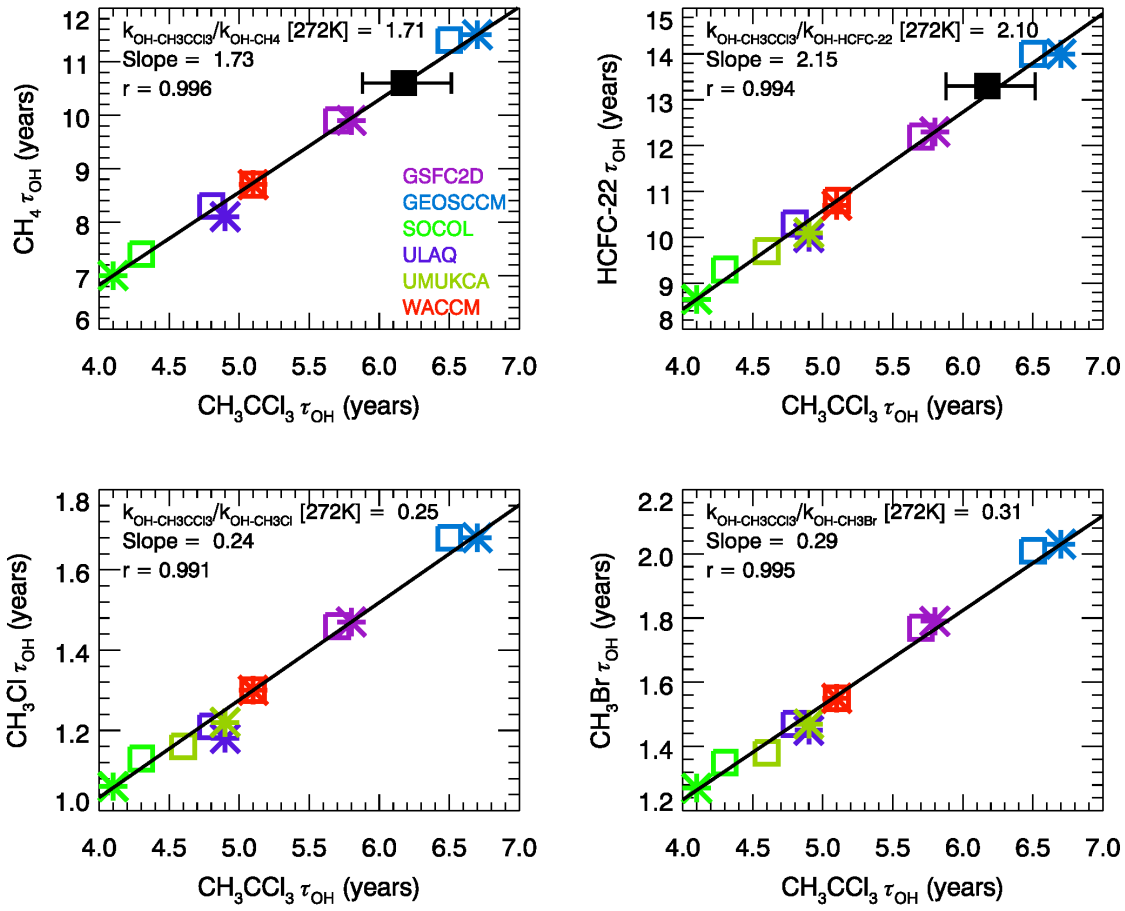

Figure 5.20. Correlation of modelled OH partial lifetimes (yrs) for (a) CH_4, (b) HCFC-22, (c) CH_3Cl, and (d) CH_3Br with modelled OH partial lifetime of CH_3CCl_3. Results are shown from runs TS2000 (squares) and TRANS (asterisks). Results from the 2-D inverse model used in Chapter 4 are also shown for CH_4 and HCFC-22 (black filled squares with horizontal bars indicating 2-σ uncertainty).

5.4.5 Future Lifetimes Estimates

Atmospheric changes are expected to modify tracer lifetimes in various ways in the future atmosphere. For example, a speed-up in the Brewer-Dobson circulation (BDC) in the critical region for stratospheric loss would be expected to lead to a reduction in the lifetime of photolytically removed species. Lin and Fu (2013) analysed the BDC changes in CCMVal-2 model experiments and found that while models consistently simulated an acceleration of both the shallow and deep branches of the BDC, the acceleration of the deep branch (i.e., above 30 hPa) was much smaller. They also noted significant differences between models. For the TR species, a future climate would lead to changes in tropospheric OH (e.g., through humidity changes) and air temperature, thus affecting the atmospheric lifetimes. For this assessment run TS2100 can be used to investigate how lifetimes may change due to these processes. Recall, however, that not all models have interactive tropospheric OH.

Table 5.9 compares the lifetimes for the TS2000 and TS2100 runs for six models that have conducted both runs. The six participating models predict different responses in future atmospheric lifetimes of SR species. GEOSCCM, SOCOL, and UMUKCA show a decrease

in lifetimes in most of the SR species while WACCM show a slight increase in all SR species. The future lifetime changes predicted by the GSFC2D and ULAQ are somewhat mixed, with increases for some and decreases in the others. A comparison of change in mean age-of-air between the simulations for 2100 and 2000 suggests that all models, except WACCM, show a speeding up of the Brewer-Dobson circulation although the magnitude of this change varies (Figure 5.21). GEOSCCM, GSFC2D, and SOCOL show only a small decrease in mean age (~1-3 months) while UMUKCA and ULAQ show larger changes. WACCM shows a slight speed-up (~0-1 month) of the shallow branch of the Brewer-Dobson circulation but a slow-down (~0-2 months) of the deep branch of the Brewer-Dobson circulation. However, such a weak change in circulation in WACCM might not be statistically significant. On the other hand, all models predict a decrease in photolysis (J) rates under 2100 conditions with the recovered ozone layer and a cooler stratosphere, though the relative changes in J rates vary among models and species. ULAQ and UMUKCA predict the strongest reduction in J rates, e.g., ~13% decrease in $J_{CFC\text{-}11}$ in the tropical lower stratosphere between 10-100 hPa with respect to the 2000 conditions, while GSFC2D, WACCM and GEOSCCM show a much weaker reduction of 5-6%. SOCOL displays a medium response of ~9% reduction in the corresponding $J_{CFC\text{-}11}$ rate. From a multi-model mean perspective, the decrease in lifetime due to a faster Brewer-Dobson circulation cancels with the increase in lifetime due to weaker photolysis. Therefore, the atmospheric lifetimes for SR species under 2100 conditions do not change significantly from the lifetimes under 2000 conditions.

With the exception of SOCOL, all models predict shorter lifetimes for TR tracers. The decrease in TR species lifetimes in GSFC2D and GEOSCCM is due to increases in air temperature while the decreases in ULAQ, UMUKCA, and WACCM are due to a combined impact of increasing OH (Table 5.3) and increasing air temperature. For all the models that calculate tropospheric OH interactively, the SOCOL model is the only model that predicts a decrease in $[OH]_{GM}$ from 1.26×10^6 molecules/cm^3 in 2000 to 1.08×10^6 molecules/cm^3 in 2100, therefore leading to an increase in lifetimes of TR tracers. However, the marked difference between its simulated OH concentration and vertical profile under present day conditions and the other models, as well as the previously published results, raises questions over the robustness of such a response.

It is important to point out that our projection of how lifetimes of ODSs will change in a future climate is dependent upon the choice of GHGs scenario used to drive the TS2100 run, as higher levels of CH_4 and CO_2 from RCP 6.5 (the more likely scenario) or RCP 8.5 will lead to a different response in atmospheric circulation, ozone concentration, as well as OH abundance, therefore a different future lifetime for both the SR and TR species.

5.5 Synthesis

The model results for the individual high priority species (Tables 5.5 and 5.6) indicate:

- **CFC-11**: Lifetime is ~23% larger than given in WMO (2011).
- **CFC-12**: The models overall show a similar lifetime to that given in WMO (2011) (5% smaller).
- **N_2O**: The models show a very similar lifetime to that given in WMO (2011).
- **CCl_4**: Modelled atmospheric lifetime is ~39% larger than that given in WMO (2011).
- **CH_3CCl_3**, **CH_4, HCFC-22**: Modelled lifetimes are similar to previous estimates and models show a large range of lifetime estimates.

Table 5.9. Steady state τ_{atmos} for 2000 and 2100 conditions from the TS2000 and TS2100 model simulations. For best-estimate lifetime for all targeted species, refer to Tables 6-1, 6-2, and 6-3 in Chapter 6.

Species	Model Mean		GSFC2D		GEOSCCM		SOCOL		ULAQ		UMUKCA		WACCM	
	2000[a,b]	2100	2000	2100	2000	2100	2000	2100	2000	2100	2000	2100	2000	2100
CFC-11	**56.5**	**55.2**	58.6	57.7	58.3	54.7	50.8	49.3	58.6	57.6	56.8	55.2	56.9	57.7
CFC-12	**95.8**	**95.3**	103.7	103.5	96.0	90.6	84.1	81.9	99.4	104.2	101.5	98.8	93.1	96.7
CFC-113	**88.5**	**87.8**	95.4	94.4	88.9	83.4	80.5	79.1	92.8	96.6	87.4	85.5	87.4	90.6
CFC-114	**189**	**193**	204	206	--	--	169	171	205	205	--	--	184	192
CFC-115	**991**	**1015**	961	981	--	--	--	--	--	--	--	--	1022	1052
CCl_4	**49.9**	**48.6**	50.7	49.9	52.2	48.7	41.4	40.2	54.3	52.9	52.0	50.4	51.3	51.8
N_2O	**117**	**118**	125	125	117	111	107	107	127	132	--	--	112	118
H1202	**1.8**	**2.0**	2.1	2.5	--	--	--	--	--	--	--	--	1.6	1.6
H1211	**11.5**	**11.9**	13.5	13.4	--	--	--	--	9.8	10.0	12.3	13.5	11.0	11.4
H1301	**73.4**	**73.1**	77.4	76.8	72.8	68.6	67.1	66.1	78.0	79.2	74.7	76.2	71.4	73.5
H2402	**14.5**	**14.8**	13.9	14.0	--	--	--	--	13.9	14.2	--	--	15.9	16.4
CH_4	**9.2**	**8.7**	9.6	9.2	11.1	10.6	7.3	8.1	8.2	7.5	--	--	8.4	8.0
CH_3CCl_3	**5.2**[c]	**4.9**	5.2	4.9	5.8	5.6	4.0	--	--	--	--	--	4.6	4.4
CH_3Cl	**1.3**	**1.3**	1.5	1.4	1.7	1.6	1.1	1.3	1.2	1.1	1.1	1.1	1.3	1.2
CH_3Br	**1.6**	**1.5**	1.7	1.6	1.9	1.9	1.3	1.5	1.4	1.3	1.4	1.3	1.5	1.4
HCFC-22	**11.0**	**10.5**	12.0	11.5	14.0	13.4	9.1	9.9	10.1	9.4	9.5	9.2	10.6	10.0
HCFC-141b	**8.3**	**7.9**	9.2	8.8	--	--	7.1	7.8	7.8	7.3	--	--	8.1	7.7
HCFC-142b	**14.5**	**13.6**	17.5	16.6	--	--	13.6	15.2	14.7	13.6	--	--	12.2	11.5
HFC-23	**242**	**229**	226	213	260	247	--	--	--	--	--	--	--	--
HFC-32	**5.5**	**5.3**	5.2	5.0	5.9	5.7	--	--	--	--	--	--	--	--
HFC-125	**31.3**	**30.1**	29.3	28.1	33.7	32.4	--	--	--	--	--	--	--	--
HFC-134a	**14.4**	**13.8**	13.6	13.0	15.4	14.8	--	--	--	--	--	--	--	--
HFC-143a	**53.2**	**50.7**	50.1	47.5	56.8	54.3	--	--	--	--	--	--	--	--
HFC-152a	**1.5**	**1.4**	1.5	1.4	1.6	--	--	--	--	--	--	--	--	--
HFC-227ea	**45.3**	**40.3**	42.4	40.3	48.6	--	--	--	--	--	--	--	--	--
HFC-245fa	**7.8**	**7.5**	7.8	7.5	--	--	--	--	--	--	--	--	--	--

[a] Model mean lifetimes for 2000 listed in this table are calculated without LMDZrepro results for a meaningful comparison with the 2100 lifetimes.
[b] The lifetime of all TR species for 2000 and 2100 conditions are calculated without SOCOL results.
[c] The CH_3CCl_3 lifetimes from ULAQ and UMUKCA in 2100 are not realistic due to very low concentrations of CH_3CCl_3 in the TS2100 run, therefore we exclude CH_3CCl_3 lifetimes from these two models in this comparison.

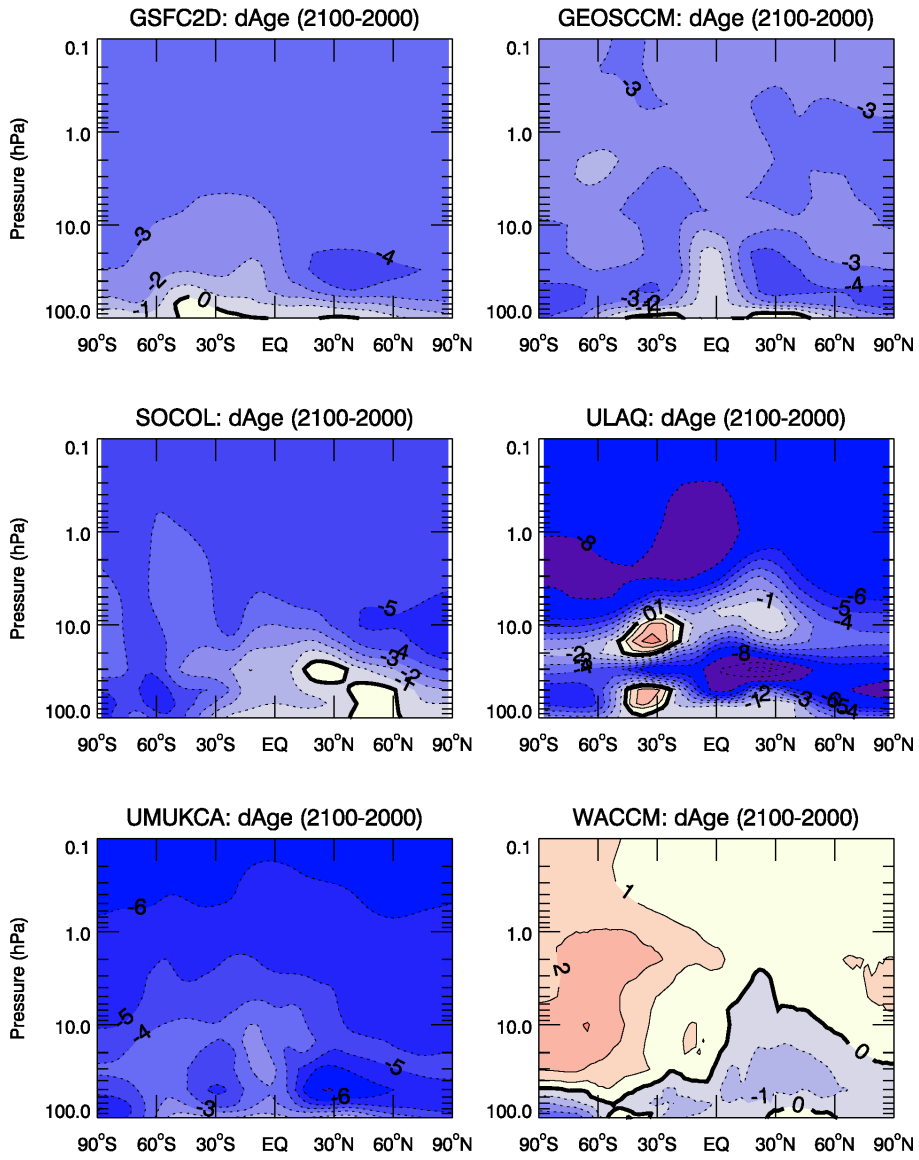

Figure 5.21. Difference in mean age-of-air (months) between CCM runs for 2100 and 2000 conditions. (Note: LMDZrepro did not perform TS2100 run and so is not included here).

Other SR species with notable results:

- **Halon-1202, Halon-1211, and Halon-2402**: Modelled lifetimes are significantly smaller (~30%) than given in WMO (2011).
- **Halon-1301**: Lifetime longer (11%) than that given in WMO (2011).

Other TR species with notable results:

- **CH_3Br**: Lifetime smaller (20%) than given in WMO (2011).
- **HCFC-141b** and **HCFC-142b**: Modelled lifetimes are shorter (13-17%) than given in WMO (2011).
- **HFC-143a**: Lifetime longer than that given in WMO (2011).
- **HFC-227ea**: Lifetime longer than that given in WMO (2011).

5.6 Summary

This chapter has analysed results from seven global models (six 3-D CCMs and a 2-D model) which were run with the same standard photochemical data. We diagnosed both instantaneous and steady-state lifetimes for species with sinks mainly in the troposphere (tropospheric removal, TR) and stratosphere (stratospheric removal, SR) for present-day and 2100 conditions. The key results are:

Quantification of Lifetimes

- The transient lifetimes of, for example, CFC-11 and CFC-12 before the 1990s are larger than steady-state lifetimes but decrease to approach the steady-state lifetime after this time. N_2O, CH_3CCl_3, and CH_4 show little differences between transient and steady-state lifetimes. The strong variations in CFC emissions over this period cause this difference.
- Flux Boundary Condition (FBC) tracers show similar lifetimes to Mixing Ratio Boundary Condition (MBC) tracers within the same model, despite significant differences in their atmospheric distributions and total burden.
- Species that are destroyed in the stratosphere show a range of model-calculated lifetimes. The lifetimes show a clear correlation with the simulated tropical mean age profile, which depends on the Brewer-Dobson circulation. In particular, the tropical ascent rate through the altitudes of large loss is critical to the calculated lifetimes with faster ascent rates produce shorter lifetimes.
- Species that are predominantly removed by OH show a large range of lifetime estimates between models. However, for many models the large range of lifetimes show a good straight-line correlation with the simple metrics of global mean tropospheric OH and CH_3CCl_3 lifetime.
- A global mean OH abundance of 1.09×10^6 molecules/cm^3 has been inferred using CH_3CCl_3 observations in the 2-D inverse model. This is likely representative of the true global mean OH because the results were confirmed by using observationally derived surface CH_3CCl_3 from the flux boundary condition tracer in the WACCM and GEOSCCM simulations as pseudo-observational constraints to derive τ_{OH} and $[OH]_{GM}$ in the inverse model (Chapter 4). This implies that the four 3-D CCMs that calculate OH interactively with full tropospheric chemistry have high-biased tropospheric OH, thus shorter TR lifetimes.
- Overall best model estimates have been calculated using the multi-model mean. Species for which the new mean modelled lifetimes show a significant increase with respect to WMO (2011) and IPCC (2007) are CFC-11, CCl_4, Halon-1301, HFC-143a, and HFC-227ea.
- Species for which the new mean modelled lifetimes show a significant decrease with respect to WMO (2011) and IPCC (2007) are Halon-1202, Halon-1211, Halon-2402, CH_3Br, HCFC-141b, and HCFC-142b.
- For 2100 some models indicate a speed-up of the Brewer-Dobson circulation and a younger age-of-air. However, for other models the circulation change is not so clear. A thicker (recovered) ozone layer in 2100 leads to reduced photolysis. These two processes lead to cancelling effects in the models and hence there is no clear trend in the lifetimes of SR tracers between 2000 and 2100. However, these impacts will depend on the future GHG scenario used.

- For a 2100 atmosphere the majority of models indicate a decrease in TR species lifetime due to the combined impact of increasing OH and increasing air temperature. Similar to the SR species, these impacts are likely to vary when a different future GHG scenario is used.

Modelling Recommendations

From a modelling point of view, recommendations for future assessments are:

- The runs presented here are the first attempts at running ODSs with flux boundary conditions (FBC) in long-term assessment simulations. Modelled distributions vary between the MBC and FBC tracers. This shows that models will diverge significantly if assessments adopt FBCs for future runs. Another complication is that full emission and sink information will be needed for all halocarbons. That information is likely not yet available so FBCs might be used for a subset of species at most.
- Scenarios which predict the future evolution of ODSs, and which are used in MBC model simulations, should be updated using new lifetimes.

5.7 Appendix A: Model Description and Updates Since CCMVal-2

SPARC CCMVal (2010) provided a comprehensive description of the CCMs used in this report. Since SPARC CCMVal (2010) the models have evolved and this section provides a brief summary of the key updates and improvements.

GEOSCCM

For this assessment, we use the GEOS CCM V2 that couples the GEOS-5 GCM version Fortuna 2-4 with an updated stratospheric chemistry module originally described by Douglass and Kawa (1999). The photochemical scheme includes all important gas-phase reactions for the stratosphere (Douglass and Kawa, 1999). The model uses a flux-form semi-Lagrangian dynamical core (Lin, 2004). Moist processes in GEOS-5 are represented using a convective parameterisation and prognostic cloud scheme. Convection is parameterised using the relaxed Arakawa Schubert (RAS) scheme developed by Moorthi and Suarez (1992). The simulations are run with spatial resolution of 2° latitude by 2.5° longitude and 72 layers extending from the surface to 0.01 hPa.

Changes since CCMVal-2 (SPARC CCMVal 2010):

- The chemical kinetics and photolysis rates were updated to the recommendations of JPL 10-6 (Sander *et al*., 2011).
- Two very-short-lived bromocarbons, CH_2Br_2 and $CHBr_3$, are added and interact with full stratospheric chemistry scheme.
- The model now uses 3-D monthly mean OH from Spivakovsky *et al.* (2000) in the troposphere instead of the original zonal mean OH archived in a previous tropospheric full chemistry Chemical Transport Model (CTM) simulation from GEOS-Chem.
- For this assessment, GEOSCCM added HFC-23, HFC-32, HFC-134a, HFC-143a, HFC-125, HFC-152a, and HFC-245fa to the chemistry scheme.

LMDZrepro

For this assessment we use a new version of the LMDZrepro CCM which couples the LMDZ-CM5 GCM version, developed for the CMIP5 exercise (Szopa *et al*., 2012; Dufresne *et al*., 2012), with an updated version of the REPROBUS chemistry module (Jourdain *et al*., 2008). The dynamical part of the LMDZ GCM is based on a finite-difference formulation of the primitive equations of meteorology on a staggered and stretchable (the Z of LMDZ standing for zoom) longitude-latitude grid. The radiation scheme is inherited from the European Centre for Medium-Range Weather Forecasts (Fouquart and Bonnel, 1980; Morcrette *et al*., 1986). The photolysis rates are calculated off-line with the Tropospheric and Ultraviolet Visible (TUV) radiative model (Madronich and Flocke, 1998). The dynamical effects of the subgrid-scale orography are parameterised according to Lott (1999). Turbulent transport in the planetary boundary layer is treated as a vertical eddy diffusion (Laval *et al*., 1981) with counter-gradient correction and dry convective adjustment. The surface boundary layer is treated according to Louis (1979). A statistical cloud scheme is used to predict the cloud properties with a different treatment for convective clouds (Bony and Emanuel, 2001) and large-scale condensation (Hourdin *et al.*, 2006). Vapour and liquid water, and atmospheric trace species are advected with a monotonic second-order finite volume scheme (Hourdin and Armengaud, 1999). Instead of using the recommended tropospheric 3-D monthly mean OH from Spivakovsky *et al*. (2000), the model calculates tropospheric OH. However, the model is forced below 400 hPa by 3-D monthly mean 1990s

climatologies of NO_x, CO and O_3 taken from a simulation by a well-established 3-D tropospheric CTM, the TOMCAT model (Savage *et al*., 2004).

Changes since CCMVal-2 (SPARC CCMVal 2010):

- The number of hybrid sigma-pressure vertical levels has been reduced from 50 in the stratospheric version of LMDZ (Lott *et al*., 2005) to 39, with 15 levels above 20 km. The top layer is about at the same altitude as the CCMVal-2 L50 version and is fine enough to resolve the propagation of the mid-latitude waves in the stratosphere and to produce sudden stratospheric warming.
- The horizontal resolution has been increased from 96 points in longitude by 72 in latitude (3.75^o x 2.5^o) to 96 points in longitude by 95 in latitude (3.75^o x 1.9^o).
- The chemical kinetics and photolysis rates were updated according to the latest recommendations in the JPL 10-6 evaluation (Sander *et al*., 2011).

SOCOL

For this assessment SOCOL v3.0 was used. In contrast to its predecessor SOCOL v2.0 described by Schraner *et al.* (2008) and evaluated in SPARC CCMVal-2 report (SPARC CCMVAL 2010), the new version exploits MA-ECHAM5 instead of MA-ECHAM4 as the underlying GCM. The advection of the chemical species is calculated by the flux-form advection scheme of Lin and Rood (1996) instead of the hybrid scheme by Zubov *et al.* (1999). From a technical point of view, the coupling between GCM and CTM has been much simplified. The chemical module has been transferred from Fortran77 to Fortran95 and completely rewritten according to the ECHAM5 infrastructure. In contrast to the previous versions, the model can be executed in parallel mode, which enables a substantial reduction of the wall clock time. ECHAM5 includes several changes in the model physics and numerics.

A new parameterization of stratiform clouds has been developed, including a separate treatment of cloud water and cloud ice, advanced cloud microphysics and a statistical model for the calculation of the cloud cover. The description of coupling processes between land surface and atmosphere has been improved, including a new data set of land surface data. Water vapour, cloud variables, and chemical species are transported by a flux-based, mass-conserving, and shape-preserving transport scheme (Lin and Rood, 1996) instead of the semi-Lagrangian approach used in ECHAM4. The shortwave radiation code is basically the same as in ECHAM4; however, the spectral resolution has been increased from 2 to 6 bands. The new longwave radiation code is based on k-correlated scheme and the number of spectral intervals has been increased to 16. The chemical scheme remains the same, but the reaction rates were updated using the latest JPL evaluation (Sander *et al.,* 2011). Preliminary analysis of the 26-year long model run results shows substantial improvement of the transport-related model quantities such as total inorganic chlorine and methane over the southern high latitudes in October and tropical water vapour tape recorder speed.

ULAQ

For this report the ULAQ model was updated in the following ways:

- Vertical resolution: 126 log-pressure levels from the surface (1000 hPa) to 0.04 hPa, with an approximate pressure altitude increment of 568 m.
- Horizontal resolution: T21 (5.6^o x 5.6^o).

- Species cross sections were updated using JPL 10-6 (Sander *et al.*, 2011) recommendations. Schumann-Runge bands are treated following the parameterisation of Minschwaner *et al.* (1993) based on (fixed-T) ODF formulation. As an alternative, the ULAQ-CCM can also use the SRB parameterisation of Allen and Frederick (1982). Diurnal averages are calculated with a 5-point Gaussian quadrature.
- Photolysis and solar heating rates are calculated with a new radiative transfer module, covering wavelengths from Lyman-alpha up to the solar NIR. Solar heating rates are calculated for O_3, O_2, NO_2, SO_2, H_2O, CO_2, aerosols. Radiative transfer is treated with a two-stream delta-Eddington approximation model (Toon *et al.,* 1989). Sphericity is included by means of Chapman functions (Dahlback and Stamnes, 1991). Refraction is treated with an iterative ray-tracing technique (Gallery *et al.,* 1983) in a simple exponential refraction model. Rayleigh-scattering cross sections are calculated with the WMO-1985 approximation. Aerosol and cirrus cloud extinction values are passed daily from the ULAQ-CCM aerosol module to the radiative module, with appropriate values of Q-ext, g, and single scattering albedo, given the calculated size distribution of the particles. Warm clouds are not included. Surface albedo is taken from MERRA 2-D hourly averaged data (http://gdata1.sci.gsfc.nasa.gov). Sun-earth distance is calculated daily as a function of orbit eccentricity. Solar cycle is included. Top-of-atmosphere solar fluxes are taken from the CCMVal web page and are carefully integrated on the wavelength bins used in the ULAQ model.
- Upper tropospheric cirrus ice particle formation is included via homogeneous and heterogeneous freezing (Kärcher and Lohmann, 2002).

UMUKCA

The current model is a further development of the version described in Morgenstern *et al.* (2009). Both the Unified Model (UM) climate model and the UKCA stratospheric chemistry module have been updated. The current version of the climate model is 7.3 as compared to 6.1 for CCMVal-2 (SPARC CCMVal 2010). It runs at a horizontal resolution of 3.75^o x 2.5^o (Arakawa C grid) with 60 levels in the vertical (hybrid geometric height coordinate), ranging from the surface up to approximately 84 km. The model solves the three-dimensional equations of motion, with vertical velocity being a prognostic quantity. Consequently monthly mean diagnostics on pressure levels are processed from the monthly mean pressure and the monthly mean of a quantity on model levels. Many physical parameterisations (including convection) have been changed between 6.1 and 7.3. For more details see Hewitt *et al.* (2011), which describes the HadGEM3 modelling framework from which the atmospheric model used in this intercomparison is derived.

The chemistry has been extended to meet the requirements of the lifetime assessment, including rate updates following JPL 10-6 recommendations. The stratospheric chemistry used in CCMVal-2 distinguished between two chlorine (CFC-11 and CFC-12) and one bromine (CH_3Br) source gas. Contributions from other species were 'lumped' into these three gases. The current version considers explicitly seven chlorine (CCl_4, CFC-11, CFC-12, CFC-113, HCFC-22, CH_3CCl_3, CH_3Cl) and five bromine (H-1211, H-1301, CH_3Br, CH_2Br_2, $CHBr_3$) source gases. Photolysis for all species is now calculated using Fast-Jx (Neu *et al.*, 2007; Telford *et al.*, 2013). The radiative transfer calculations in the climate model use the trace gas distributions determined by the interactions of transport and chemistry.

WACCM

The Whole-Atmosphere Community Climate Model, Version 4 (WACCM4) is a comprehensive numerical model, spanning the range of altitude from the Earth's surface to the lower thermosphere (Garcia *et al.,* 2007). WACCM4 is a fully interactive model, wherein the radiatively active gases (CO_2, H_2O, N_2O, CH_4, CFCs, HCFCs, halons, NO, O_3) affect heating and cooling rates and therefore dynamics. WACCM4 is based on the software framework of the National Center for Atmospheric Research's Community Atmospheric Model, version 4 (CAM4), which is contained in the Community Earth System Model (CESM) version 1.0.3.

Changes since CCMVal-2 (SPARC CCMVal 2010):

- The gas-phase chemical reaction and photolysis rates were updated to the recommendations of JPL 10-6 (Sander *et al*., 2011).
- The chemical mechanism has been expanded to include a detailed representation of tropospheric chemistry (Emmons *et al.,* 2010). The WACCM version used in CCMVal-2 had 59 species and 234 chemical reactions. The mechanism used in this report contains 144 species and 443 chemical reactions.
- Time-dependent surface emissions for CO, NO, and non-methane hydrocarbons were taken from the IPCC ACCMIP emission inventory (Lamarque *et al*., 2011).
- In CCMVal-2 the WACCM mechanism included 10 organic halogens: CH_3Cl, CFC-11, CFC-12, CFC-113, HCFC-22, CCl_4, CH_3CCl_3, H-1211, H-1301, and CH_3Br. For this report an additional eight organic halogens were added: CFC-114, CFC-115, HCFC-141b, HCFC-142b, CH_2Br_2, $CHBr_3$, Halon-1202, and Halon-2402.

GSFC2D

The NASA/Goddard Space Flight Center (GSFC) two-dimensional (2-D) model was originally developed in the 1980s for studies pertaining to the chemistry of the middle atmosphere and has been used in stratospheric assessments since 1989. The specified transport version of the model, in which the transport and temperature fields are derived offline from meteorological data, was originally described in Douglass *et al*. (1989) and Jackman *et al*. (1990) with subsequent updates discussed in Considine *et al*. (1994); Jackman *et al*. (1996); and Fleming *et al*. (1999, 2007). The model now uses the year-to-year transport and temperature fields for 1979-2010 derived from the MERRA meteorological analyses. The coupled version of the model, in which the chemistry, radiation, and dynamics are computed interactively, was originally discussed in Bacmeister *et al*. (1995) and Rosenfield *et al*. (1997). This version of the model has recently undergone significant improvements (Fleming *et al*., 2011) and simulates long term (1960-2100) changes in stratospheric ozone, temperature, and age-of-air that are in good agreement with the GEOSCCM. Both versions of the model are used in this assessment.

Both the specified transport and coupled versions of the model use the same chemistry solver and kinetic and photochemical calculations. While neither model version was included in CCMVal-2 (SPARC CCMVal, 2010), several of the model components are very similar to those used in the GEOSCCM which was evaluated in CCMVal-2. These components include: the infrared (IR) radiative transfer scheme (Chou et al., 2001); the photolytic calculations (Anderson and Lloyd, 1990; Jackman *et al*., 1996); and the microphysical model for polar stratospheric cloud (PSC) formation (Considine *et al*., 1994). The chemistry solver includes all gas-phase reactions important for the stratosphere and computes a full diurnal

cycle for 35 fast chemical constituents. This scheme was shown to be in good agreement with photochemical steady state box model calculations (Park *et al*., 1999). The latest JPL 10-6 recommendations are used for the photolytic cross sections and reaction rate constants (Sander *et al*., 2011). The model domain extends from the ground to approximately 92 km, with a grid resolution of 4° latitude by 1 km altitude.

5.8 Appendix B: Description of Model Simulations

TRANS is a 50-year transient run from 1960 to 2010, based on the definition of the REF-B1 simulation used in CCMVal-2 (SPARC CCMVal, 2010, Chapter 2). All forcings in this simulation are taken from observations, and are mostly identical to those used by Eyring *et al.* (2006) and Morgenstern *et al.* (2010) for REF-B1. This transient simulation includes all anthropogenic and natural forcings based on changes in trace gases, solar variability, volcanic eruptions, QBO, and SSTs/SICs.

- **GHGs** (N_2O, CH_4, and CO_2) Coupled Model Intercomparison Project (CMIP) RCP 4.5 Scenario.
- **ODS** (CFC-11, CFC-12, CFC-113, CFC- 114, CFC-115, CH_3CCl_3, HCFC-22, HCFC-141b, HCFC-142b, Halon-1211, Halon-1202, Halon-1301, and Halon-2402) are prescribed at the surface according to Table 5A-3 (baseline A1 scenario) of WMO (2011).
- **HFCs** (HFC-23, HFC-32, HFC-125, HFC-134a, HFC-143a, HFC-152a, HFC-245fa), except HFC-23, are from high scenario A1 of Velders *et al.* (2009) merged with AGAGE measurements in 2010. HFC-23 between 1978 and 2009 is from the annual global mean in Table 3 of Miller *et al.* (2010).
- **SST and SICs** are prescribed as monthly mean boundary conditions following the observed global SIC and SST data set HadISST1 (Rayner *et al.,* 2003).
- **Solar variability**. Daily spectrally resolved solar irradiance data from 1 January 1950 to 31 Dec 2006 (in $W/m^2/nm$) are provided at http://www.geo.fu-berlin.de/en/met/ag/strat/research/SOLARIS/Input_data/index.html. The data are derived with the method described by Lean *et al.* (2005). Each modelling group was required to integrate the data over the individual wavelength intervals used in their radiation and photolysis schemes.
- **The QBO**: Models that do not produce an internally generated QBO were asked externally impose a QBO.
- **Aerosol Surface Area Densities (SADs)** from observations are considered in TRANS (Eyring *et al.,* 2010, Morgenstern *et al.,* 2010).
- **Emission of ozone and aerosol precursors** (CO, NMVOC, NO_x and SO_2) are from Representative Concentration Pathways (RCP) Scenario 4.5 (Lamarque *et al*., 2011).
- **Tropospheric OH:** Models that do not include a detailed tropospheric chemistry scheme were asked to use to prescribe their tropospheric OH values to the 3-D monthly OH documented in Spivakovsky *et al.* (2000).

TS2000 is a 30-year timeslice simulation for 2000 conditions, designed to diagnose steady-state lifetimes and to facilitate the comparison of model output against constituent observations from various measurement datasets.

- **GHGs, ODSs, and HFCs:** The surface concentrations of GHGs are based on CMIP RCP4.5 Scenario while the surface halogens are based on Table 5A-3 of WMO (2010) for the year 2000. The surface concentrations of HFCs are from the A1 scenario of Velders *et al.* (2009) for the year 2000. All ODSs, GHGs and HFCs repeat every year.
- **Emission of ozone and aerosol precursors** (CO, NMVOC, NO_x and SO_2) are from the RCP4.5 Scenario and are repeating annually.
- **Tropospheric OH:** Models that do not include a detailed tropospheric chemistry scheme are asked to use OH fields of Spivakovsky *et al.* (2000) in the troposphere.

TS2100 is a 30-year timeslice simulation for 2100 conditions, designed to diagnose steady-state lifetimes in a future climate with recovered stratospheric ozone layer and a faster Brewer-Dobson circulation.

- **GHGs, ODSs, and HFCs:** The surface concentrations of GHGs and ODSs are based on projections of the CMIP RCP4.5 Scenario and Table 5A-3 of WMO (2011) for the year 2100, respectively. There are no projections available for HFCs in 2100 and no recommendation was made for this experiment.
- **Ozone and aerosol precursors, and tropospheric OH:** OH in the troposphere is controlled by a delicate balance between its sources and sinks and responds to changes in tropospheric concentrations of CO, CH_4, H_2O, O_3, NO_x, as well as overhead O_3 column. In this assessment, we only seek to address how OH responds to climate changes, i.e., changes in O_3 column, H_2O and CH_4, under 2100 conditions. Therefore, models that calculate realistic tropospheric OH were asked to use the same precursors emissions as run TS2000. Models which do not include a detailed tropospheric chemistry scheme were asked to use OH fields of Spivakovsky *et al.* (2000) in the troposphere.

FBC tracer emissions

- **Annual global emission**: The surface emissions used in TRANS are time-dependent annual bottom up emissions computed using time series of data on production and sales into various end-use categories having different release functions (McCulloch *et al.,* 2001, 2002).
- **Emission distribution:** The geographical resolved distribution is based on the distribution of 1986 for CFC-11 and CFC-12, 1990 for HCFC-22 and CH_3CCl_3 for 1950-1995. From 1995 to 2010, the distribution is calculated using the geographical resolved fractionation of 2000 for CFC-11 and CFC-12. The calculated global emissions were distributed among countries using the distribution of individual national fractions of the world total Gross Domestic Product **(**McCulloch *et al.,* 2001, 2002**)**. Within each country, emissions were distributed to individual grid squares using a population distribution (McCulloch *et al.,* 2001, 2002; AFEAS, 2001).
- **Surface emission for TS2000:** Surface emissions of year 2000 are used repeatedly for the entire 30-year simulation. Due to the difference in source vs. sink balance for each species, individual FBC tracers evolve differently, with CFC-11_FBC and CH_3CCl_3_FBC behaving as trace gases with an increasing trend and CFC-12_FBC and HCFC-22_FBC behaving as time-decaying tracers.
- **Surface emission for TS2100:** All emissions of the above four species become zero (or have a very small value) in 2100. Models used zero emissions for all four FBC tracers repeatedly for the entire simulation.

5.9 Appendix C

Table 5.A1. Comparison of model steady-state lifetime (τ_{ss}) from the TS2000 simulation with the transient lifetime ($\tau_{transient}$) for MBC high priority species and their FBC and CONST tracers in year 2000 from the transient simulation. Note part of the differences in the lifetimes between the FBC and MBC tracers are due to the unaccounted topography impact on the FBC tracers as discussed in Box 5.1.

Species		GSFC2D	GEOSCCM	LMDZ -repro	SOCOL	ULAQ	UMUKCA	WACCM
CFC-11	τ_{SS}	58.6	58.3	49.1	50.2	58.6	56.8	56.9
	$\tau_{transient, MBC}$	56.6	60.0	47.0	49.5	58.2	56.3	55.1
	$\tau_{transient, FBC}$	60.0	58.7	--	--	60.6	61.4	55.2
	$\tau_{transient, CONST}$	--	60.4	--	--	--	--	57.1
CFC-12	τ_{SS}	103.7	96.0	88.2	84.1	99.4	101.5	93.1
	$\tau_{transient, MBC}$	102.1	98.5	85.0	80.5	101.4	99.9	93.3
	$\tau_{transient, FBC}$	99.1	96.1	--	--	105.0	109.7	93.0
	$\tau_{transient, CONST}$	--	97.5	--	--	--	--	92.1
CCl_4	τ_{SS}	50.7	52.2	42.0	41.4	54.3	52.0	51.3
	$\tau_{transient, MBC}$	49.2	53.5	40.0	41.0	53.8	51.2	50.1
N_2O	τ_{SS}	125	117	105	107	127	--	112
	$\tau_{transient, MBC}$	124	120	--	105	130	--	113
	$\tau_{transient, CONST}$	--	119	--	--	--	--	112
CH_3CCl_3	τ_{SS}	5.2	5.8	--	4.0	4.1	4.3	4.6
	$\tau_{transient, MBC}$	5.2	5.8	--	3.7	4.5	4.5	4.6
	$\tau_{transient, FBC}$	5.2	5.8	--	--	4.5	4.5	4.6
	$\tau_{transient, CONST}$	--	--	--	--	--	4.5	4.5
CH_4	τ_{SS}	9.6	11.1	--	7.3	8.2	--	8.4
	$\tau_{transient, MBC}$	10.0	11.2	--	6.9	8.5	--	8.4
	$\tau_{transient, CONST}$	--	10.9	--	--	--	--	8.5
HCFC-22	τ_{SS}	12.0	14.0	--	9.1	10.1	9.5	10.6
	$\tau_{transient, MBC}$	12.4	13.9	--	8.5	10.3	9.9	10.1
	$\tau_{transient, FBC}$	12.4	14.0	--	--	11.7	9.8	10.3

5.10 Appendix D: Additional Figures

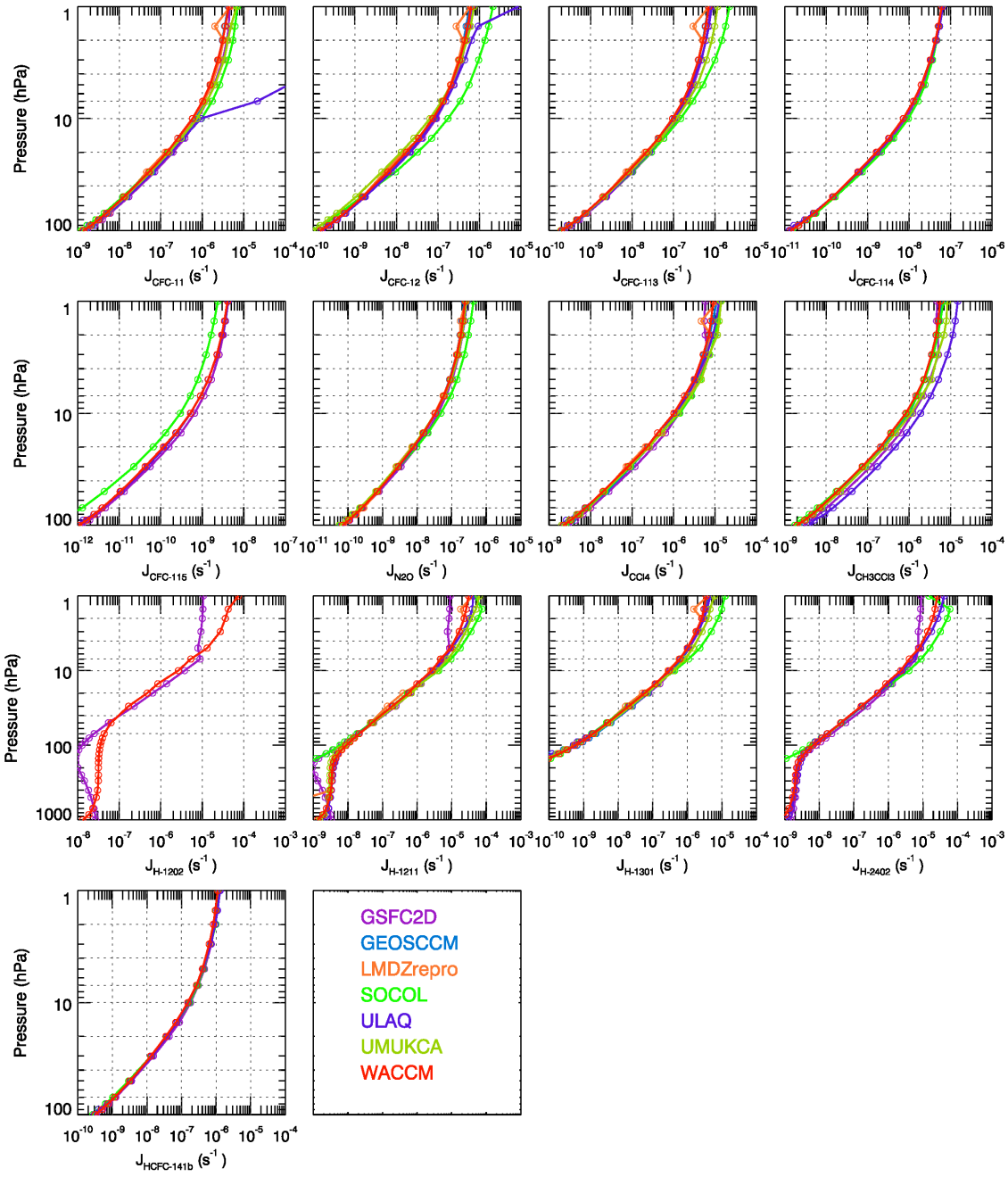

Figure 5.A1. Comparison of modelled 30-year mean J_{ODS} rates from the TS2000 simulation averaged between 30°S-30°N.

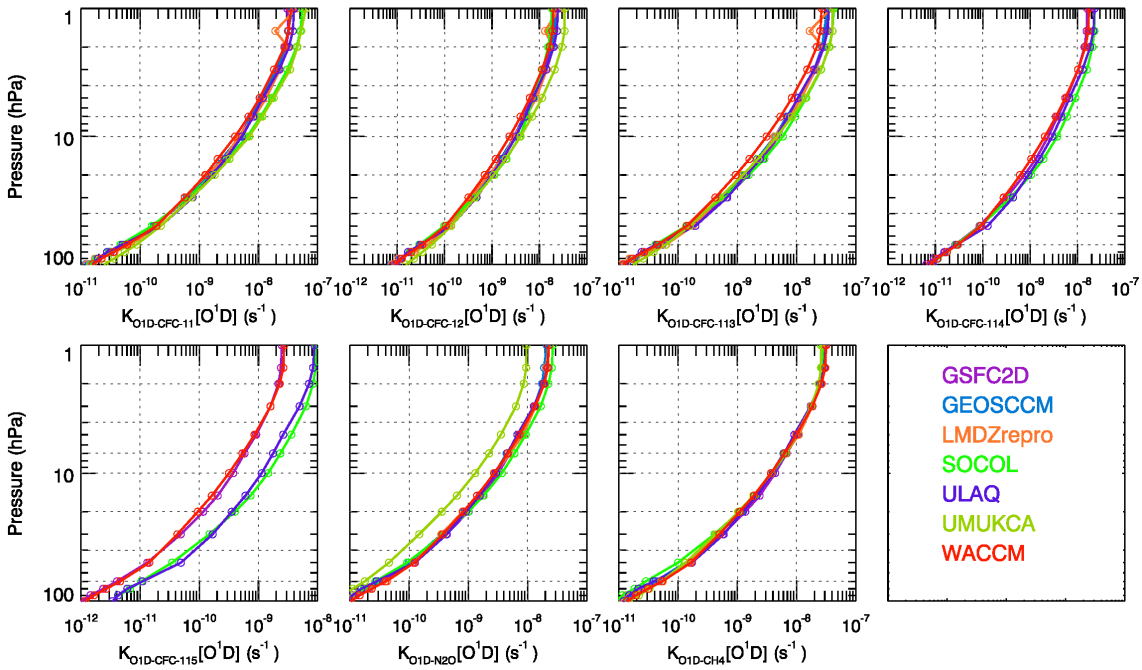

Figure 5.A2. Comparison of modelled 30-year mean $k_{O1D\text{-}ODS}[O^1D]$ rates from the TS2000 simulation averaged between 30°S-30°N.

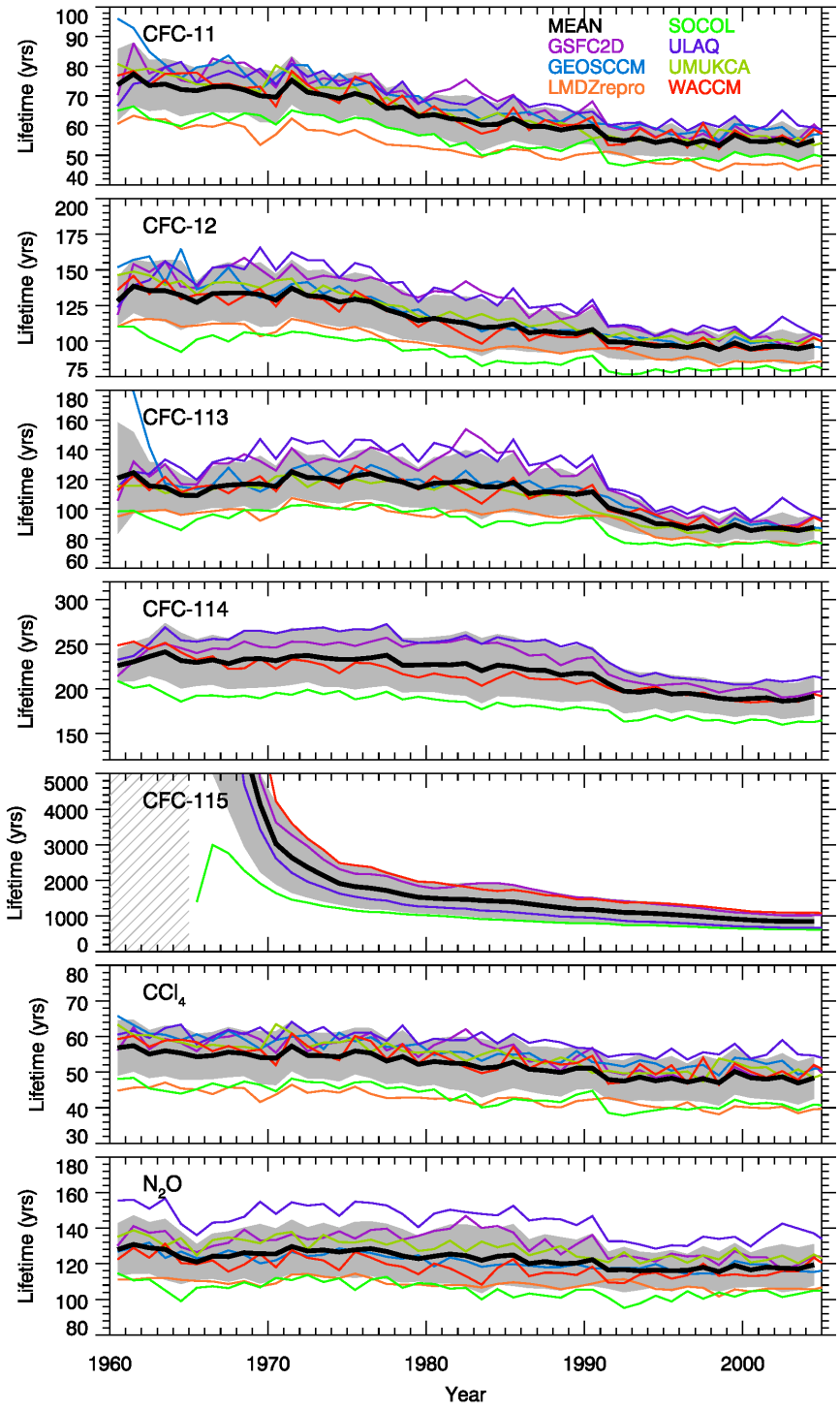

Figure 5.A3. Time evolution of modelled atmospheric partial lifetimes, τ_{atmos}, (yrs) of SR species between 1960 and 2006 from the TRANS simulations. Model mean lifetimes (thick black lines) and 1-σ variance (gray shadings) are also shown. The gray hatching area indicates where atmospheric concentrations of the corresponding ODS are close-to-zero.

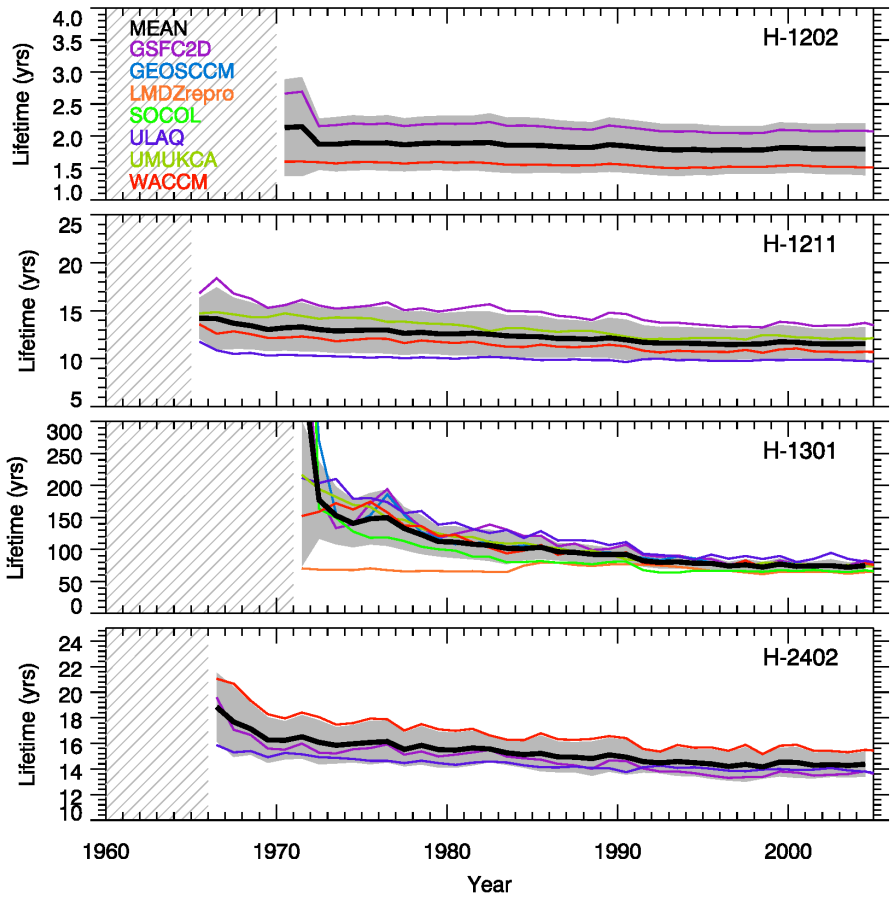

Figure 5.A4. As Figure 5.A3, but for modelled Halon lifetimes.

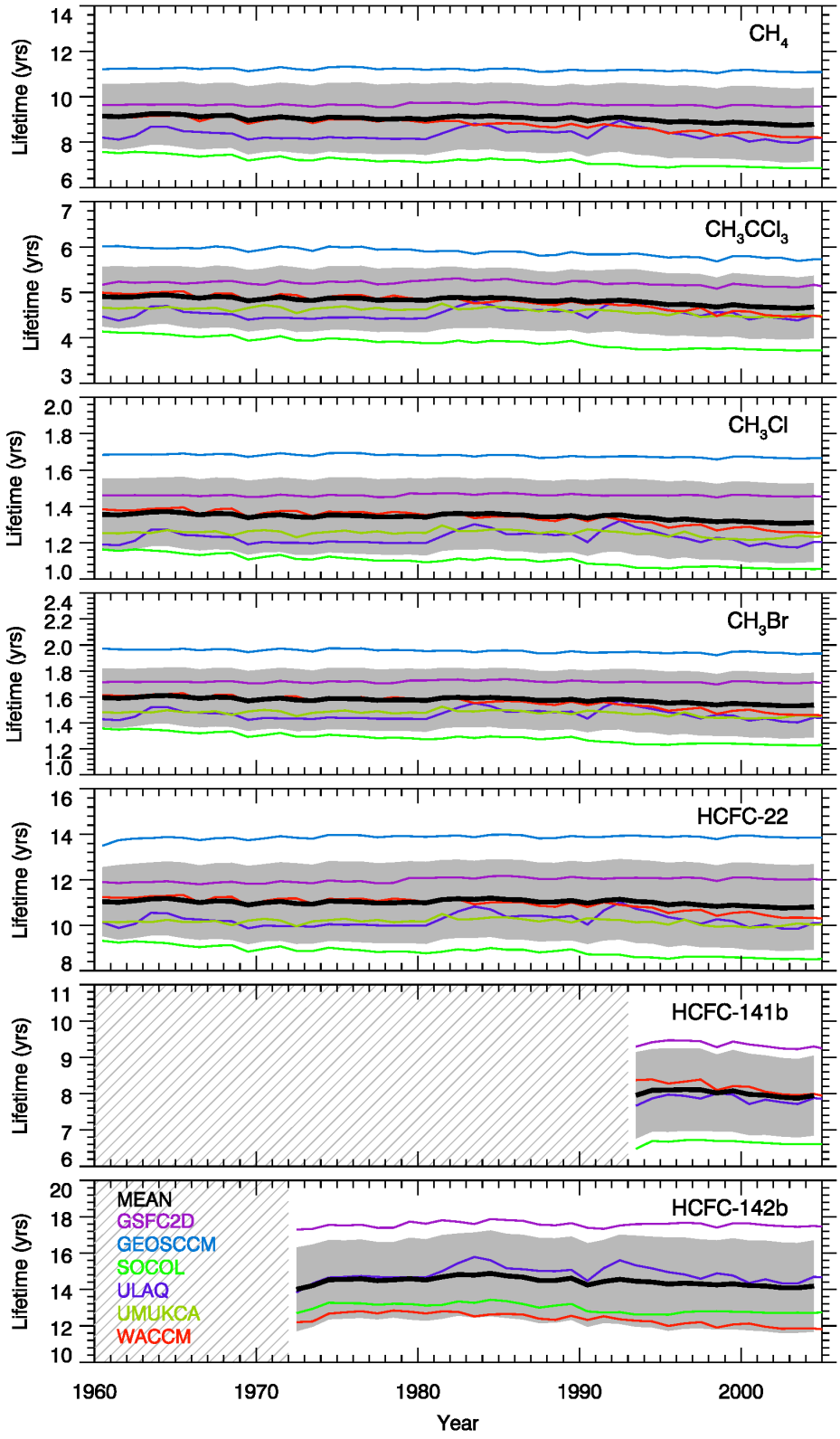

Figure 5.A5. As Figure 5.A3, but for modelled lifetimes of TR species.

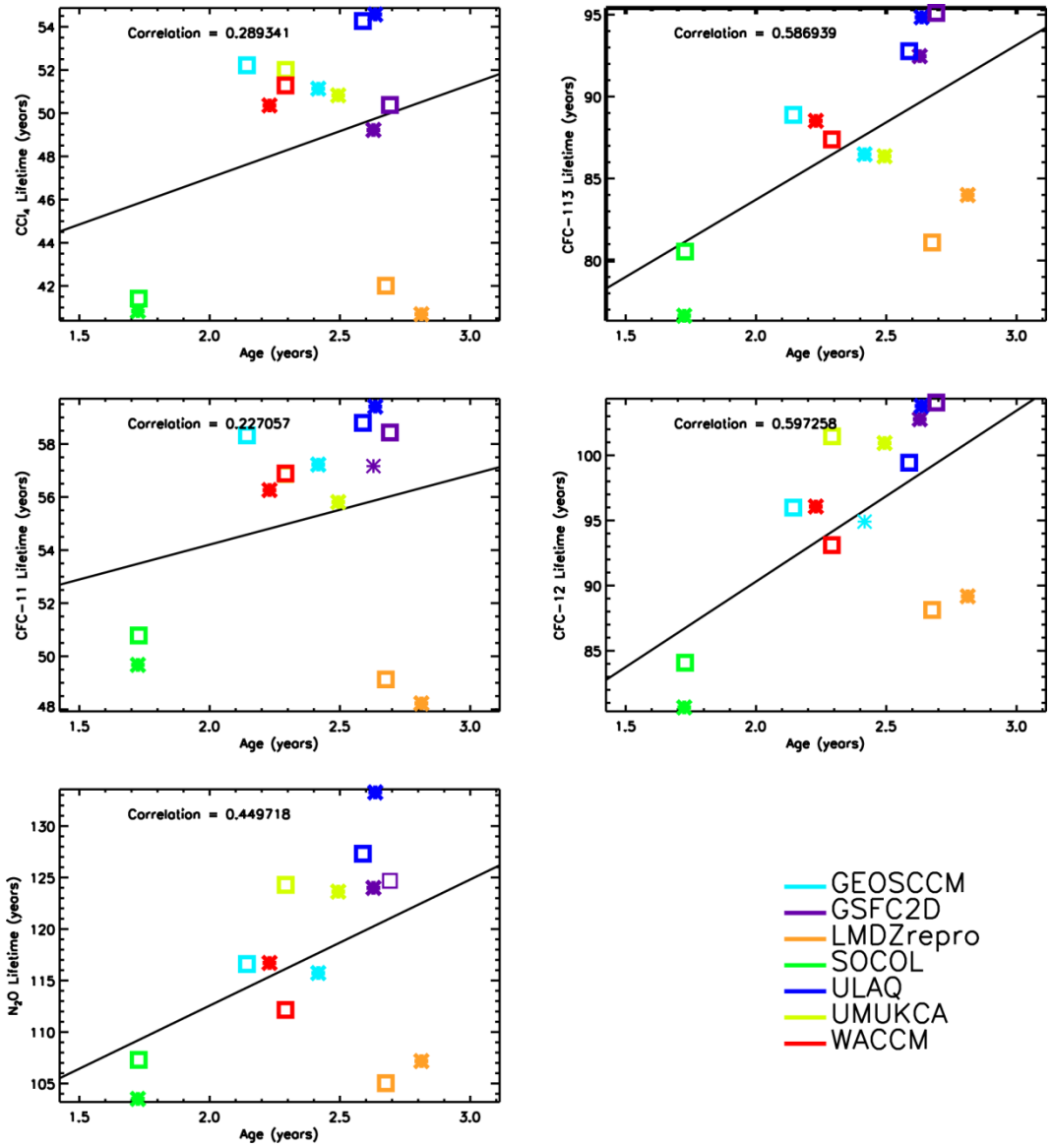

Figure 5.A6. As Figure 5.17, but with results for LMDZrepro.

5.11 References

AFEAS (Alternative Fluorocarbons Environmental Acceptability Study), *Production, Sales and Atmospheric Releases of Fluorocarbons through 2000*, Arlington, VA, USA, 2001.

Allen, M., and J. E. Frederick, Effective photodissociation cross sections for molecular oxygen and nitric oxide in the Schumann-Runge bands, *J. Atmos. Sci.*, *39,* 2066-2075, 1982.

Anderson Jr., D. E., and S. A. Lloyd, Polar twilight UV-visible radiation field: Perturbations due to multiple scattering, ozone depletion, stratospheric clouds, and surface albedo, *J. Geophys. Res*., 95, 7429-7434, 1990.

Bacmeister, J. T., M. R. Schoeberl, M. E. Summers, J. E. Rosenfield, and X. Zhu, Descent of long-lived trace gases in the winter polar vortex, *J. Geophys. Res., 100,* 11669-11684, 1995.

Bony, S., and K. A. Emanuel, A parameterization of the cloudiness associated with cumulus convection; evaluation using TOGA COARE data, *J. Atmos. Sci*., *58*, 3158-3183, 2001.

Bousquet, P., D. A. Hauglustaine, P. Peylin, C. Carouge, and P. Ciais, Two decades of OH variability as inferred by an inversion of atmospheric transport and chemistry of methyl chloroform, *Atmos. Chem. Phys*., *5*, 2635-2656, 2005.

Butchart, N., A. J. Chariton-Perez, I. Cionni, S. C. Hardiman, P. H. Haynes, K. Krüger, P. J. Kushner, P. A. Newman, S. M. Osprey, J. Perlwitz, M. Sigmond, L. Wang, H. Akiyoshi, J. Austin, S. Bekki, A. Baumgaertner, P. Braesicke, C. Brühl, M. Chipperfield, M. Dameris, S. Dhomse, V. Eyring, R. Garcia, H. Garny, P. Jöckel, J.-F. Lamarque, M. Marchand, M. Michou, O. Morgenstern, T. Nakamura, S. Pawson, D. Plummer, J. Pyle, E. Rozanov, J. Scinocca, T. G. Shepherd, K. Shibata, D. Smale, H. Teyssèdre. W. Tian, D. Waugh, and Y. Yamashita, Multimodel climate and variability of the stratosphere, *J. Geophys. Res., 116*, D05102, doi: 10.1029/2010JD014995, 2011.

Chou, M.-D., M. J. Suarez, X.-Z. Liang, and M.-H. Yan, *A thermal infrared radiation parameterization for atmospheric studies,* NASA Tech. Memo, NASA/TM-2001-104606, 9, 56 pp., Greenbelt, MD, USA, 2001.

Considine, D. B., A. R. Douglass, and C. H. Jackman, Effects of a polar stratospheric cloud parameterization on ozone depletion due to stratospheric aircraft in a two-dimensional model, *J. Geophys. Res., 99*, 18879-18894, 1994.

Crutzen, P., and P. H. Zimmermann, The changing photochemistry of the troposphere, *Tellus*, *43* AB, 136-151, 1991.

Dahlback, A., and K. Stamnes, A new spherical model for computing the radiation field available for photolysis and heating at twilight, *Planet. Space Sci.*, *39,* 671-683, 1991.

Douglass, A. R., and S. R. Kawa, Contrast between 1992 and 1997 high-latitude spring Halogen Occultation Experiment observations of lower stratospheric HCl, *J. Geophys. Res., 104* (D15), 18739-18754, doi: 10.1029/1999JD900281, 1999.

Douglass, A. R., C. H. Jackman, and R. S. Stolarski, Comparison of model results transporting the odd nitrogen family with results transporting separate odd nitrogen species, *J. Geophys. Res., 94*, 9862-9872, 1989.

Douglass, A. R., R. S. Stolarski, M. R. Schoeberl, C. H. Jackman, M. L. Gupta, P. A. Newman, J. E. Nielsen, and E. L. Fleming, Relationship of loss, mean age of air and the distribution of CFCs to stratospheric circulation and implications for atmospheric lifetimes*, J. Geophys. Res., 113*, D14309, doi: 10.1029/2007JD009575, 2008.

Dufresne, J.-L., M.-A. Foujols, S. Denvil, A. Caubel, O. Marti, O. Aumont, Y. Balkanski, S. Bekki, H. Bellenger, R. Benshila, S. Bony, L. Bopp, P. Braconnot, P. Brockmann, P. Cadule, F. Cheruy, F. Codron, A. Cozic, D. Cugnet, N. de Noblet, J.-P. Duvel, C. Ethé, L. Fairhead, T. Fichefet, S. Flavoni, P. Friedlingstein, J.-Y. Grandpeix, L. Guez, E. Guilyardi, D. Hauglustaine, F. Hourdin, A. Idelkadi, J. Ghattas, S. Joussaume, M. Kageyama, G. Krinner, S. Labetoulle, A. Lahellec, M.-P. Lefebvre, F. Lefevre, C. Levy, Z. X. Li, J. Lloyd, F. Lott, G. Madec, M. Mancip, M. Marchand, S. Masson, Y. Meurdesoif, J. Mignot, I. Musat, S. Parouty, J. Polcher, C. Rio, M. Schulz, D. Swingedouw, S. Szopa, C. Talandier, P. Terray, N. Viovy, and N. Vuichard, Climate change projections using the IPSL-CM5 Earth System Model: From CMIP3 to CMIP5, *Clim. Dynam., 40,* 2123-2165, doi: 10.1007/s00382-012-1636-1, 2013.

Egorova, T., E. Rozanov, V. Zubov, E. Manzini, W. Schmutz, and T. Peter, Chemistry-climate model SOCOL: A validation of the present-day climatology, *Atmos. Chem. Phys.*, *5*, 1557-1576, doi: 10.5194/acp-5-1557-2005, 2005.

Emmons, L. K., S. Walters, P. G. Hess, J.-F. Lamarque, G. G. Pfister, D. Fillmore, C. Granier, A. Guenther, D. Kinnison, T. Laepple, J. Orlando, X. Tie, G. Tyndall, C. Wiedinmyer, S. L. Baughcum, and S. Kloster, Description and evaluation of the Model for Ozone and Related chemical Tracers, version 4 (MOZART-4), *Geosci. Model Dev.*, *3*, 43-67, 2010.

Eyring, V., N. R. P. Harris, M. Rex, T. G. Shepherd, D. W. Fahey, G. T. Amanatidis, J. Austin, M. P. Chipperfield, M. Dameris, P. M. De F. Forster, A. Gettelman, H. F. Graf, T. Nagashima, P.A. Newman, S. Pawson, M. J. Prather, J. A. Pyle, R. J. Salawitch, B. D. Santer, and D. W. Waugh, A strategy for process-orientated validation of coupled chemistry-climate models, *Bull. Am. Meteorol. Soc.*, *86*, 1117-1133, 2005.

Eyring, V., N. Butchart, D. W. Waugh, H. Akiyoshi, J. Austin, S. Bekki, G. E. Bodeker, B. A. Boville, C. Brühl, M. P. Chipperfield, E. Cordero, M. Dameris, M. Deushi, V. E. Fioletov, S. M. Frith, R. R. Garcia, A. Gettelman, M. A. Giorgetta, V. Grewe, L. Jourdain, D. E. Kinnison, E. Mancini, E. Manzini, M. Marchand, D. R. Marsh, T. Nagashima, P. A. Newman, J. E. Nielsen, S. Pawson, G. Pitari, D. A. Plummer, E. Rozanov, M. Schraner, T. G. Shepherd, K. Shibata, R. S. Stolarski, H. Struthers, W. Tian, and M. Yoshiki, Assessment of temperature, trace species, and ozone in chemistry-climate model simulations of the recent past, *J. Geophys. Res.*, *111*, D22308, doi: 10.1029/2006JD007327, 2006.

Eyring, V., I. Cionni, G. E. Bodeker, A. J. Charlton-Perez, D. E. Kinnison, J. F. Scinocca, D. W. Waugh, H. Akiyoshi, S. Bekki, M. P. Chipperfield, M. Dameris, S. Dhomse, S. M. Frith, H. Garny, A. Gettelman, A. Kubin, U. Langematz, E. Mancini, M. Marchand, T. Nakamura, L. D. Oman, S. Pawson, G. Pitari, D. A. Plummer, E. Rozanov, T. G. Shepherd, K. Shibata, W. Tian, P. Braesicke, S. C. Hardiman, J. F. Lamarque, O. Morgenstern, D. Smale, J. A. Pyle, and Y. Yamashita, Multi-model assessment of stratospheric ozone return dates and ozone recovery in CCMVal-2 models, *Atmos. Chem. Phys.*, *10*, 9451-9472, doi: 10.5194/acp-10-9451-2010, 2010.

Fleming, E. L., C. H. Jackman, D. B. Considine, and R. S. Stolarski, Simulation of stratospheric tracers using an improved empirically based two-dimensional model transport formulation, *J. Geophys. Res., 104*, 23911-23934, 1999.

Fleming, E. L., C. H. Jackman, D. K. Weisenstein, and M. K. W. Ko, The impact of inter-annual variability on multidecadal total ozone simulations, *J. Geophys. Res., 112*, D10310, doi: 10.1029/2006JD007953, 2007.

Fleming, E. L., C. H. Jackman, R. S. Stolarski, and A. R. Douglass, A model study of the impact of source gas changes on the stratosphere for 1850-2100, *Atmos. Chem. Phys.*, *11*, 8515-8541, doi: 10.5194/acp-11-8515-2011, 2011.

Fouquart, Y., and B. Bonnel, Computations of solar heating of the Earth's atmosphere: A new parameterization, *Contrib. Atmos. Phys*., *53*, 35-62, 1980.

Gallery, W. O., F. X. Kneizys, and S. A. Clough, Air Mass Computer Program for Atmospheric Transmittance/Radiance Calculations: FSCATM, AFGL-TR-83-0065, 1983.

Garcia, R. R., D. Marsh, D. E. Kinnison, B. Boville, and F. Sassi, Simulations of secular trends in the middle atmosphere, 1950-2003, *J. Geophys. Res.*, *112*, D09301, doi: 10.1029/2006JD007485, 2007.

Hall, T., D. Waugh, K. Boering, and R. Plumb, Evaluation of transport in stratospheric models, *J. Geophys. Res*., *104*, 18815-18839, 1999.

Hewitt, H. T., D. Copsey, I. D. Culverwell, C. M. Harris, R. S. R. Hill, A. B. Keen, A. J. McLaren, and E. C. Hunke, Design and implementation of the infrastructure of HadGEM3: The next-generation Met Office climate modelling system, *Geosci. Model Dev.*, *4*, 223-253, doi: 10.5194/gmd-4-223-2011, 2011.

Hourdin, F., and A. Armengaud, The use of finite-volume methods for atmospheric advection trace species: 1. Tests of various formulations in a general circulation model, *Mon. Weather Rev*., *127*, 822-837, 1999.

Hourdin, F., I. Musat, S. Bony, P. Braconnot, F. Cordron, J. Dufresne, L. Fairhead, M.-A. Filiberti, P. Friedlingstein, J.-Y. Grandpeix, G. Krinner, and P. Levan, The LMDZ4 general circulation model: Climate performance sensitivity to parameterized physics with emphasis on tropical convection, *Clim. Dynam., 27* (7-8), 787-813, doi: 10.1007/s00382-006-0158-0, 2006.

IPCC, *Climate Change 2007: The Physical Science Basis. Contribution of Working Group I to the Fourth Assessment Report of the Intergovernmental Panel on Climate Change* (S. Solomon, D. Qin, M. Manning, Z. Chen, M. Marquis, K. B. Averyt, M. Tignor, and H. L. Miller (eds.), Cambridge University Press, Cambridge, United Kingdom, and New York, NY, USA, 996 pp., 2007.

Jackman, C. H., A. R. Douglass, R. B. Rood, R. D. McPeters, and P. E. Meade, Effect of solar proton events on the middle atmosphere during the past two solar cycles as computed using a two-dimensional model, *J. Geophys. Res.*, *95*, 7417-7428, 1990.

Jackman, C. H., E. L. Fleming, S. Chandra, D. B. Considine, and J. E. Rosenfield, Past, present, and future modeled ozone trends with comparisons to observed trends, *J. Geophys. Res., 101*, 28753-28767, 1996.

Jourdain, L., S. Bekki, F. Lott, and F. Lefevre, The coupled chemistry-climate model LMDz-REPROBUS: description and evaluation of a transient simulation of the period 1980-1999, *Ann. Geophys., 26*, 1391-1413, 2008.

Kärcher, B., and U. Lohmann, A parameterization of cirrus cloud formation: homogeneous freezing including effects of aerosol size, *J. Geophys. Res.*, *107*, 4698, doi: 10.1029/2001JD001429, 2002.

Krol, M. C., J. Lelieveld, D. E. Oram, G. A. Sturrock, S. A. Penkett, C. A. M. Brenninkmeijer, V. Gros, J. Williams, and H. A. Scheeren, Continuing emissions of methyl chloroform from Europe, *Nature*, 421 (6919), 131-135, doi: 10.1038/nature01311, 2003.

Lamarque, J.-F., T. C. Bond, V. Eyring, C. Granier, A. Heil, Z. Klimont, D. Lee, C. Liousse, A. Mieville, B. Owen, M. G. Schultz, D. Shindell, S. J. Smith, E. Stehfest, J. van Aardenne, O. R. Cooper, M. Kainuma, N. Mahowald, J. R. McConnell, V. Naik, K. Riahi, and D. P. van Vuuren, Historical (1850-2000) gridded anthropogenic and biomass burning emissions of reactive gases and aerosols: methodology and application, *Atmos. Chem. Phys., 10*, doi: 10.5194/acp-10-7017-2010, 7017-7039, 2010.

Lamarque, L., G. P. Kyle, M. Meinshausen, K. Riahi, S. J. Smith, D. P. van Vuuren, A. J. Conley, and F. Vitt, Global and regional evolution of short-lived radiatively-active gases and aerosols in the Representative Concentration Pathways, *De Change*, *109*, 191-212, doi: 10.1007/s10584-011-0155-0, 2011.

Laval, K., R. Sadourny, and Y. Serafini, Land surface processes in a simplified general circulation model, *Geophys. Astrophys. Fluid Dyn., 17*, 129-150, 1981.

Lawrence, M. G., P. Jöckel, and R. von Kuhlmann, What does global mean OH concentration tell us, *Atmos. Chem. Phys.*, *1*, 37-49, doi: 10.5194/acp-1-37-2001, 2001.

Lean, J., G. Rottman, J. Harder, and G. Kopp, Source contributions to new understanding of global change and solar variability, *Solar Phys., 230*, 27-53, 2005.

Liang, Q., R. S. Stolarski, A. R. Douglass, P. A. Newman, and J. E. Nielsen, Evaluation of emissions and transport of CFCs using surface observations and their seasonal cycles and simulation of the GEOS CCM with emissions-based forcing, *J. Geophys. Res., 113*, D14302, doi: 10.1029/2007JD009617, 2008.

Lin, P., and Q. Fu, Changes in various branches of the Brewer-Dobson circulation from an ensemble of chemistry climate models, *J. Geophys. Res.*, *118*, 73-84, doi: 10.1029/2012JD018813, 2013.

Lin, S.-J., A "vertically Lagrangian" finite-volume dynamical core for global models, *Mon. Weather Rev., 132* (10), 2293-2307, 2004.

Lin, S. J., and R. B. Rood, Multidimensional flux-form semi-Lagrangian transport schemes, *Mon. Wea. Rev.*, *124*, 2046-2068, 1996.

Lott, F., Alleviation of stationary biases in a GCM through a mountain drag parameterization and a simple representation of mountain lift forces, *Mon. Weather Rev., 127*, 788-801, 1999.

Lott, F., L. Fairhead, F. Hourdin, and P. Levan, The stratospheric version of LMDz: dynamical climatologies, Arctic oscillation, and impact on the surface climate, *Clim. Dynam., 25*, 851-868, doi: 10.1007/s00382-005-0064-x, 2005.

Louis, J.-F., A parametric model of vertical eddy fluxes in the atmosphere, *Boundary-Layer Meteorol., 17*, 187-202, 1979.

Madronich, S., and S. Flocke, The role of solar radiation in atmospheric chemistry, Handbook of Environmental Chemistry, edited by P. Boule, Springer-Verlag, Heidelberg, pp. 1-26, 1998.

Martinerie, P., E. Nourtier-Mazauric, J.-M. Barnola, W. T. Sturges, D. R. Worton, E. Atlas, L. K. Gohar, K. P. Shine, and G. P. Brasseur, Long-lived halocarbon trends and budgets from atmospheric chemistry modelling constrained with measurements in polar firn, *Atmos. Chem. Phys., 9,* 3911-3934, 2009.

McCulloch, A., P. Ashford, and P. M. Midgley, Historic emissions of fluorotrichloromethane (CFC-11) based on a market survey, *Atmos. Environ.*, *35* (26), 4387-4397, 2001.

McCulloch, A., P. M. Midgley, and P. Ashford, Releases of refrigerant gases (CFC-12, HCFC-22, and HFC-134a) to the atmosphere, *Atmos. Environ.*, *37* (7), 889-902, 2002.

Miller, B. R., M. Rigby, L. J. M. Kuijpers, P. B. Krummel, L. P Steele, M. Leist, P. J. Fraser, A. McCulloch, C. Harth, P. Salameh, J. Mühle, R. F. Weiss, R. G. Prinn, R. H. J. Wang, S. O'Doherty, B. R. Greally, and P. G. Simmonds, HFC-23 (CHF_3) emission trend response to HCFC-22 ($CHClF_2$) production and recent HFC-23 emission abatement measures, *Atmos. Chem. Phys.*, *10*, 7875-7890, doi: 10.5194/acp-10-7875-2010, 2010.

Minschwaner, K., R. Salawitch, and M. McElroy, Absorption of solar radiation by O2: Implications for O_3 and lifetimes of N_2O, $CFCl_3$ and CF_2Cl_2, *J. Geophys. Res., 98,* 10543-10561, 1993.

Montzka, S. A., M. Krol, E. Dlugokencky, B. Hall, P. Jöckel, and J. Lelieveld, Small interannual variability of global atmospheric hydroxyl, *Science, 331* (67), doi: 10.1126/science.1197640, 2011.

Morcrette, J.-J., L. Smith, and Y. Fouquart, Pressure and temperature dependence of the absorption in longwave radiation parameterizations, *Contrib. Atmos. Phys., 59* (4), 455-469, 1986.

Moorthi, S., and M. J. Suarez, Relaxed Arakawa–Schubert, A parameterization of moist convection for general circulation models, *Mon. Wea. Rev., 120*, 978-1002, 1992.

Morgenstern, O., P. Braesicke, F. M. O'Connor, A. C. Bushell, C. E. Johnson, S. M. Osprey, and J. A. Pyle, Evaluation of the new UKCA climate-composition model – Part 1: The stratosphere, *Geosci. Model Dev.*, *2*, 43-57, doi: 10.5194/gmd-2-43-2009, 2009.

Morgenstern, O., M. A. Giorgetta, K. Shibata, V. Eyring, D.W. Waugh, T. G. Shepherd, H. Akiyoshi, J. Austin, A. J. G. Baumgaertner, S. Bekki, P. Braesicke, C. Brühl, M. P. Chipperfield, D. Cugnet, M. Dameris, S. Dhomse, S. M. Frith, H. Garny, A. Gettelman, S. C. Hardiman, M. I. Hegglin, D. E. Kinnison, J.-F. Lamarque, E. Mancini, E. Manzini, M. Marchand, M. Michou, T. Nakamura, J. E. Nielsen, G. Pitari, D. A. Plummer, E. Rozanov, J. F. Scinocca, D. Smale, H. Teyssèdre, M. Toohey, W. Tian, and Y. Yamashita, Review of the formulation of present-generation stratospheric chemistry-climate models and associated external forcings, *J. Geophys. Res.*, *115*, D00M02, doi: 10.1029/2009JD013728, 2010.

Neu, J. L., M. J. Prather, and J. E. Penner, Global atmospheric chemistry: Integrating over fractional cloud cover, *J. Geophys. Res., 112*, D11306, doi: 10.1029/2006JD008007, 2007.

Park, J. H., M. K.W. Ko, C. H. Jackman, R. A. Plumb, J. A. Kaye, and K. H. Sage (Eds.): *Models and Measurements Intercomparison II,* NASA Tech. Memo., TM-1999-209554, Hampton, VA, USA, 1999.

Pawson, S., R. S. Stolarski, A. R. Douglass, P. A. Newman, J. E. Nielsen, S. M. Frith, and M. L. Gupta, Goddard Earth Observing System chemistry-climate model simulations of stratospheric ozone-temperature coupling between 1950 and 2005, *J. Geophys. Res*., *113*, D12103, doi: 10.1029/2007JD009511, 2008.

Pitari, G., E. Mancini, V. Rizi, and D. Shindell, Impact of future climate and emission changes on stratospheric aerosol and ozone, *J. Atmos. Sci*., *59*, 414-440, 2002.

Prather, M. J., and C. M. Spivakovsky, Tropospheric OH and the lifetimes of hydrochlorofluorocarbons, *J. Geophys. Res*., *95*, 18723-18729, 1990.

Poisson, N., M. Kanakidou, and P. J. Crutzen, Impact of nonmethane hydrocarbons on tropospheric chemistry and the oxidizing power of the global troposphere: 3-dimensional modeling results, *J. Atmos. Chem*., *36*, 157-230, 2000.

Prinn, R. G., R. F. Weiss, B. R. Miller, J. Huang, F. N. Alyea, D. M. Cunnold, P. J. Fraser, D. E. Hartley, and P. G. Simmonds, Atmospheric trends and lifetime of CH_3CCl_3 and global OH concentrations, *Science*, *269*, 187-192, 1995.

Prinn, R. G., J. Huang, R. F. Weiss, D. M. Cunnold, P. J. Fraser, P. G. Simmonds, A. McCulloch, C. Harth, P. Salameh, S. O'Doherty, R. J. J. Wang, L. Porter, and B. R. Miller, Evidence for substantial variations of atmospheric hydroxyl radicals in the past two decades, *Science*, *292*, 1882-1888, 2001.

Prinn, R. G., J. Huang, R. F. Weiss, D. M. Cunnold, P. J. Fraser, P. G. Simmonds, A McCulloch, C. Harth, S. Reimann, P. Salameh, S. O'Doherty, R. H. J. Wang, . W. Porter, B. R. Miller, and P. B. Krummel, Evidence for variability of atmospheric hydroxyl radicals over the past quarter century, *Geophys. Res. Lett., 32*, L07809, doi: 10.1029/2004GL022228, 2005.

Rayner, N. A., D. E. Parker, E. B. Horton, C. K. Folland, L. V. Alexander, D. P. Rowell, E. C. Kent, and A. Kaplan, Global analyses of SST, sea ice and night marine air temperature since the late nineteenth century. *J. Geophys. Res., 108*, 4407, doi: 10.1029/2002JD002670, 2003.

Rigby, M., R. G. Prinn, S. O'Doherty, S. A. Montzka, A. McCulloch, C. M. Harth, J. Mühle, P. Salameh, R. F. Weiss, D. Young, P. G. Simmonds, B. D. Hall, G. S. Dutton, D. Nance, D. J. Mondeel, J. W. Elkins, P. B. Krummel, L. P. Steele, and P. J. Fraser, Re-evaluation of the lifetimes of the major CFCs and CH_3CCl_3 using atmospheric trends, *Atmos. Chem. Phys., 13*, 2691-2702, doi: 10.5194/acp-13-2691-2013, 2013.

Rosenfield, J. E., D. B. Considine, P. E. Meade, J. T. Bacmeister, C. H. Jackman, and M. R. Schoeberl, Stratospheric effects of Mount Pinatubo aerosol studied with a coupled two-dimensional model, *J. Geophys. Res., 102,* 3649-3670, 1997.

Sander, S. P., J. Abbatt, J. R. Barker, J. B. Burkholder, R. R. Friedl, D. M. Golden, R. E. Huie, C. E. Kolb, M. J. Kurylo, G. K. Moortgat, V. L. Orkin, and P. H. Wine, *Chemical Kinetics and Photochemical Data for Use in Atmospheric Studies, Evaluation No. 17*, JPL Publication 10-6, Jet Propulsion Laboratory, Pasadena, 2011 http://jpldataeval.jpl.nasa.gov, 2011.

Savage, N. H., K. S. Law, J. A. Pyle, A. Richter, H. Nüß, and J. P. Burrows, Using GOME NO_2 satellite data to examine regional differences in TOMCAT model performance, *Atmos. Chem. Phys., 4*, 1895-1912, 2004.

Schraner, M., Rozanov, E., Schnadt Poberaj, C., Kenzelmann, P., Fischer, A. M., Zubov, V., Luo, B. P., Hoyle, C. R., Egorova, T., Fueglistaler, S., Brönnimann, S., Schmutz, W., and T. Peter, Technical Note: Chemistry-climate model SOCOL: Version 2.0 with improved transport and chemistry/microphysics schemes, *Atmos. Chem. Phys.*, *8*, 5957-5974, doi: 10.5194/acp-8-5957-2008, 2008.

SPARC CCMVal (Stratospheric Processes And their Role in Climate), *Report on the Evaluation of Chemistry-Climate Models,* edited by V. Eyring, T. G. Shepherd, and D. W. Waugh, SPARC Report No. 5, WCRP-132, WMO/TD-No. 1526, available: http://www.atmosp.physics.utoronto.ca/SPARC/ccmval_final/index.php, 2010.

Spivakovsky, C. M., R. Yevich, J. A. Logan, S. C. Wofsy, M. B. McElroy, and M. J Prather, Tropospheric OH in a three-dimensional chemical tracer model: An assessment based on observations of CH_3CCl_3, *J. Geophys. Res.*, 95, 18441-18471, 1990.

Spivakovsky, C. M., J. A. Logan, S. A. Montzka, Y. J. Balkanski, M. Foreman-Fowler, D. B. J. Jones, L. W. Horowitz, A. C. Fusco, C. A. M. Brenninkmeijer, M. J. Prather, S. C. Wofsy, and M. B. McElroy, Three-dimensional climatological distribution of tropospheric OH: Update and evaluation, *J. Geophys. Res.*, *105* (D7), 8931-8980, doi: 10.1029/1999JD901006, 2000.

Szopa, S., Y. Balkanski, M. Schulz, S. Bekki, D. Cugnet, A. Fortems-Cheiney, S. Turquety, A. Cozic, C. Déandreis, D. Hauglustaine, A. Idelkadi, J. Lathière, F. Lefevre, M. Marchand, R. Vuolo, N. Yan, and J.-L. Dufresne, Aerosol and ozone changes as forcing for climate evolution between 1850 and 2100, *Clim. Dynam.,* doi: 10.1007/s00382-012-1408-y, 2012.

Telford, P. J., N. L. Abraham, A. T. Archibald, P. Braesicke, M. Dalvi, O. Morgenstern, F. M. O'Connor, N. A. D. Richards, and J. A. Pyle, Implementation of the Fast-JX photolysis scheme (v6.4) into the UKCA component of the MetUM chemistry climate model (v7.3), *Geosci. Model Dev.*, *6*, 161-177, doi: 10.5194/gmd-6-161-2013, 2013.

Toon, O., C. McKay, T. Ackerman, and K. Santhanam, Rapid calculation of radiative heating rates and photodissociation rates in inhomogeneous multiple scattering atmospheres, *J. Geophys. Res., 94,* 16287-16301, 1989.

Velders, G. J. M., D. W. Fahey, J. S. Daniel, M. McFarland, and S. O. Andersen, The large contribution of projected HFC emissions to future climate forcing, *Pro. Nat. Acad. Sci.*, doi: 10.1073/pnas.0902817106, 2009.

Wang, Y., J. A. Logan, and D. J. Jacob, Global simulation of tropospheric O**3**-NO**x**-hydrocarbon chemistry, 2. model evaluation and global ozone budget, *J. Geophys. Res.*, *103*, 10727-10755, 1998.

Wang, J. S., M. B. McElroy, J. A. Logan, P. I. Palmer, W. L. Chameides, Y. Wang, and I. A. Megretskaia, A quantitative assessment of uncertainties affecting estimates of global mean OH derived from methyl chloroform observations, *J. Geophys. Res.*, *113*, D12302, doi: 10.1029/2007JD008496, 2008.

Waugh, D., and V. Eyring, Quantitative performance metrics for stratospheric-resolving chemistry-climate models, *Atmos. Chem. Phys.*, *8*, 5699-5713, 2008.

WMO, *Scientific Assessment of Ozone Depletion: 2010, Global Ozone Research and Monitoring Project-Report No. 52*, 516 pp., Geneva, Switzerland, 2011.

Zubov, V., E. Rozanov, and M. E. Schlesinger, Hybrid scheme for three-dimensional advective transport, *Mon. Weather Rev.*, *127*(6), 1335-1346, 1999.